Wear Study on Polymer Matrix Composite Materials for Brake shoe Applications

A thesis submitted to the Department of Materials and Metallurgical Engineering, Dhaka, in partial fulfillment of the requirement for the degree of Master of Science in Engineering (Metallurgical)

By

Muhammad Monjur Morshed

Roll No: 9511004 F

#93586#

Department of Materials and Metallurgical Engineering, Bangladesh University of Engineering and Technology, Dhaka, Bangladesh
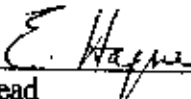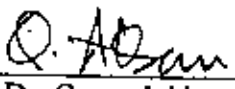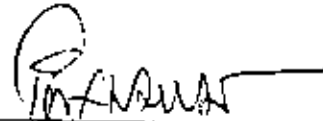
August, 1999

DECLARATION

This is to certify that this research work has been carried out by the
author under the supervision of Dr. A. S. M. A. Haseeb, Associate
Professor, Materials and Metallurgical Engineering Department,
BUET, Dhaka, and it has not been submitted elsewhere for the
award or degree of any kind.

Coutersigned by

E. Haque
for Dr. A. S. M. A. Haseeb.
Singnature of the Supervisor

Muhammad Monjur Morshed
Singnature of the Author

The undersigned examiners appointed by the Committee of Advanced Studies and Research (CASR) hereby recommend to the Department of Metallurgical Engineering of Bangladesh University of Engineering and Technology (BUET), Dhaka, the acceptance of the thesis entitled "**WEAR STUDY ON POLYMER MATRIX COMPOSITE MATERIALS FOR BRAKE SHOE APPLICATIONS**" submitted by Muhammad Monjur Morshed, B.Sc. Engg (Metallurgical) in partial fulfilment of the requirements for the degree of Master of Science in Engineering (Metallurgical).

1. _____ 12/8/99

Dr. A.S.M.A Haseeb
Associate Professor
Department of Materials and Metallurgical Engineering
BUET, Dhaka

Chairman
(Supervisor)

2. _____

Head
Department of Materials and Metallurgical Engineering
BUET, Dhaka

Member

3. _____

Dr. Qumrul Ahsan
Assistant Professor
Department of Materials and Metallurgical Engineering
BUET, Dhaka

Member

4. _____

Prof. Dr. Md. Serajul Islam
Retired Professor
Department of Materials and Metallurgical Engineering
BUET
256/2/A, Sultanganj
Rayer Bazar, Dhaka

Member
(External)

DEDICATION

In The Name Of Allah
The Most Beneficent
The Most Merciful

ABSTRACT

A polymer based automotive brake shoe lining material manufactured in Bangladesh has been compared with those of three imported brake shoes sold in the local market. X-ray diffraction, infrared spectroscopy, and optical microscopic techniques of the four materials were used upon to identify the constituents. Relevant physical properties of Materials viz. density, water absorption and swelling characteristics were also determined using standard analyzed methods. The friction and wear behaviour of the materials were tested in a pin-on-disc type apparatus under ambient conditions. Linear speed and load employed were 2.97 and $1.88m^{-1}$ and 15N respectively. During the tests, friction force was measured with an on-line load cell. It has been observed that all of the four friction materials contain phenol formaldehyde as the matrix. Other major ingredients were also the same in all the samples. These include asbestos as fiber reinforcement, barium sulphate as filler, brass particles and cashew nut shell/pre cured resin as friction modifiers. It was found that the swell resistance of the friction material manufactured in Bangladesh compares favourably with that of the improved materials, but the bulk density of the Bangladeshi material was the lowest and its water absorption the highest. The room temperature friction coefficient of the Bangladeshi material was found to be about 0.4 which lies well with in the acceptable range. Among the four materials tested the Bangladeshi material was found to rank third in respect of wear resistance. Besides the above, a wear testing machine based on SAE J661a has been developed to correspond closely to the wear and frictional condition of an actual automobile.

i

ACKNOWLEDGEMENT

CONTENT

Chapter One

1. INTRODUCTION

Brakes are essential and crucial components in automobiles, trains, aircrafts, cranes and other moving systems. Automotive brakes must satisfy a certain set of consumer expectations, which include safety, comfort, durability and reasonable cost. In technical terms these expectations are translated into a set of specific requirements such as high and stable friction, no or minimal vibration and noise and low wear rates for the rotor and friction material (brake shoe lining material). The brake shoe lining materials must also be compatible with the rotor materials. All these technical goals have to be achieved simultaneously at a reasonable cost. Particularly, the friction coefficient has to remain high and stable under varying application conditions involving high and low temperatures, high and low humidity, high and low speed stop, high and low deceleration rates and occasional to many consecutive stops [1]. To stop the movable automobile, four kinds of drum brakes are used in the service brake system (Fig.1.1). These brakes are distinguished by the features of force interaction between the brake shoes and the expanding device and drum. Conditionally, the brake linings are shown to be symmetrical relative to the horizontal diameter of the brake; the resultants of normal force N and of the forces of friction fN are applied in the middle linings arc of the drum [2].

The brake shoe lining of heavy dnty, cars and light duty vehicles are molded from a mixture of fibrous asbestos or nonasbestos and binder (rubber, mineral and vegetable oils, synthetic resin). Polymer matrix composites have been developed for some time for brake shoe. These materials have been continuing to attract a great deal of interest in recent year because of a lot room is there for further improvement of their performance. For light duty vehicles these brake shoes are stamped and welded. Owing to small heat capacity, high adaptability to manufacturer and pliability which aids in equalizing pressures along the length and width of friction lining, the stamped-and-welded brake shoes are in general use [2].

Many of the brake shoe lining used today in our country are made from polymer based composites. These brake linings are mainly imported from abroad. A couple of industries have been trying in recent years to produce brake shoe lining. However, local producers find it difficult to market their products partly because of inferior quality.

The objective of the present study is to characterize and compare locally produced brake shoe lining material with the imported ones. For this purpose, one locally produced material and three imported ones were selected. Major constituents in the selected materials are identified, their physical properties as well as wear and frictional behavior were investigated.
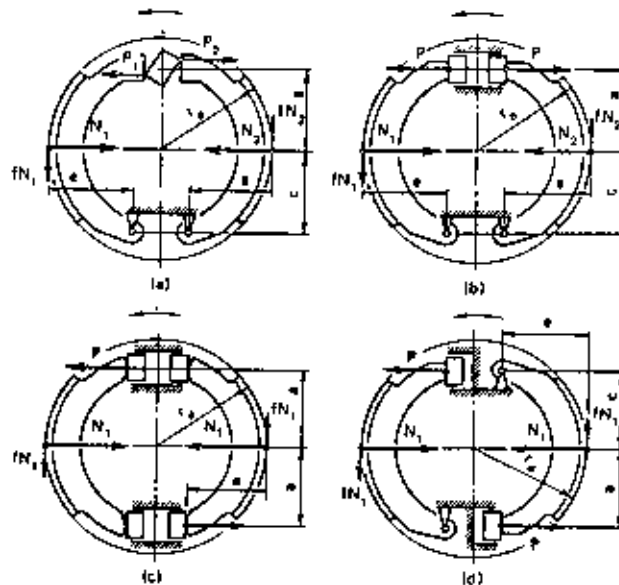
Fig. 1.1 Schematics of drum brakes
a) with equal displacement of shoes; b) reversing unbalanced brake; c) non-reversing balanced brake; d) reversing brake with leading shoes

Chapter Two

2. THEORETICAL BRACKGROUND

2.1 COMPOSITE MATERIALS

Fibrous polymeric composites are nonhomogeneous compound materials. Their base is a polymeric matrix, reinforced by fiber or particles. For a sound selection of the experimentally determinable characteristics and mathematical apparatus for processing the test results, it must be determined to which class the composites belong-to isotropic or anisotropic materials. Depending on the size relationships of reinforcing elements and their arrangement in the polymeric matrix, two large groups of reinforced materials can be identified: randomly reinforced (matrix+particles) and regularly reinforced or oriented (matrix+continuous fibers) materials. The first group of materials incorporates reinforcement consisting of particle sizes of which are commensurate in all direction, or of discrete fibers, for example, short fiber lengths, whiskers, etc. These particles are randomly arranged in the polymeric matrix, so that the material is quasi-isotropic, i.e., anisotropic in microvolumer but isotropic in macrovolumer. However, it should be remembered that in the conversion process, for example, in cast-molding the product as a whole can become anisotropic, similar to metals in after pressure processing [3]. The role of the matrix in a fiber-reinforced composite is to transfer stresses between the fibers, to provide a barrier against an adverse environment, and to protect the surface of the fibers from mechanical abrasion. The matrix plays a minor role in the tensile load-carrying capacity of a composite structure. However, selection of a matrix has a major influence on the interlaminar shear as well as in-plane shear properties of the composite material. The interlaminar shear strength is an important design consideration for structures under bending loads, whereas the in-plane shear strength is important under torsional loads. The matrix provides lateral support against the possibility of fiber buckling under compression loading, thus influencing to some extent the compressive strength of the composite material. The interaction between fibers and matrix is also important in designing damage-tolerant structures. Finally, the processability and defects in a composite material depend strongly on the physical and chemical characteristics, such as viscosity, melting point, and curing temperature of the matrix. The primary consideration in the selection of a matrix is

its basic mechanical properties. For high-performance composites, the most desirable mechanical properties of a matrix are:

(a) High tensile modulus, which influences the compressive strength of the composite
(b) High tensile strength, which control the intraply cracking in a composite laminate
(c) High fracture toughness, which controls ply delamination and crack growth

For a polymeric matrix composite, there may be other considerations, such as good dimensional stability at elevated temperatures, and resistance to moisture and solvents. The former usually means that the polymer must have a high glass transition temperature T_g. In practice, the glass transition temperature should be higher than the maximum service temperature. Resistance to moisture and solvent means that the polymer should not dissolve, swell, crack (craze), or otherwise degrade in hot/ wet environments or when exposed to solvents.

Traditionally, thermoset polymers (also called resins) have been used as a matrix material for fiber reinforced composites. Starting materials used in the polymerization of thermoset polymers are usually low molecular weight liquid chemicals with very low viscosities. Fibers are either pulled through or immersed in these chemicals before the polymerization reaction begins. Since the viscosity of the polymer at the time of fiber incorporation is very low, it is possible to achieve a good wet-out between the fibers and the matrix without the aid of high temperature or pressure. Among other advantages of using thermoset polymers are their thermal stability and chemical resistance. They also exhibit much less creep and stress relaxation than thermoplastic polymers. The disadvantages are their limited storage life (before the final shape is molded) at room temperature, long fabrication time in the mold, and low strain to failure, which also contribute to their low impact strengths [4].

2.2 TYPE OF COMPOSITE MATERIALS

There is no generally accepted classification of fibrous polymeric composites. The mechanics of materials has its specific requirements for division of fibrous composites into separate classes. The general principles by which materials obtain their names are specified in classification of fibrous composites. Fibrous composites are then divided into quasi-isotropic and anisotropic materials, the type of anisotropy is established, and the transition to a uniform medium is accomplished. The following general principles may underline classification of fibrous composites: materials, i.e., classification by reinforcement or matrix material; structure, i.e., by type of reinforcement and its layup; technology, i.e., by the method of conversion in to end products.

More often the fibrous composites obtain their names from the reinforcing fibers: glass fiber, boron, carbon, graphite, organic (aramid), glass fiber/boron etc., composites. Classification by matrix material is less wide spread. It is difficult because of the broad selection of resins and their combinations. This principle is nsed for more precise definition of the name of the material only: for example, unidirectional boron-epoxy composite.

Classification by method of conversion or the technological classification divides fibrous composites into cast, and wound. Randomly reinforced materials are processed by casting and molding, and oriented ones by winding, press molding and contact molding. The processing method has a strong effect on the properties of the material. The specimen technology and shape must correspond to the production method and intended use of the material. This explains the different approaches to wound and molded materials.

Even the most successful material mechanics or technological nomenclature for a material does not address the details of mechanical tests of fibrous composites. Type of reinforcement and its lay up in the polymeric matrix are the most important classification criteria in this regard. The main requirement for classification, from the point of view of the mechanics of materials, is to determine the law of

5

deformation and the relationship of the properties to angular coordinates. By assuming, in the first approximation, that fibrous composites follow Hooke's law, the entire variety of fibrous composites can be divided into isotroppic and anisotropic materials [3].

2.3 MANUFACTURING METHOD OF COMPOSITE MATERIALS

The early manufacturing method for fiber reinforced composite structural parts used a hand lay-up technique. Although hand lay-up is a reliable process, it is by nature very slow and labor intensive. In recent year, particularly due to the interest generated in the automotive industry, there is more emphasis on the development of manufacturing methods that can support mass production rates. Compression molding, pultrusion, and filament winding represent there such manufacturing methods. Although they have existed for many years, investigation in their basic characteristics and process optimization started mostly in the mid -1970s. With the introduction and automation, fast curing resins, new fiber forms, high-resolution control tools, and so on, the manufacturing technology for fiber- reinforced polymer composites is advancing at a remarkably rapid place.

Transformation of uncured or partially cured-reinforced thermosetting polymers into composite parts or structure involves curing the material at elevated temperatures and pressure for a predetermined length of time. High cure temperatures are required to initiate and snstain the chemical reaction that transforms the uncured or partially cured material into a fully cured solid. High cure pressures are used to provide the force needed for the flow of the highly viscous fiber-resin mixture in the mold, as well as for the consolidation of individual unbonded plies into a bonded laminate. The magnitude of these two important process parameters, as well as their duration, significantly affects the performance of the molded product. The length of time required to properly cure a part is called the cure cycle. Since the cure cycle determines the production rate for a part, it is desirable to achieve the proper cure in the shortest amount of time. It should be noted that the cure cycle depends on a number of factors, including resin chemistry, catalyst reactivity, cure temperature, and the presence of inhibitors or accelerators [4].

2.4 EFFECT OF PARAMETERS ON COMPOSITE MATERIALS

2.4.1 Degree of Cure

A number of investigators have experimentally measured the heat evolved in a curing reaction and related into the degree of cure achieved at any time during the curing process. Experiments are performed in a differential scanning calorimeter (DSC) in which a small sample, weighing a few milligram, is heated either isothermally (i.e., at constant temperature) or dynamically (i.e., with uniformly increasing temperature). The instrumentation in DSC monitors the rate of heat generation as a function of time, which is displayed on a strip chart recorder. Fig. 2.1 schematically illustrates the rate of heat generation curves for isothermal and dynamic heating.
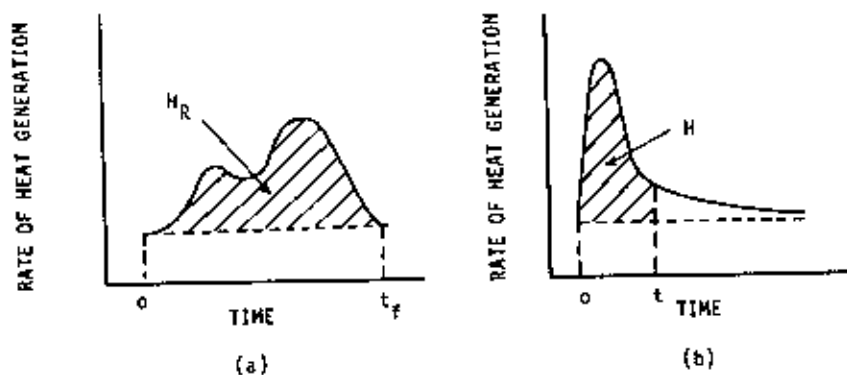
Fig. 2.1 Schematic representation of the rate of heat generation in (a) dynamic and (b) isothermal heating of a thermoset polymer in a different scanning calorimeter

The total heat generation to complete a curing reaction (i.e., 100% degree of cure) is equal to the area under of heat generation-time curve obtained in a dynamic heating experiment. It is expressed as

$$H_R = \int_{t_o}^{t_f} (dQ/dt)_d \, dt$$

Where

H_R = heat of reaction

$(dQ/dt)_d$ = rate of heat generation in a dynamic test

t_f = time required to complete the reaction

The amount of heat released in time t at a constant curing temperature T is determined from isothermal experiments. The area under the rate of heat generation-time curve is expressed as

$$H = \int_{o}^{t} (dQ/dt)_i \, dt$$

Where

H = amount of heat released in time t

$(dQ/dt)_i$ = rate of heat generation in an isothermal test conducted at constant temperature T

Fig. 2.2 shows a number of curves relating the degree of cure to cure time for a vinyl resin at various cure temperatures.
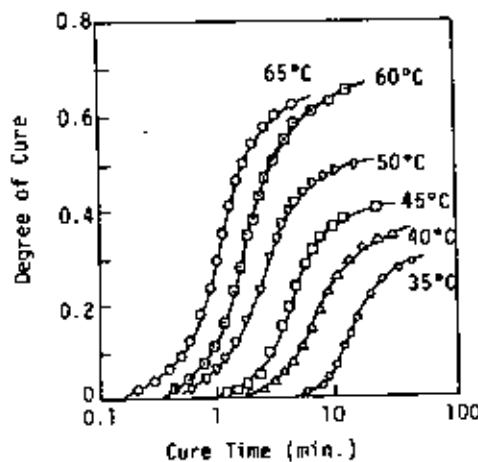
Fig. 2.2 Degree of cure for a vinyl ester resin at various cure temperature.

The degree of cure at any time t is defined as

$$\alpha_c = H/H_R$$

From 2.2 figure it can be seen that α_c increases with both time and temperature; however, the rate of cure is decreased as the degree of cure attains asymptotically a maximum value. If the cure temperature is too low, the degree of cure $d\alpha_c/dt$, obtained from the slopes of α_c versus t curves and plotted in Fig. 2.3, exhibits a maximum value at 10-40% of the total cure achieved. Higher cure temperatures increase the rate of cure and produce the maximum degree of cure in shorter periods of time [4].
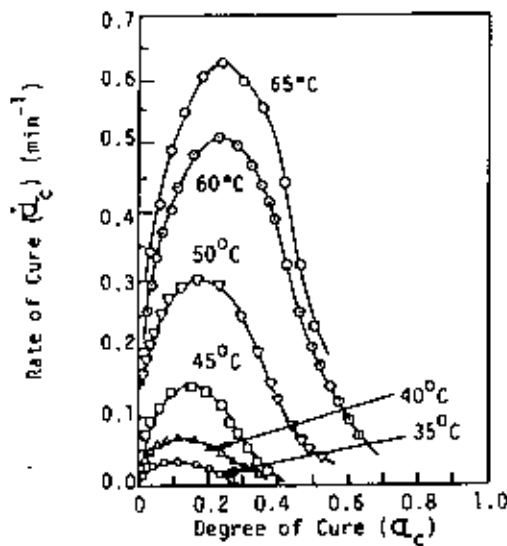
Fig. 2.3 Rate of cure for a vinyl ester resin at various cure temperature

2.4.2 Viscosity

The two most important factors determining the viscosity of a fluid are the temperature and shear rate. For all fluids, the viscosity decreases with increasing temperature. Shear rate does not have any influence on the viscosity of low

molecular-weight fluids, whereas it tends to either increase (shear thickening) or decrease (shear thinning) the viscosity of a high molecular fluid (Fig. 2.4). Polymer melts, in general, are shear-thinning fluids since their viscosity decreases with increasing intensity of shearing. The starting material for a thermosetting resin is a low viscosity fluid. However, its viscosity increases with curing and approaches a very large value as it transforms in to a solid mass. In all cases, the viscosity increases with increasing curing time and temperature. The rate of viscosity increase is low at early stages of curing. After a threshold degree of cure is achieved, the resin viscosity increases at a very rapid rate. The time at which this occurs is called the gel time. The gel time is an important molding parameter, since the flow of resin in the mold becomes increasingly difficult at the end of this time period.
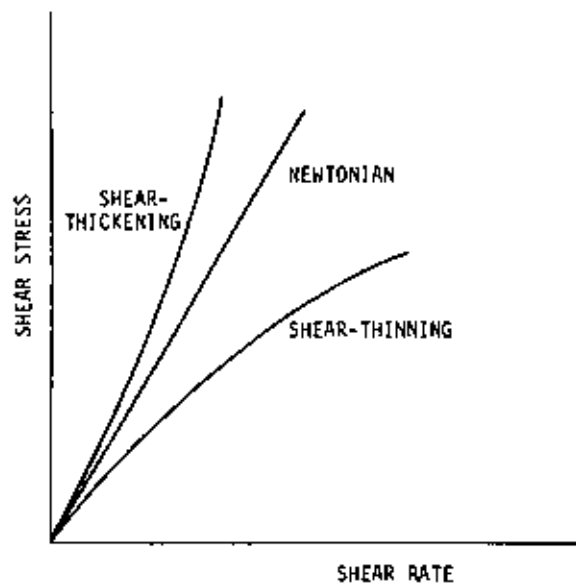
Fig. 2.4 Schematic shear stress versus shear rate curve for various type of liquid.

A number of important observations can be made from the viscosity data listed below:

a) A B-staged or a thickened resin has a much higher viscosity than the neat resin at all stages in the curing.

b) The addition of fillers, such as $CaCO_3$, to the neat resin increases its viscosity as well as the rate of viscosity increase during curing. On the other hand, the addition

10

of thermoplastic additives tends to reduce the rate of viscosity increase during curing.

c) The increasing in viscosity with cure time is less if the shear rate is increased. This phenomenon, known as shear thinning, is more pronounced in B-staged or thickened resins than in neat resins. Fillers and thermoplastic additives also tend to increase the shear-thinning phenomenon.

d) The viscous η of a thermosetting resin during the curing process is a function of cure temperature T, shear rate γ, and the degree of cure α_c.

$$\eta = \eta \, (T, \gamma, \alpha_c)$$

It is important to note that the viscosity function for thermosets is significantly different from that for thermoplastic. Since no insitu chemical reaction occurs during the processing of a thermoplastic polymer, its viscosity depends only on temperature and shear rate.

e) At a constant shear rate and for the same degree of cure, the η versus $1/T$ plot is linear (Fig. 2.5).
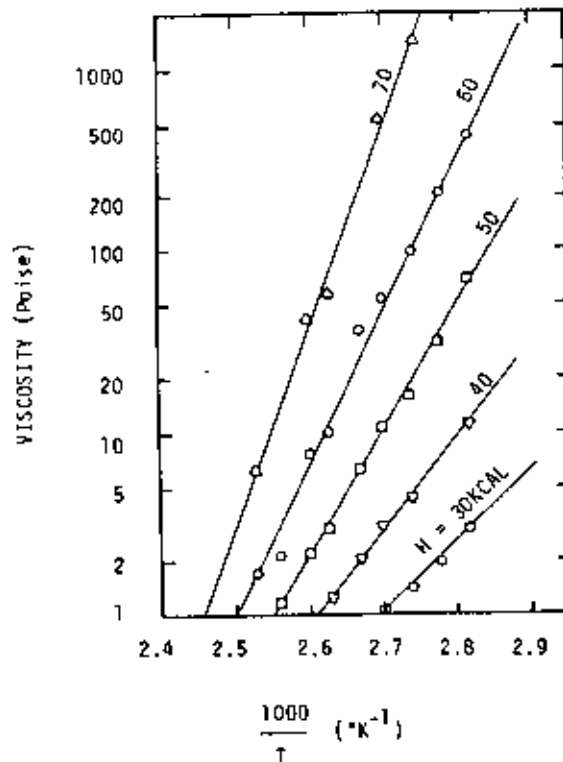
Fig. 2.5 Viscosity-temperature relationships for an epoxy resin at different level of cure.

This suggests that the viscous flow of a thermosetting polymer is an energy-activated process. Thus, its viscosity as a function of temperature can written as

$$\eta = \eta_0 \exp(-E/RT)$$

Where

η= viscosity (pa-s or centipoise)

E= flow activation energy (cal/g-mol)

R= universal gas constant

T= curing temperature ($^\circ$K)

η_0 = constant

It should be noted that the activation energy for viscous flow increases with the degree of cure and approaches high value near the gel point [4].

2.4.3 Resin Flow

Proper flow of resin through fiber network or lay-ups is critical in producing void-free parts and good fiber wet out. In thermoset resins, curing may take place simultaneously with resin flow, and if the resin viscosity rises too rapidly due to curing, its flow may be inhibited, causing voids and interlaminer adhesion. Resin flow through fiber network has been modeled using Dacry's equation, which was derived for flow of Newtonian fluids through a porous medium. This equation relates the volumetric resin flow rate q per unit area to the pressure gradient that causes the flow of occur. For one dimensional flow in the x direction,

$$q = -p_0/\eta \, (dp/dx)$$

Where

q= volumetric flow rate per unit area (m/s) in the x direction

p_0 = permeability (m^2)

12

η = viscosity (N-s/m^2)

dp/dx= Pressure gradient (N/m^3), which is negative in the direction of flow (positive x direction)

The permeability is determined by the following equation known as the Carman-Kozney equation;

$$P_o = d_f^2 (1-v^f)^3 / (16K \, v_f^2)$$

Where
d_f= fiber diameter
v_f= fiber volume fraction
K = Kozney constant.

2.4.4 Shrinkage

Shrinkage is the reduction in volume or linear dimensions caused by curing as well as thermal contraction. Curing shrinkage occurs because of the rearrangement of polymer molecules into a more compact mass as the curing reaction proceeds. The thermal shrinkage occurs during the cooling period that follows the curing reaction and may take place both inside and outside the mold. The volumetric shrinkage for cast epoxy resins is of the order of 1-5%. The addition of fibers or fillers reduces the volumetric shrinkage of a resin. However, in the case of unidirectional fibers, the reduction of shrinkage in the longitudinal direction is higher than in the transverse direction. High resin shrinkage is desirable for easy release of the part from the mold surface; at the same time, high resin shrinkage can contribute to many molding defects, such as warpage and sink marks.

2.4.5 Voids

Among the various defects produced during the molding of a composite laminate, the presence of voids is considered the most critical defect in influencing its mechanical properties. The most common cause for void formation is the inability of

the resin to displace air from the fiber surface during the time fibers are coated with the liquid resin. The rate at which the fibers are pulled through the liquid resin, the resin viscosity, the relative values of fiber and resin surface energies, and the mechanical manipulation of fibers in the liquid resin affect air entrapment at the fiber-resin interface. Voids may also be caused by air bubbles and volatile entrapment in the liquid resin. Solvents used for resin viscosity control, moisture, and chemical contamination in the resin, as well as styrene monomer, may remaining dissolved in the resin mix and volatilize during elevated temperature curing. In addition air is also entrapped between various layers during the lamination process.

Much of the air or volatiles entrapped at the pre molding stages can be removed by degassing the liquid resin, applying vacuum during the molding process, and allowing the resin mix to flow freely in the mold, which helps in carrying the air and volatiles out through the vents in the mold. The presence of large volume fractions of voids in a composite laminate can significantly reduce the tensile, compressive, and flexural strengths. The presence of voids generally increases the rate and amount of moisture absorption in a humid environment, which in turn increases the physical dimensions of the part and reduces its matrix-dominated properties [4].

2.5 FACTORS CONTROLLING THE COMPOSITE PROPERTIES

2.5.1 Water Absorption

The rate of water absorption has two chief functions: first, as a guide to the proportion of water absorbed by a material and consequently, in those cases where the relationships between moisture and electrical or mechanical properties, dimensions, or appearance have been determined, as a guide to the effects of exposure to water or humid conditions on such properties; and second, as a control test on the uniformity of a product. This second function is particularly applicable to sheet, rod, and arms when the test is made on finished product.

The moisture content of a composite is very intimately related to such properties as electrical insulation resistance, dielectric losses, mechanical strength, appearance, and dimensions. The effect upon these properties of change in moisture content due to water absorption depends largely on the type of exposure (by immersion in water or by exposure to high humidity), shape of the part, and inherent properties of the composite. With nonhomogeneous materials, such as laminated forms, the rate of water absorption may be widely different through each edge and surface. Even for otherwise homogeneous materials, it may be slightly greater through cut edges than through molded surfaces. Consequently, attempts to correlate water absorption with the surface area must generally be limited to closely related materials and to similarly shaped specimens. For materials of widely varying density, relation between water-absorption values on a volume as well as a weight basis may need to be considered [8].

When exposed to humid air or water environments, many polymeric matrix composites absorb water/moisture by instantaneous surface absorption followed by diffusion through the matrix. Analysis of water/moisture absorption for composite materials shows that the water concentration increases initially with time and approaches an equilibrium (saturation) level after several days of exposure to humid environments. Its thickness as well as the ambient temperature determines the rate at which the composite laminate attains the equilibrium water concentration. Upon drying, the water concentration is continually reduced until the composite laminate returns to the original as dry state. In general, the rate of desorption is higher than the rate of absorption, although for the purposes of analysis they are assumed to be equal.

The moisture concentration M, average over the thickness, of a composite laminate at any time during its exposure to humid environment at a given temperature can be calculated from the following equation:

$$M = M_i + G (M_m - M_i)$$ ---------------- (2.5.1)

Where

M_i = initial moisture concentration, which is equal to zero if the material is completely dried,

M_m = equilibrium (maximum) moisture concentration in the saturated condition and

G = time dependent dimensionless parameter related to the diffusion coefficient of the material

or

$$\% \text{ of water absorption} = \frac{\text{Wet wt.- Dry wt.}}{\text{Dry wt.}} \times 100 \quad \text{------------------(2.5.2)}$$

For a material immersed in water, the equilibrium moisture concentration M_m is a constant. If the material is exposed to humid air, the equilibrium moisture concentration M_m increases with increasing relative humidity of the surrounding air; however, it is found that M_m is relatively insensitive to the ambient temperature. For the humid air environment, M_m is expressed as

$$M_m = A\,(RH)^B \quad \text{----------------(2.5.3)}$$

Where

RH = Relative humidity (percent) of the surrounding air and

A, B = Constants that depend primarily on the type of polymer; the exponent B has a value between 1 and 2

Assuming a Fickian diffusion through the laminate thickness, the time dependent parameter G can be approximated as

$$G \approx 1 - \frac{8}{\pi^2}\,\exp\left(-\pi^2 D_z t/c^2\right) \quad \text{------------(2.5.4)}$$

Where

D_z = Diffusion coefficient (mm²/s) of the material in the direction normal to the surface (moisture diffusion is in the thickness direction)

c = lamination thickness h if both sides of the laminate are exposed to humid environment; for exposure on one side, c = 2h

t = time (s)

Equation (2.5.3) is valid at sufficiently large values of t . For shorter times, the average moisture concentration increases linearly with $t^{1/2}$, and the parameter G can be approximated as

$$G = 4 \, (D_z t \, / \, \pi^2 c)^{1/2} \text{------------}(2.5.5)$$

The diffusion coefficient D_z is related to the matrix diffusion coefficient D_m by the following equation:

$$D_z = D_{11} \cos^2\phi + D_{22} \sin^2\phi \text{ -------------}(2.5.6)$$

Where

$$D_{11} = D_m \, (1 - v_f)$$

$D_{22} = D_m \, \{ \, 1 - 2\sqrt{(v_f / \pi)} \}$ [Assuming fiber diffusivity to be small compared to matrix diffusivity (i.e., $D_f \ll D_m$)]

ϕ = fiber angle with the z direction (ϕ = 90 ⁰ for fibers parallel to the laminate surface)

v_f = fiber volume fraction

Equation (2.5.1) and (2.5.3) through (2.5.6) and equation (2.5.2) which is established by ASTM D 570-77 can be used to estimate the moisture concentration in a composite laminate. However, the following internal and external parameters may cause deviations from the calculated moisture concentrations.

2.5.1.1 Void content

The presence of voids has a dramatic effect on increasing the equilibrium moisture concentration as well as the diffusion coefficient.

2.5.1.2 Fiber type

Equation (2.5.6) assumes that the fiber diffusivity is negligible compared with the matrix diffusivity. This assumption is valid for glass, carbon and boron fibers. However, Kevlar 49 fibers are capable of absorbing and diffusing significant amounts of moisture from the environment. As a result, Kevlar 49 fiber reinforced composites absorb much more moisture than other composites.

2.5 1.3 Resin type

Moisture absorption in a resin depends on its chemical structure and the curing agent as well as the degree of cure. Analysis of the water absorption data of various epoxy resin compositions shows that the weight gain due to water absorption may differ by a factor of 10 or more between different resin chemical structures and by a factor of 3 or more for the same resin having different curing formulation [5]. For many resin systems, the water absorption process may continue for a long time and equilibrium may not be attained for months or even years.

2.5.1.4 Temperature

Moisture diffusion in a polymer is an energy-activated process, and the diffusion coefficient depends strongly on the temperature (Table 2.1). In general, the temperature dependence can be predicated from an Arrhenius-type equation:

$$D_z = D_{zo} \exp(- E / RT)$$

Where

E = activation energy (cal/g-mol)

R = universal gas constant = 1.987cal/(g-mol-K)

T = absolute temperature (K)

D_{zo} = constant (mm^2/s)

Table 2.1 Diffusion coefficients for absorption and desorption in an epoxy resin at 100% relative humidity

Temperature (°C)	Diffusion coefficient (10^{-8} mm^2/s)	
	Absorption	Desorption
2	3	3
25	21	17
37	41	40
50	102	88
60	179	152
70	316	282
80	411	489
90	630	661

2.5.1.5 Stress level

Gillat and Broutman have shown that increasing the applied stress level on a T-300 carbon-epoxy cross-ply laminate produces higher diffusion coefficients but does not influence the equilibrium moisture content. Similar experiment by Marom and Broutman [6] show that the moisture absorption is a function of fiber orientation angle relative to the loading direction. The maximum effect is observed at $\theta = 90°$.

2.5.1.6 Microcracks .

The moisture concentration in a laminate may exceed the equilibrium moisture concentration if microcracks develop in the material. Moisture absorption is

accelerated owing to capillary action at the microcracks as well as exposed fiber-matrix interfaces at the laminate edges. On the other hand, there may be an "apparent" reduction in moisture concentration if there is a loss of material from leaching or cracking.

2.5.1.7 Thermal spikes

Diffusion characteristics of composite laminates may alter significantly if they are rapidly heated to high temperatures followed by rapid cooling to the ambient condition, a process known as thermal spiking. McKague et al. [7] have shown that the moisture absorption in specimens exposed to 75% relative humidity at 24°C and occasional (twice weekly) thermal spikes (rapid heating to 149°C followed by rapid cooling to 24°C) is twice that of specimens not exposed to spikes. Additionally, thermally spiked specimens exhibit a permanent change in their moisture absorption characteristics. The increased diffusion rate and higher moisture absorption are attributed to microcracks formed owing to stress gradients caused by thermal cycling and resin swelling. The service temperature in a spike environment should be limited to the glass transition temperature T_g of the resin, since spike temperatures above the T_g cause much higher moisture absorption than those below the T_g.

2.5.1.8 Reverse thermal effect

Adamson [8] has observed that cast epoxy resins or epoxy-based laminates containing an equilibrium moisture concentration exhibit a rapid rate of moisture absorption when the ambient temperature is reduced. For example, an AS carbon fiber reinforced epoxy laminate attained an equilibrium moisture concentration of 2.3 wt % after 140 days of exposure at 74°C. When the exposure temperature was reduced to 25°C, the equilibrium moisture concentration increased to 2.6% within 40 days. This inverse temperature dependence of moisture absorption is called the reverse thermal effect.

2.5.2 Physical Effect of Moisture Absorption

Moisture absorption produces volumetric change (swelling) in the resin, which in turn cause dimensional changes in the material. Assuming that the swollen volume of the resin is equal to the volume of absorbed water, the resulting volume change can be computed from the following relationship:

$$\frac{\Delta V(t)}{V_o} = \frac{\rho_m}{\rho_w} M$$

Where

ρ_m = matrix density

ρ_w = water density($\approx$ 1 Kg/mm3)

M = moisture content at time t

The corresponding dilatational (volumetric) strain in the resin is

$$\varepsilon_m = \frac{1}{3} \frac{\Delta V}{V_o} = \frac{1}{3}(\rho_m/\rho_w) M = \beta_m M$$

Where

$$\beta_m = \frac{1}{3} (\rho_m/\rho_w)$$

Which is called the swelling coefficient.

In practice, swelling is negligible until a threshold moisture concentration M_o is exceeded. Therefore, the dilatational strain is

$$\varepsilon_m = 0 \qquad \qquad \text{for } M < M_o$$

$$= \beta_m (M - M_o) \qquad \qquad \text{for } M > M_o$$

The threshold moisture concentration M_o represents the amount of water absorbed in the free volume as well as microvoids present in the resin. For a variety of cast

epoxy resins, the measured swelling coefficient ranges from 0.26 to 0.33 and the threshold moisture concentration is in the range of 0.3-0.7% [9].

The dimensional strain in a unidirectional 0° composite laminate due to moisture absorption can be calculated as

Longitudinal : $\varepsilon_{mL} = 0$

Transverse : $\varepsilon_{mT} = \beta_T (M-M_v)$

Where

$\beta_T = (1+\nu_m) \beta_m (\rho_m/\rho_c)$

ρ_c = composite density

ν_m = matrix Poisson's ratio

$M_v = V_v (\rho_w/\rho_c)$

V_v = void volume fraction

Another physical effect of moisture absorption is the reduction in glass transition temperature of the resin (Fig. 2.6). Although the room temperature performance of a resin may not change with a reduction in T_g, its elevated temperature properties are severely affected. For example, the modulus of an epoxy resin at $150^\circ C$ ($300^\circ F$) decreases from 2070MPa (300,000psi) to 20.7MPa (3000psi) as its T_g is reduced from $215^\circ C$ ($420^\circ F$) to $127^\circ C$ ($260^\circ F$). Similar effects may be expected for the matrix-dominated properties of a polymeric matrix composite.

Finally, the dilatation expansion of the matrix around the fiber reduces the residual compressive stresses at the fiber-matrix interface caused by curing shrinkage. As a result, the mechanical interlocking between the fiber and the matrix may be relieved [4].
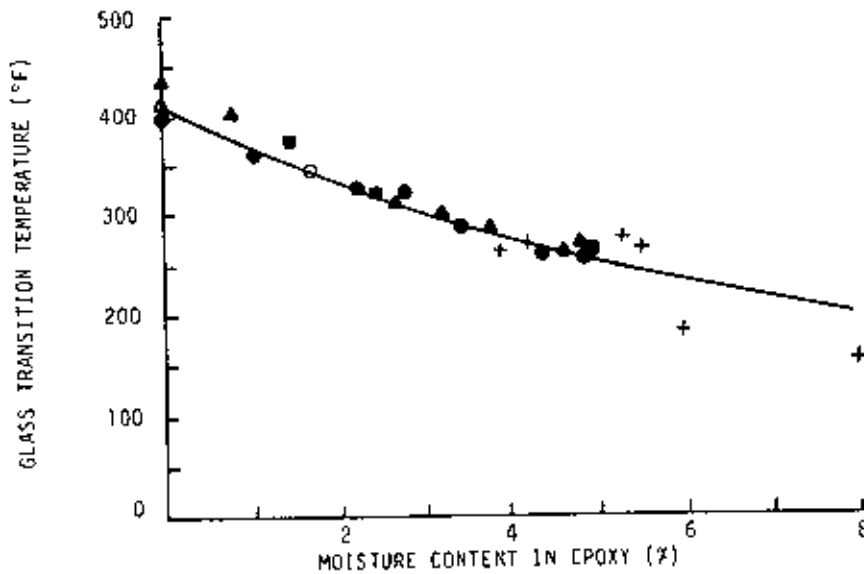
Fig.2.6 Variation of glass transition temperature of various epoxy matrices and their composites with moisture content

2.5.3 Environmental Effect

The influence of environmental factors, such as elevated temperatures, high humidity, corrosive fluids, and ultraviolet (UV) rays, upon the performance of polymeric matrix composites is of concern in many applications. These environmental conditions may cause degradation in the mechanical and physical properties of a fiber-reinforced polymer because of one or more of the following reason:

1. Physical and/or chemical degradation of the polymeric matrix, for example, reduction in modulus due to increasing temperature and scission or alteration of polymer molecules due to chemical attack or ultraviolet rays. However, it is important to note that different groups of polymers or even different molecular

configurations within the same group of polymers would respond differently to the same environment.

2. Loss of adhesion or debonding at the fiber-matrix interface, which may be followed by diffusion of water or other fluids into this area. In turn, this may cause a reduction in fiber strength due to stress corrosion. Many experimental studies have shown that compatible coupling agents are capable of either slowing down or preventing the debonding process even under sever environmental conditions, such as exposure to boiling water.

3. Reduction in fiber strength and modulus. For a short-term or intermitten temperature rise up to 150-294⁰C, reduction in the properties of most commercial fibers is insignificant. However, depending on the fiber type, other environmental conditions may cause deterioration in fiber properties. For example, moisture is known to accelerate the static fatigue in glass fiber. Kevlar 49 fibers are capable of absorbing moisture from the environment, which reduces its tensile strength and modulus. The tensile strength of Kevlar 49 fibers is also reduced with direct exposure to ultraviolet rays.

2.5.4 Coefficient of Thermal Expansion

The coefficient of thermal expansion (CTE) represents the change in unit length of a material due to unit temperature rise or drop. Its value is used for calculating dimensional changes as well as thermal stresses caused by temperature variation.

The CTEs of unreinforced polymers are higher than those of metals. The addition of fibers to a polymeric matrix generally lowers its CTE. Depending on the fiber type, orientation, and fiber volume friction, the CTE of fiber-reinforced polymers cau vary over a wide range of values. In unidirectional 0° laminates, the longitudinal CTE,α, reflects the fiber characteristic. Thus, both carbon and Kevler 49 fibers produce a negative CTE, and glass and boron fibers produce a positive CTE in the longitudinal direction. As in the case of elastic properties, the CTEs for unidirectional 0° lamiuates, are different in longitudinal and transverse directions. Compared with carbon fiber-reinforced epoxies, Kevlar 49 fiber-reinforced epoxies exhibit a greater anisotropy in their CTE due to grater anisotropy in the CTE of Kevlar 49 fibers [10].

In quasi-isotropic laminates as well as randomly oriented discontinuous fiber laminates, the CTEs are equal in all directions in the plane of the laminate. Furthermore, with proper fiber type and lamination configuration, CTE in the plane of the laminate can be made close to zero. An example is shown in Fig.2.7, in which the proportions of fibers in 0, 90 and $\pm 45°$ layers were controlled to obtain a variety of CTEs in the [0/±45]s, and [90/±45]s laminates [11].

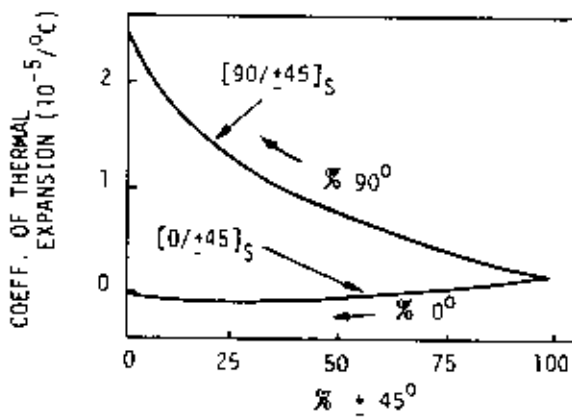

Fig. 2.7 Coefficient of thermal expansion of [0/±45]s and [90/±45]s laminates.

2.6 WEAR AND FRICTION OF POLYMERS

2.6.1 Wear of Polymers

Wear rate could be defined as the mass or volume of material removed per unit time or since sliding speed is frequently held constant, the wear rate is commonly expressed as mass or volume per unit sliding distance [12].

The wear of polymers is determined by the nature of materials, the surface and bulk mechanical. physical and chemical properties of the frictionally interacting bodies, the operating parameters. the macro and micro geometry and the working environment [13]. Investigation by Rymuza [14] shows that the wear dynamics of

polymer-polymer and polymer-metal systems are determined by properties of the polymer such as surface energy, modulus of elasticity, specific heat, thermal conductivity and various operating conditions. The wear characterization of polymer running against polymer are rather different from those of polymer against metal. Partly this is due to the different thermal characteristics of metal and polymer but the actual mechanism of wear also seems to be different. Ratner, et al [15]. Lew's [16], Rhee [17], Lancaster [18], Atkinson et al. [19], Eiss et al. [20], Dowson et al [21]. and others have developed various forms of equation and relationships for the wear of polymers. All these models have expressed wear volume as a function of either the operating variables such as load/pressure, speed, sliding length/duration or include properties such as hardness of the counterface, asperity height, shear strength of polymer, etc.

A. Writh reported that friction material wear rates and friction coefficients are not interrelated i.e., high friction coefficient did not necessarily produce a high friction material wear rate and vice versa. Experimental investigations on polymeric composites have shown that the wear and friction behavior of such material exhibits anisotropic characteristics. Moreover, studies on the effect of sliding velocity on wear rate and coefficient of friction revealed some discrepancies. Such discrepancies may be explained by reviewing the material and testing condition in each case. The effect of fiber volume friction on both wear and friction has been investigated.

2.6.2 Friction Coefficient of Polymer

In comparison to the metal, the coefficient of frictions of polymers are relatively low, but this is not generally correct. Because most polymers exhibit visco-elastic behavior, the magnitude of the coefficient of friction involves an appreciable component arising from deformation and elastic hysteresis loss, and this component varies markedly with the conditions of sliding, and particularly with speed. At high speed or light loads, PTFE sliding on metals or against itself may exhibit friction coefficient as high as 0.3. Similar, though less marked, effects occur with their polymers. The addition of fillers to polymers also affects the coefficient of friction. If the filler is a solid lubricant, particles may transfer to the counter-face, establish a

lubricating film and reduce friction. Alternatively with hard, rigid fillers such as glass, mica or asbestos, the load may be preferentially supported by the filler particles and the coefficient of friction is then largely characteristic of the filler/counterface interactions [22].

The cheaper phenol formaldehyde and polyester resins are somewhat brittle and are almost always used in fiber-reinforced form. The simplest method of producing reinforced thermosetting materials is by impregnation of fibrous mat or cloth-cellulose, cotton, asbestos, glass, carbon etc-by the liquid resin, or a solution thereof, pressing into an appropriate shape and curing at elevated temperature.

Because reinforced thermosets do not soften appreciably on heating, they continue to be useable up to the temperatures at which thermal or oxidative degradation of the resin or reinforcement begin to be significant. The rates of wear then tend to increase, but not so rapidly as for thermoplastics near their softening points. Reinforced thermosets will continue to operate for short periods at temperature well in excess because thermal or oxidative degradation is both time and temperature dependent.

2.7 BRAKE SHOE LINING MATERIALS

2.7.1 Introduction

Automobile brake materials usually consist of several ingredients which are classified as fibrous reinforcement, binder, filler and friction modifier [23-24]. A high performance friction material must possess stable friction and low wear under varying operating speed, applied loads, temperatures and environments [24, 25-27]. Although the normal operating temperature of the rotor is 150-250°C for passenger cars [23], high temperatures of 370°C and above can be encountered in front disk pads [28]. When an organic friction material is subjected to such high temperatures, the normal low-temperature coefficient of friction decreases temporarily and this phenomenon is called fade [23, 27-29]. After a friction material is engaged at high temperature, prefade coefficient of friction must be regained at lower temperatures

and this characterization is termed as recovery [23, 29] which is essential for reliable repeatable braking performance. A phenolic resin is generally chosen as the binder in polymeric brake materials due to its excellent thermal stability. Another unique characteristic of many fiber reinforced composites is their internal damping. This leads to better vibrational energy absorption within the material and results in reduced transmission of noise and vibration to neighboring structures. High damping capacity of composite materials can be beneficial in many automotive applications in which noise, vibration and harshness (NVH) is a critical issue for passenger comfort. Fillers, such as baryte, clay, barium sulphate, calcium carbonate, mica and glass microspheres (solid as well as hollow) are added to a polymeric matrix for one or more of the following reasons:

1. Reduce cost (since most fillers are much less expensive than the matrix resin, its primary role is to increase the volume of the friction lining and improve its dimensional stability [4] and thus to cut the overall cost of a composite on a volume basis).
2. Increase modulus
3. Reduce mold shrinkage
4. Control viscosity
5. Produce smoother surface

The binder is generally a thermosetting phenolic resin, which holds together all the components of the material. Since the binder is an organic polymer, special consideration should be given to its thermal stability and oxidation resistance at elevated temperature. In thermosetting polymers, the liquid resins are converted in to hard brittle solids by chemical cross linking which leads to the formation of a tightly bound three dimensional network of polymer chains. The mechanical properties depend on the molecular units making up the network and on the length and density of the cross-links. The former is determined by the initial chemical used and the latter by the control of the cross linking process which are involved in the cure. Finally, the friction modifier has diverse roles including the altering of the friction behavior. For example, brass chips and copper powder are used in heavy-duty organic linings to break up surface film and improve the fade performance [30].

Dry brake lining materials may still include some asbestos-impregnated resin materials even though asbestos is generally begin eliminated as a brake materiel. Other materials include wood, cast iron, polymers, and molded materials (phenolic resins, rubber) which may contain brass and/or zinc chips to aid heat conduction, stabilize friction, and improve the strength of the lining. Cashew nutshell oil, graphite, and newer proprietary compounds are added to control friction.

Heavy-duty disk brake pads of sintered iron and graphite display a static coefficient of friction on the order of 0.4 and a dynamic coefficient of the order of 0.3. They have been used on heavy equipment of weight through 200 tons.

Wet brake materials include a paper-based materials, cork, molded graphitics, fluoroelastomers, and sintered metal. The paper-based materials are the cheapest, have moderate strength, and good static and dynamic friction characteristics. Sintered materials are more expensive than the other materials and have better thermal conductivity and better thermal shock resistance but generally lower coefficients of friction. The other materials listed have properties whose values usually lie between those of the paper-based and sintered metal linings.

Since there is as yet no general agreement on the surface phenomena that cause friction, there is no generally accepted theory in the open literature to guide the lining manufacturer in the selection of materials for improved lining performance. Phenomena suggested to date are that friction is due to asperities (surface hills and valleys) which collide and are bent or broken as two surfaces slide on one another, that is due to braking of temporary bonds that form under pressure, that is due to electrical attraction between atoms of different surfaces, and so on. The shear strength of the brake lining does not explicitly appear in the formulas relating activating force to braking torque because it is assumed that

$$\tau \leqq \mu \, p_{max}$$

Where τ is the maximum shear stress that the lining can support without failure. Shear strength measurements by Anderson and Knapp indicate that in the direction

of the reinforcing fibers the shear strengths vary from about 9 to 16 MPa (1300 to 2300 Psi) [31].

2.7.2 Phenolic Based Friction Material

Brake linings are bonded largely with phenolic resins. Automotive applications are the largest outlet for friction elements, though many other vehicles and machines depend on such composites, including aircraft, trains, drilling rigs, etc. Two important recent developments have occurred in automotive-brake elements: conversion from drum brakes to disk brakes and the development of nonasbestos composites. Both developments require that the binder resins exhibit higher temperature performance without deleteriously affecting the coefficient of friction coefficient stability over a broad temperature range, wear of the composite, and improve adhesion to the semi metallic additive which replace asbestos.

Manufacturing processes include impregnation, extrusion, dough molding, or dry compounding, depending on the type of friction element being produced. The phenolic resiu, either a novolak/hexa blend or a liquid or solid resole, generally is employed at 10-20wt % of the composite mix. Other ingredients including fillers at 20-30wt % friction granules, i.e., a cross-linked particle based on alkenyl phenol extracted from cashew-nnt shells; asbestos or semi metallic fibers at 40-60wt %; etc. The combination of the different additives, phenolic resin type, conceutration and cross-link density, and the process employed determines the friction properties, wear characteristics, noise development level, and thermal resistance of the finished composite.

2.8 CHARACTERISTICS AND PROPERTIES OF BRAKE SHOE LINING MATERIALS

2.8.1 Materials and Processing of Brake Shoe Lining Materials

A cashew-modified Phenol-formaldehyde, NC-126 (Cardolite Corporation, Newark) resin uses as as the matrix for brake shoe lining. The resin is a dry powder and

contains hexamethylenetettraamine (HEXA), a curing agent. The friction modifier consisted of pre cured modified phenolic resin. The fiber uses as milled fiber which has a sufficient modulus and strength. The friction material formulation consists of 30/25/15/20/10 by weight percent which correspond to 34.5/34.0/21.6/7.6/2.3 by volume percent of fibers/phenolic resin/phenolic particles/barium sulphate/ friction modifier (brass particles) respectively. The addition of brass particles aid the mixing of the component and to improve the thermal conductivity of the composite. The proper proportions of the various components are blended in a laboratory mixer in the following sequence so as to obtain satisfactory mixing. First, the filler and brass particles are churned together in the mixer since it appear that the brass particles help to brake down the barium sulphate clumps. Fibers are added next, followed by the friction particles and resin. Mixing occurs for a few seconds at the addition of each component and finally for about two minutes after the addition of resin. The mixer is hot pressed at 170 ^{0}C and 7 MPa for about 10 minutes. The molded plates are post cured in an oven at 170 ^{0}C for about 3h.

2.8.2 Wear of Brake Shoe Lining Material

Although brake wear depends primarily on the temperature during braking, protecting the lining from foreign materials that may increase the wear rate, and from moisture and other agents that may cause the brake lining and/or its additives to deteriorate, may alter the wear rate, so some manufactures provide wear rate data for particular reference conditions. The commonly accepted formula for the wear rate, defined as the decrease δ in thickness per unit time, assumes that the rate of wear is proportional to the product of the pressure and the velocity, written as

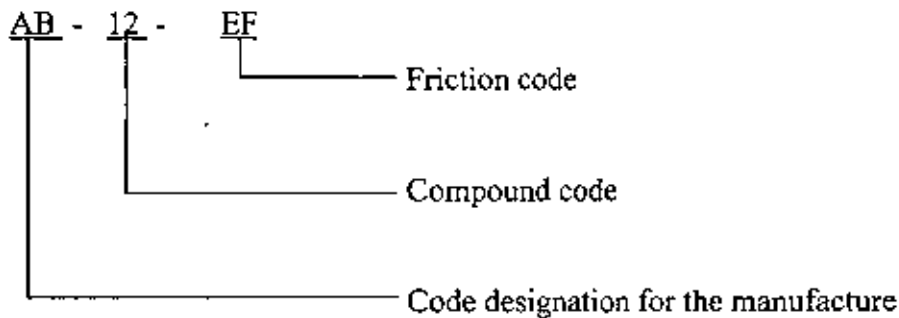$$\frac{\delta}{t} = \frac{K}{\sigma_h} pv \quad \text{------------------(2.8.1)}$$

in which K is a dimensionless wear constant that depends on the lining materials and the conditions of the test (temperature, moisture, lining cleanliness, etc.), σ_h is the surface hardness in units of stress, p is the pressure applied to the brake lining, and v is the relative velocity between the lining and the friction surface–the slip velocity.

As in any test on brake lining, the designer must remember that these tests are to provide a comparison between lining materials for specified reference conditions. They are not for design purposes because the pressure in an actual brake usually varies over the area of the lining, and the braking temperatures and the cooling between brake applications can cause appreciable differences, as can the presence of harmful foreign material.

The rate of application of a brake may also affect the life of the lining. For example, very slow application may cause excessive heat accumulation, so that a greater lining pressure, which may produce some lining crushing, is required to supply a torque that could be realized with a lower lining pressure on a cool brake. Very slow application increases the lining wear for each application, so that the lining wear per application increases. Very rapid application associated with large pressure may cause excessive shear stress either in the lining itself or at the adhesive or mechanical bond between the lining and backing plate. If wear is sufficiently important, equation (2.8.1) may be used together with the load, the variation of the friction coefficient with slip velocity, and the equation of motion of the system to calculate the wear for a family of actuation rates that either stop the driven machine or bring it up to speed in the required time. With the aid of computer control we may then follow that pressure-time profile which provides a low wear rate during starting and stopping [31].

2.8.3 Friction Coefficient for Brake Linings

The usual range of the dynamic friction coefficient for those friction materials normally used in dry brake linings is given in the Society of Automotive Engineers (SAE) coding standard SAE J866a, which lists the code letters and friction ranges shown in Table 2.2. According to this code, the first letter in the lining edge code indicates the normal friction coefficient and the second letter indicates the hot friction coefficient. Thus a lining material whose normal friction coefficient is 0.29 and whose hot friction coefficient is 0.40 would be as follows :

```
AB  -  12  -    EF
                 └──────── Friction code

            └──────────── Compound code

     └────────────────── Code designation for the manufacture
```

Temperatures for normal and hot friction coefficient are defined in SAE J661a, which also describes the measurement method to be used.

Static and dynamic coefficient of frictions are usually different for most brake materials. If a brake is used to prevent shaft rotation during a particular operating phase, with its stopping torque and heat dissipation of secondary importance (i.e., a holding break on a press), the static friction coefficient is the design parameter used. If, on the other hand, the brake is to be designed its stopping torque and heat dissipation, the design parameters used are the dynamic friction coefficient and its change with temperature.

Table.2.2 Friction identification system for brake linings and brake block for motor vehicles

Code Letter	Friction coefficient
C	Not over 0.15
D	Over 0.15 but not over 0.25
E	Over 0.25 but not over 0.35
F	Over 0.35 but not over 0.45
G	Over 0.45 but not over 0.55
H	Over 0.55
Z	Unclassified

Typical coefficient of friction between lining materials and smooth cast iron or smooth steel and their temperature dependence are displayed in Figures 2.8-2.12. The solid lines in these figures represent coefficients of friction, shown on the left-hand ordinate, and the dashed lines represent the wear, shown on the right hand ordinate. Figure 2.8 is for a rigid-molded high–friction material which shows less

100 and 600°F (or 37.77 and 315.55°C), but wear increases with increasing temperature. The brake lining shown in Figure 2.9, designed for industrial brakes and off-the-road equipment, is made from different proprietary materials which provide good face resistance but at a lower friction coefficient, to obtain better wear characteristics under 400°F (204.44°C). This trend for improved wear at the expense of a reduced coefficient of friction is demonstrated again in Figure 2.10 for a rigid-molded asbestos material for industrial brake application. Note that for all three materials face resistance is obtained at the expense of greater wear at higher temperatures. This trade-off between wear and fade resistance (a large friction coefficient at high temperature) is also demonstrated in Figure 2.11, where greatly improved wear resistance may be had from this woven material design for plate brakes, but at the expense of poor fade resistance above about 400°F (204.44°C). As shown in Figure 2.12, friction material may be desirable for slip clutches, a form of brake, used for tension control. In such applications the low friction coefficient offers some protection against the brake actually stopping the motion if the actuating force is increased inadvertently.

The friction data displayed above were obtained according to SAE J661a, which calls for a 100-lb force to press a 1in.×1in. sample against the interior surface of a cast iron drum having an 11-in. inside diameter while the drum rotates at 417 rpm. With the drum temperature held constant the normal force is applied for 20 cycles, each cycle consisting of a 10-sec application of the force and a 20-sec rest when the lining is not in contact with the drum. The average friction coefficient from these 20 readings is the value plotted in Figures 2.8 through 2.12. The temperature was varied in100°F (37.77°C) steps, and wear was measured by the weight loss (to within 0.0001g) after each cycle. From the nature of these tests it is evident that the wear data are primarily for use in comparing friction, or lining, materials, as no indication is given of the effect on the friction coefficient of varying either the relative velocity or the lining pressure. Usually, either a single number or a range of values is given for the static friction of these materials, implying that it is constant over the usual range of lining pressure. Although it is generally accepted that the static friction coefficient is greater than the dynamic coefficient for most materials, it is evident

from these curves that this assumption is an oversimplification of the behavior of lining materials in the range 100 to 600°F (or 37.77 and 315.55°C) [31].
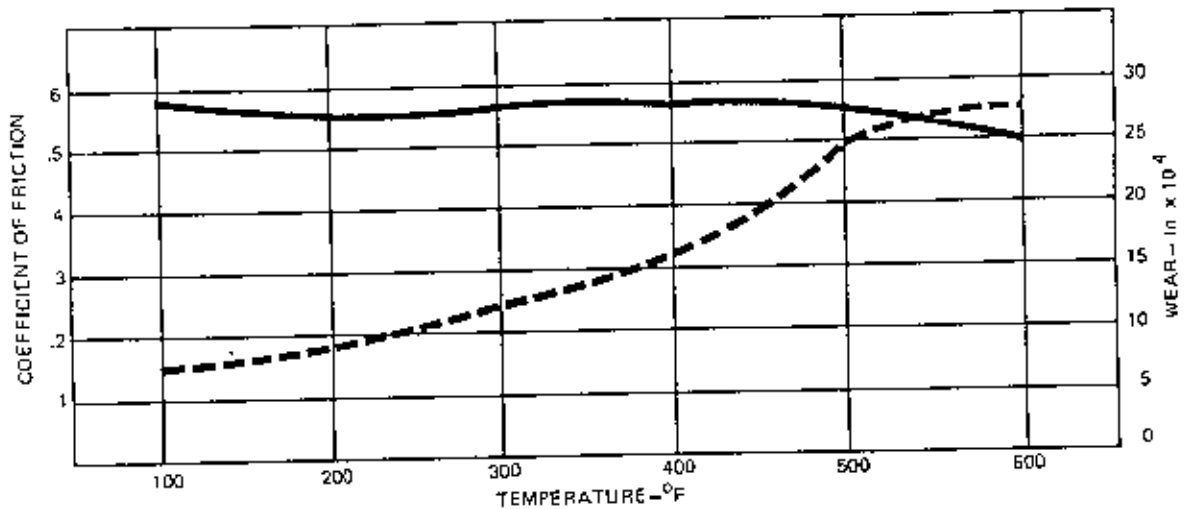
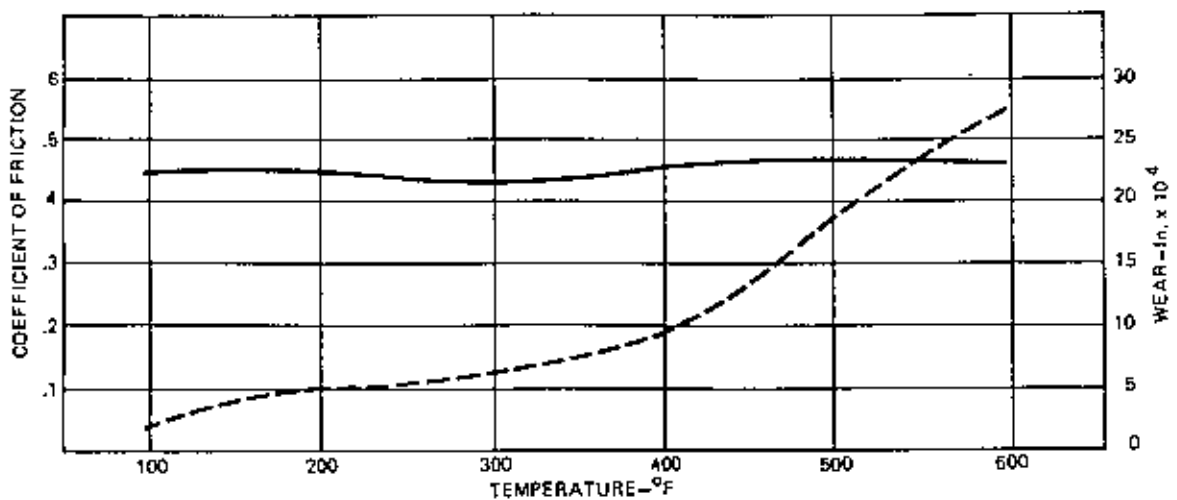Fig. 2.8 Rigid-molded high-friction material (static friction coefficient is 0.30 to 0.35)

Fig. 2.9 High friction material for industrial brakes and off-road equipment (static friction coefficient is 0.31 to 0.36).
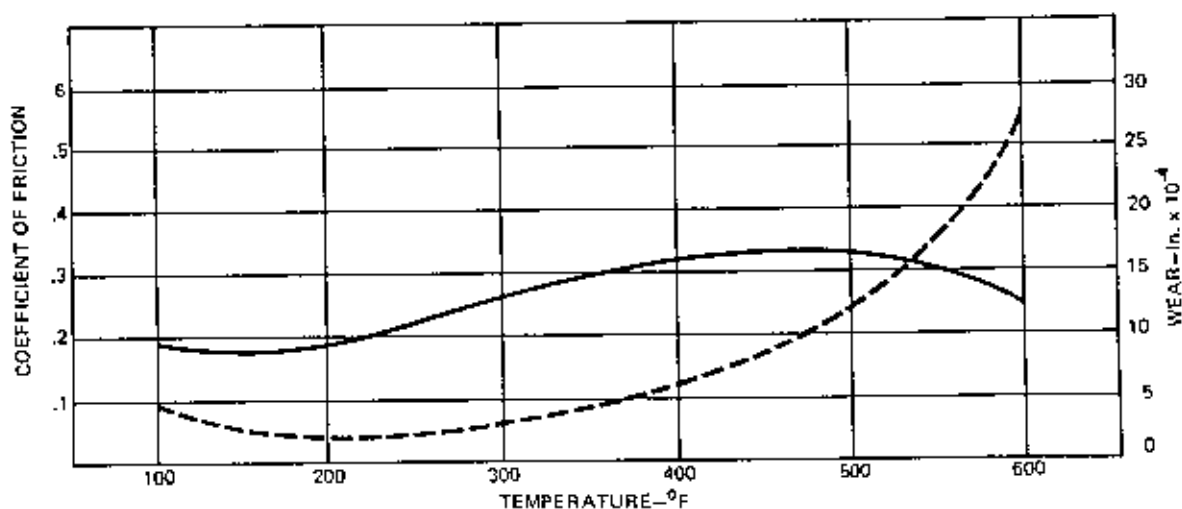
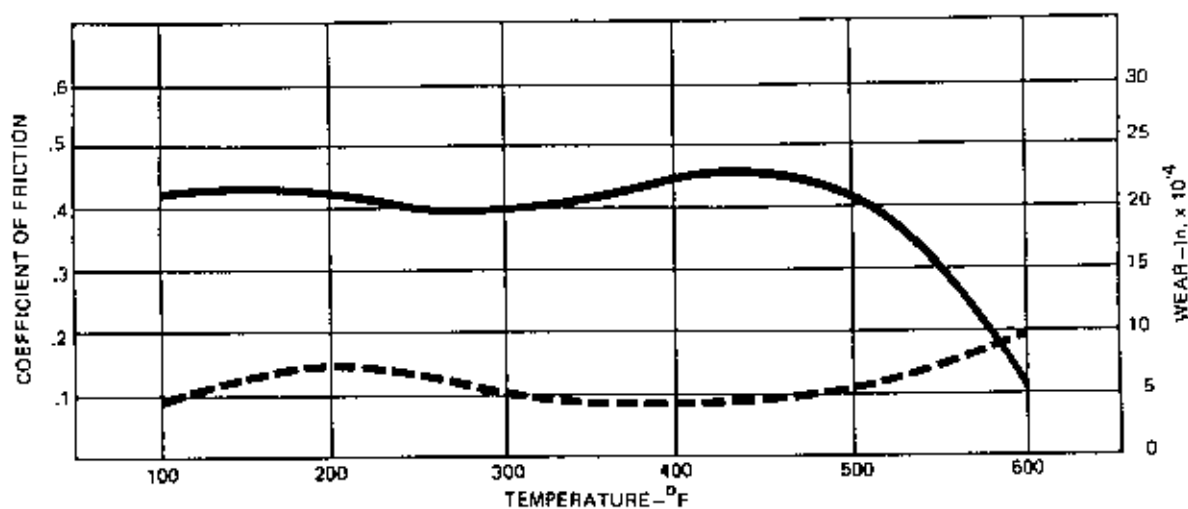Fig. 2.10 Rigid-molded asbestos materials for industrial brakes (static friction coefficient is 0.27 to 0 31).

Fig. 2.11 Woven material of asbestos yarn with brass wire inserts for face, or multiple-disk brake and clutches (static friction coefficient is 0.30 to 0.34).
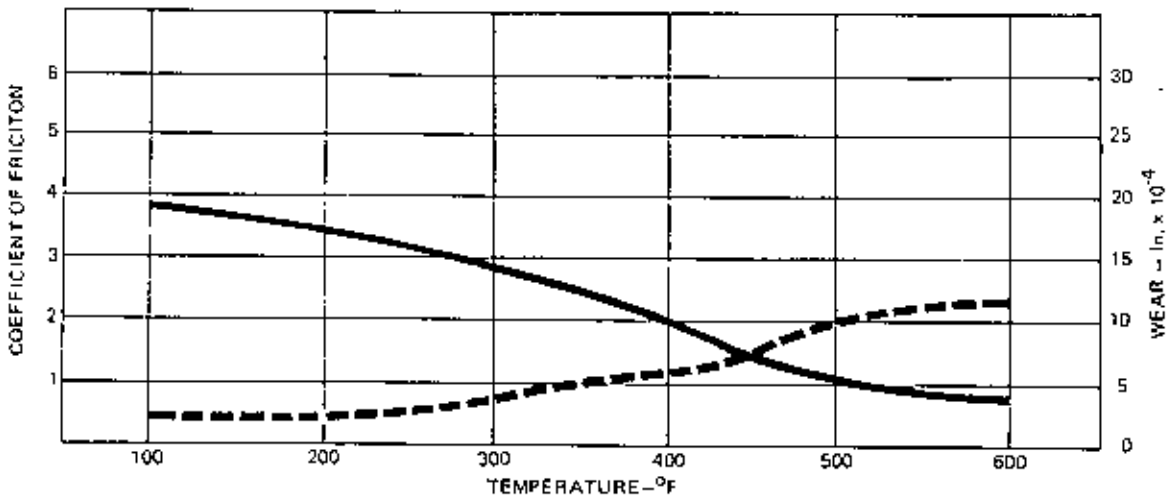
Fig. 2.12 Low-friction, rigid-molded material from phenolic resin, friction modifiers, and asbestos fibers (static friction coefficient is 0.28 to 0.31).

2.8.4 Brake Fade

Brake fade is a term that refers to the reduced effectiveness of many dry brakes as they become heated. A standard test described in SAE J661a outlines a procedure that uses controlled-temperature drums and controlled brake lining pressure to simulate actual brake fading as a basis of comparison of the brake-fading characteristics of various materials. The equipment and temperatures are essentially identical to those used in estimating the coefficient of friction as a function of temperature. Only the presentation of the data is different, as shown in Figure 2.13. The fade test mode of presentation of data provides another indication of the recovery capability of various lining materials. As with the previous test data, the fade test mode is limited to a comparison of different lining materials for these conditions only.

Limitation of the application of these data to preliminary design is emphasized because the friction coefficient is depended upon the pressure, the temperature, and

the relative velocities of the contacting surfaces, as noted earlier. Field testing is recommended before the production of any brakes design because of the uncertainty usually associated the variables involved in lining heating and in the cooling capability of the brake housing and any associated structure [31].
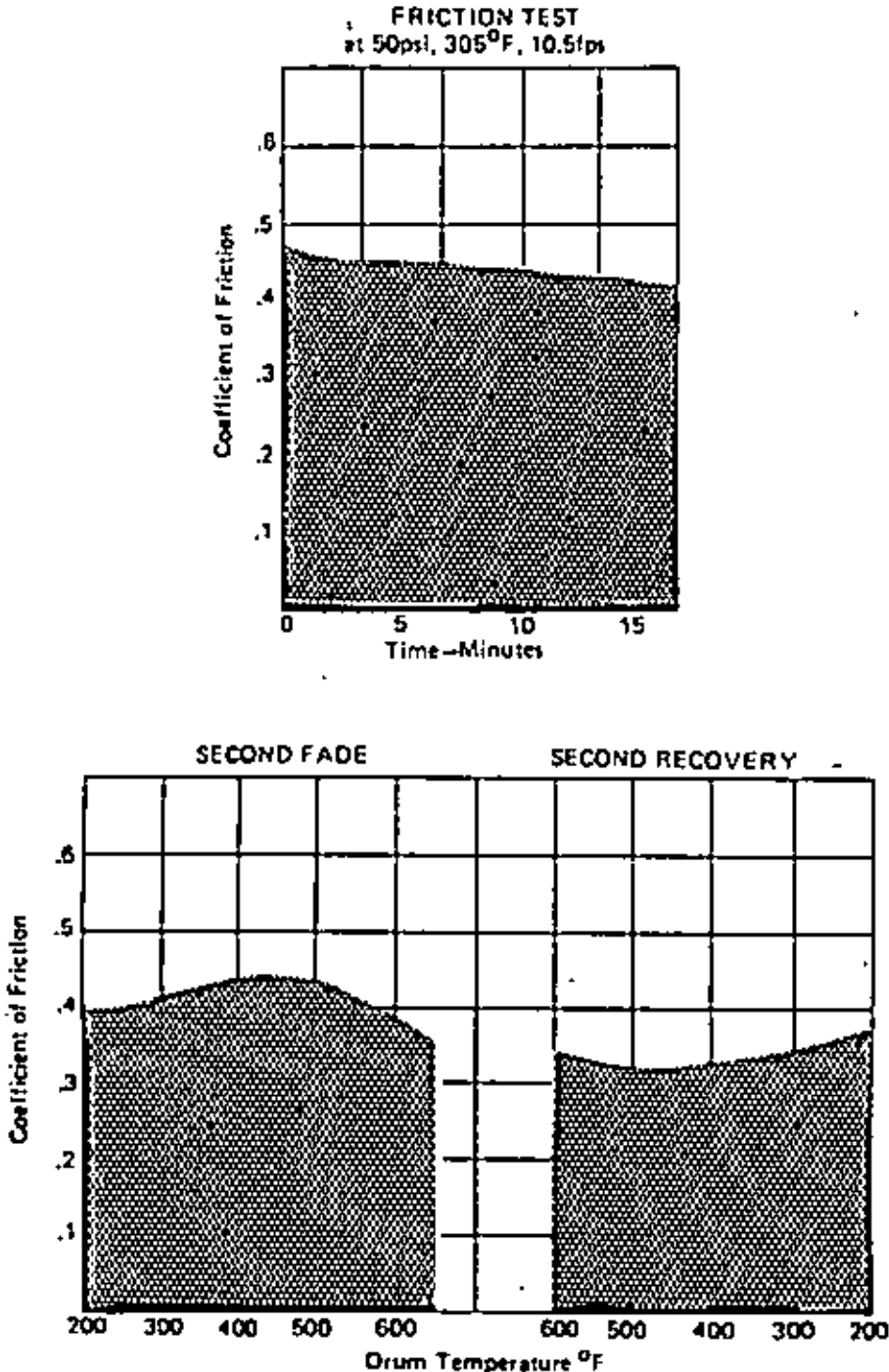
FRICTION TEST
at 50psi, 305°F, 10.5fps

SECOND FADE   **SECOND RECOVERY**

Fig. 2.13 Display of brake lining fade test result

2.8.5 Brake Lining Compressive Strength

All of the expressions for the toque capability of friction brakes represent the maximum pressure on the lining. In a particular configuration the maximum pressure can be induced by the mechanical, electrical, pneumatic, or hydraulic system used to activate the brake should obviously be less than the compressive stress of the lining material by a safety factor suitable to the intendment use. Because this value may be highly dependent on both the temperature and the relative velocity of the contacting surfaces (in which circumstance the stress field is quite different from that in idealized simple compression), brake lining manufactures usually do not list a maximum compressive stress for their products.

For purposes of preliminary design the maximum compressive stress may be taken as being on the order of 3.00 MPa (435 psi) for most commercial dry brake lining material and of the order of 2.75 MPa (400 psi) for paper-based wet brake lining material. Tensile strengths obtained experimentally by Anderson and Knapp [32] imply that these values for dry brake materials err well on the side of caution.

Copper–and ceramic–based sintered brake materials may have a compressive strength on the order of 300 MPa (43,500psi). Laboratory compressive tests have resulted in failure that was associated with shear and granular fragmentation along planes at about 45^0 to the surface that supported a static compressive load.

2.9 INFRA-RED SPECTROSCOPY

2.9.1 Principles of Infrared Spectroscopy

2.9.1.1 Introduction

Infrared spectrum is an important record, which gives sufficient information about the structure of a compound. Unlike ultraviolet spectrum, which comprises of relatively few peaks, this technique provides a spectrum containing a large number of absorption bands from which a wealth of information can be derived about the

structure of an organic compound. The absorption of infrared radiation (quantised) causes the various bands in a molecule to stretch and bend with respect to another. The most important region for an organic chemist is 2.5 μm to 15 μm in which molecular vibrations can be detected and measured in an infrared spectrum or in a Raman spectrum. The ordinary infrared region extends from 2.5 μm to 15 μm. The regions from 0.8 μm to 2.5 μm is called **Near infrared** and that from 15 μm to 200 μm is called **Far Infrared region**.

The absorption of infrared radiation can be expressed either in terms of wavelength (λ) or in wave number (ν). Mostly infrared spectra of organic compounds are plotted as percentage transmittance against wave number. The relationship between wavelength and wave number is as follows:

$$\text{Wave number } (\nu) = \frac{1}{\text{Wave-length in centimeters } (\lambda)}$$

The wavelength 15 μm corresponds to wave number equal to 667 cm^{-1}. Thus, in terms of wave number the ordinary infrared region covers 4000 cm^{-1} to 667 cm^{-1}.
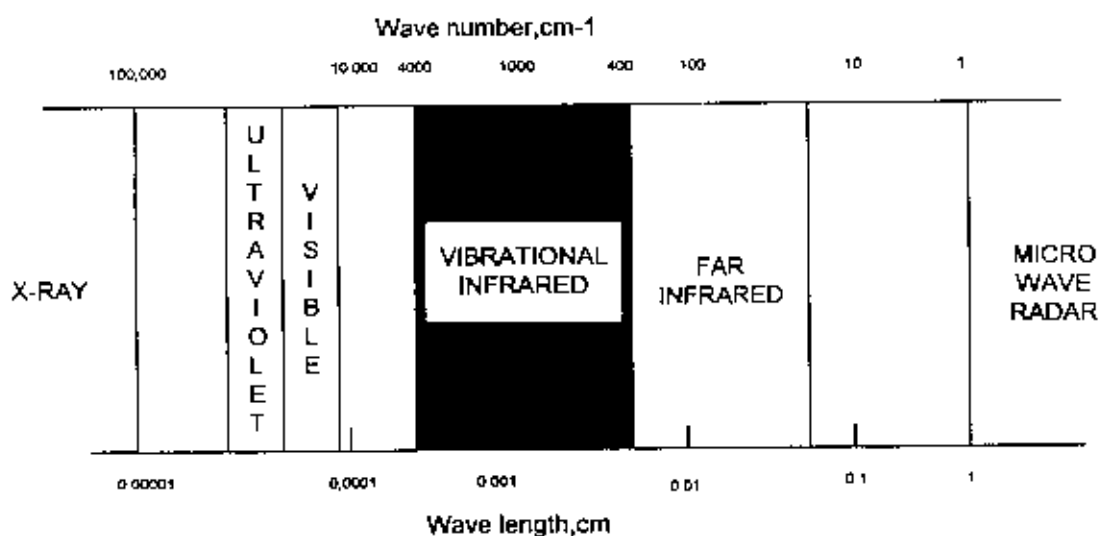
Fig.2.14 The position of the infrared region of the electromagnatic spectrum

Band intensity is either expressed in terms of absorbance (A) or Tansmittance (T).

$$A = \log_{10}(1/T)$$

This technique can be employed to establish the identity of two compounds or to determine the structure of a new compound. In revealing the structure of a new compound, it is quite useful to predict the presence of certain functional groups which absorb at definite frequencies [33].

2.9.1.2 Infrared Theory

Vibrational Spectra: Molecular vibrations can occur by two different mechanisms. Firstly, quanta of infrared radiation can excite atoms to vibrate directly–the absorption of infrared radiation gives rise to the infrared spectrum. Secondly, quanta of visible light can achieve the same result indirectly – the Raman Effect.

Most organic molecules are fairly large and their resultant vibrational spectra are complex. To introduce the basic concepts governing vibrational spectra, a simple diatomic covalent bond will be considered as a spring with the atomic masses at either end (Fig2.15).
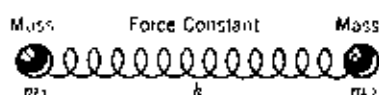
Fig. 2.15 Ball and spring representation of two atoms of a molecule vibrating in the direction of the bond.

$$v = \frac{1}{2\pi} \sqrt{\frac{k(m_1 + m_2)}{m_1 \times m_2}}$$

The stiffness of the spring is described by a *force constant*, K. If such a simple system is put in to motion (by stretching and releasing), the induced vibrations of the masses are adequately described by Hook's law of simple harmonic motion. Frequency of motion,

$$v = \frac{1}{2\pi}\sqrt{\frac{k}{\mu}}$$

Where μ is the reduced mass, that is the harmonic mean of the individual masses

$$\frac{1}{\mu} = \frac{1}{m_1} + \frac{1}{m_2}$$

$$\mu = m_1 m_2 / (m_1 + m_2)$$

To a first approximation, this assumption of harmonic forces is in agreement with actual conditions in real molecules. However, quantum theory governinng molecular motion restricts the energy stored in the vibration, E_v, such that only certain energy transitions are allowed, as determined by a quantum number, v.

$$E_v = (v + 1/2)hv \ldots\ldots\ldots\ldots(2.9.1)$$

Where $v = 0, 1, 2, 3, 4,\ldots\ldots$etc. For instance, if a molecule were to undergo a transition from the lowest level ($v=0$) to the first level ($v=1$) by absorption of infra-red radiation, the frequency of that exciting radiation would be given by the Bohr principle, $hv = E_1 - E_0$

Now equation (2.9.1) gives

$$E_0 = 1/2 hv \text{ and } E_1 = 3/2 hv$$

Therefore, by substitution:

$$(E_1 - E_2)/h = v$$

In summary, the absorption of infrared radiation causes the excitation of the molecule of higher vibrational levels and is quantized. The normal vibration has the same frequency as the electromagnetic radiation. The absorption process can occur only if there is a change in the magnitude and direction of the dipole moment of the bond [34].

2.9.1.3 Scanning of Infrared Spectrum

The most important source of infrared light for scanning the spectrum of an organic compound is **Nerst glower** which consists of a rod of the sintered mixture of the oxides of Zirconium, Ytterium and Erbium. The rod is electrically heated to $1500\ ^0C$ to produce infrared radiations.

A rod of silicon carbide (Global) can also be electrically heated to produce infrared radiations. To obtain monochromatic light, optical prism or gratings can be used. For prism material, glass or quartz can not be used since they absorb strongly through most of the infrared region. Sodium chloride or certain alkali metal halides are commonly used as cell containers or for prism materials as these are transparent to most of the infrared region under consideration. Sodium cloride is hygroscopic and is, therefore, protected from the condensation of moisture by working at suitable temperature. Gratings give better resolution than do prisms at high temperatures.

Light from the source is split into two beams. One of the beams is passed through the sample under examination and is called the sample beam. The other beam is called the reference beam. When the beam passes through the sample, it becomes less intense due to the absorption of certain frequencies. Now, there will be a difference in the intensities of the two beams. Let I_0 be the intensity of the reference beam and I be the intensity of the beam after interaction with the sample respectively.

The absorbance of the sample at a particular frequency can be calculated as:

$$A= \log(I_0/I)$$

Also transmittance, $T= I/I_0$

$$A= \log(1/T).$$
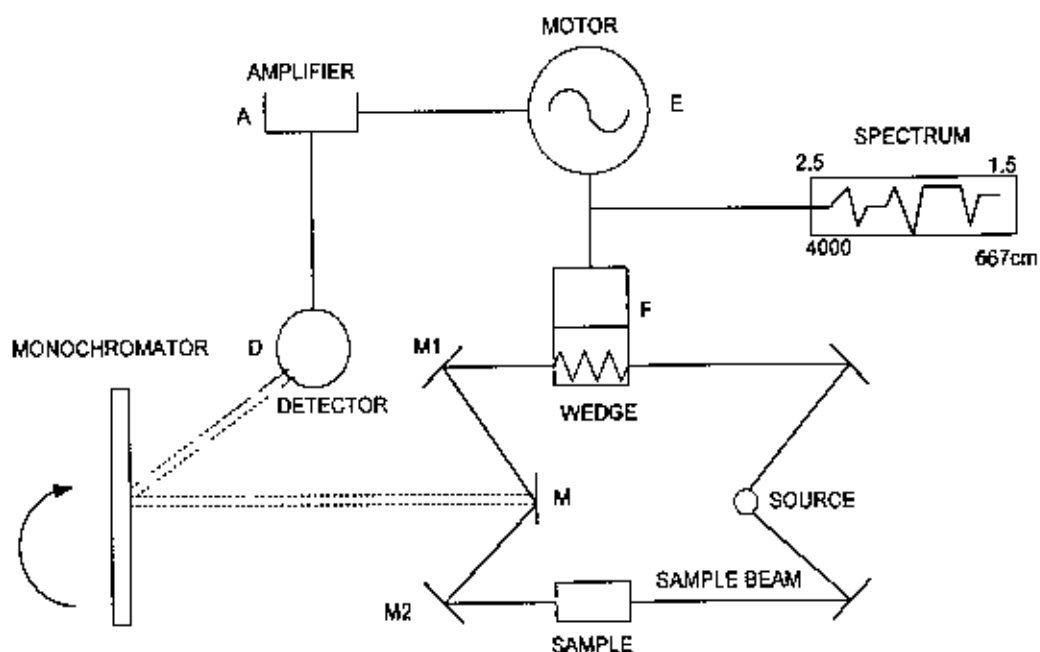
Fig. 2 9.3   Infrared Spectrometer

Intensities of the bands can be recorded as a linear function of T against the corresponding wave number. Intensities of the two beams are converted in to and measured as electrical energies with the help of detector thermopile which proceed as follows:

The two beams (sample and reference) are made to fall on a segmented mirror M (chopper) with the help of two mirrors M_1 and M_2. The chopper (M) which rotates at a definite speed reflects the sample and the reference beams to a monochromator grating (B). As the grating rotates slowly, it sends individual frequencies to M detector thermopile (D) which coverts infrared energy into electrical energy. It is then amplified with the help of amplifier (A). Due to the difference in intensities of the two beams, alternating currents start flowing from the detector thermopile to the amplifier. The amplifier is coupled to a small motor (E) which drives an optical wedge (F). The movement of the wedge continues till the detector receives light of equal intensity from the sample and the reference beams. Calibration can be carried out using spectrum of Poly-styrene [33].

2 9.1.4 Sampling Technique

Various techniques [33] can be employed for placing the sample in the path of the infrared beam depending upon whether the sample is a gas, a liquid or a solid. The intermolecular forces of attraction are most operative in solids and least in case of gases. Thus, the sample of the same substance shows shifts in the frequencies of absorption as we pass from the gaseous state. In some cases, additional bands are also observed with the change in the state of sample. Hence, it is always important to mention the state of the sample on the spectrum which is scanned for its correct interpretation. Solids: solids for the infrared spectrum may be examined as an alkali halide mixture. Alkali metal halides, usually potassium bromide which is transparent throughout the infrared region is commonly used for the purpose. The substance under investigation should be absolutely dry as water absorbs strongly at about 3710 cm^{-1} and also near 1630 cm^{-1}. The sample (solid substance) is ground with KBr and is made into a disc after drying and then pressing it under elevated temperature at high pressures. Also a blank disc is prepared with pure potassium bromide which may be placed in the path of the reference beam. It is often advisable to carry out grinding under infrared lamp to avoid condensation of atmospheric moisture. Discs obtained from poorly ground mixture scatter more light than they disperse. The particle size of the ground mixture should be less than 2μm to avoid scattering. KBr is transparent to the infrared region (2.5 μm-15μm) and thus, a complete spectrum can be scanned by mixing 1-2% of the solid sample with it and then grinding it to the desired particle size [33].

2.9.1 5 Applications of Infrared Spectroscopy

Infrared spectrum of a compound provides more information than is normally available from the electronic spectra. In this technique, almost all groups absorb characteristically within a definite range. The shift in the position of absorption for a particular group may change (within the range) with the change in the structure of the molecule [33].

Impurities in a compound can be detected from the nature of the bands, which no longer remain sharp and well defined. If the spectrum contains a strong absorption band between 1900-1600 cm^{-1}, the presence of carbonyl group (>C=O) in a compound is suspected. The position of the peak or the band not only tells the presence of a particular group but also reveals a good deal about the environments affecting the group. Further study of the spectrum reveals whether it is aldehydic, ketonic, ester, amide etc. Aldehydes can be recognized from its characteristic C-H stretching; esters from C-O stretching and amides show absorptions for N-H stretching and N-H bending absorption in addition to v C=O in the side range.

Presence of conjugation with carbonyl group can be detected as it shifts vC=O stretching to the lower wave number. The absorption values for certain groups such as vC=O, O-H are also important in detecting hydrogen bonding. In case of hydrogen bonding, the wave number of absorption is shifted downwards for both the donor as well as the acceptor group. It can also make distinction between inter-molecular hydrogen bonding and intra molecular hydrogen bonding; the absorption position due to the latter being independent of the change in concentration.

Due to the different positions of absorption, it is also possible to know the axial and the equitorial positions of certain groups in a cyclic structure.

The force constants responsible for the absorption peaks can be used to calculate bond distances and bond angles in some simple cases. When the infrared spectrum of an unknown compound is scanned, a large number of questions come to occur mind viz:

1. Which group/groups can be present in the compound?
2. What environments are influencing it?
3. What type is the carbon skeleton in the compound?
4. Is the compound aromatic? If so, what type of substitution?

2.9.1.6 Interpretation of an infra-red spectrum

Following are some useful tips for interpreting an infrared spectrum [33].

(1) Always place more reliance upon the negative evidence. The absence of a band in a particular region is a sure indication of the absence of group/groups absorbing in that region. For example if there is no absorption in the resign 1900-1600 cm^{-1}, the carbonyl group (>C=O) must be absent in the compound.

(2) Always start from the higher frequency end of the spectrum. Mostly stretching vibration occur in the region above 1500cm^{-1} and are most informative. The region 1500-1000 cm^{-1} may be used for confirming esters, alcohols, ethers etc.

(3) To distinguish between inter-molecular and intra-molecular hydrogen bonding, the spectra of the sample are scanned at two different concentrations. Various solvents may be used to study association effects.

(4) For easy detection of the varions groups present in the compound, the infra-red region (4000 to 667 cm^{-1}) may visualised as consisting of the following portion:

   (a) **3600-3200 cm^{-1}**. The appearance of the bands in this region show the presence of –OH, -NH$_2$, >NH group in the compound. The position, intensity and the breadth of the bands tell whether the group is free, intra-molecularly bonded or exhibit intra-molecular hydrogen bonding ≡ C-H str. also shows a medium band near 3300 cm^{-1}.

   (b) **3200-3000 cm^{-1}**. Absorption due to = C-H str.and Ar-H stretching occur in this region. The sharp bands of weak to medium intensities are observed.

   (c) **3000-2500 cm^{-1}**. The absorption due to C-H stretching from methyl or methylene groups occur in this region. The asymmetric C-H stretching occurs at slightly higher wave number as compared to that of symmetric C-H str. A very broad band between 3000-2500 cm^{-1} is most characteristics of acids (-COOH group). Two weak bands, one at 2720 cm^{-1} and the other near 2820 cm^{-1} are most characteristic of C-H stretching in aldehydes. The higher frequency band is seldom observed.

(d) **2300-2100-cm⁻¹**. This is the region in which alkynes, cyanides, cyanates, isocynates obsorb. The bands observed are weak and variable-C≡C stretching occur between 2140-2100cm⁻¹. -C≡N stretching shows a varialbe band between 2260-2250 cm⁻¹.

1900-1650 cm⁻¹. Strong bands due to C=O stretching occur in the region. Anhydrides show two strong bands in the region 1850-1740 cm⁻¹. Esters, aldehydes, ketoncs, lactones, carboxylic acids, amids show strong bands due to C=O stretching in this region. Imides are also recognized by two strong bands (doublet) in the region around 1700 cm⁻¹. Following points regarding C=O stretching may be helpful.

(i) α, β- unsaturation lowers the frequency of absorption by 15-40 cm⁻¹. But in amids a small absorption shift towards lower frequency is observed.

(ii) Increase in the ring strain in case of cyclic ketones raise ν C=O absorption.

(iii) Hydrogen bonding to the carbonyl compound lowers νC=O absorption by 40-60 cm⁻¹.

(e) **1600-1000 cm⁻¹**. This region is very important for identifying nitro compounds and also confirming the presence of ethers, esters, primary, secondary and tertiary alcohol. The appearance of strong bands due to C=O stretching at 1300-1050 indicates (i) an ester provided C=O stretching is observed in the region 1750-1735 cm⁻¹ and (ii) an alochol if O-H stretching free and/or bonded occurs between 3600-3200 cm⁻¹. Ethers show a strong band in the region 1150-1070 cm⁻¹ due to C-O stretching in →C-O-C←. This region also helps to identify C-H str. in aromatic compounds. For aromatic rings, medium bands around 1600 cm⁻¹, 1580 cm⁻¹ and 1500 cm⁻¹ arc observed.

(f) **Below 1000 cm⁻¹**. This region is very useful in identifying the type of substitution on the aromatic ring:

(i) a strong band at 770-730 cm⁻¹ (s) shows monosubstitution.

(ii) ortho and para distributed compounds show one band each. The latter absorbs at a higher wave number.

(iii) meta-disubstitated compounds are usually recognized by two medium bands in the region 850-710 cm^{-1} [33].

2.9.2 Experimental Method

Infrared spectroscopy was used to identify the organic compounds present in the sample. Before the test, the sample was dried in an oven at 80°C to get rid of moisture and preserved in a desicator. Sample was then pulverized with KBr using an agate mortar. To avoid scattering, the particle size of the ground mixture was prepared to less than 2.0 μm. The KBr mixed powder sample was pressed into pellet under 8 ton. The pellet was subjected to the test by using a 460 Shimadzu Infrared Spectrometer with a scanning speed of 360 cm^{-1}/min in the range of 400-4000 cm^{-1}. The absorption pattern was recorded on the chart paper. The chart paper was then analyzed and the possible groups of organic compound responsible for the recorded absorption peaks in the chart paper were identified with the help of the mannal available in the IR laboratory. IR spectroscopy was carried out at the Chemistry Department, University of Dhaka.

Chapter Three

3. EXPERIMENTAL

Materials used

Four phenolic based brake shoe lining materials collected from the market available in Bangladesh. One of the brake shoe lining materials manufactured by a local company in Bangladesh designated as B while three others designated as F1, F2 and F3 were imported from three different countries of origin.

3.1 X-RAY DIFFRACTION

X-ray diffractometry (XRD) was used to find out the phases present in the brake shoe lining materials viz. B, F1, F2, and F3. For this purpose sample was pulverized using an agate mortar. Fine powdered grains of each sample were packed tightly into the cavity of glass slide with random orientation of the powder.

The sample was subjected to the test by using a JEOL DX-GE-2P X-ray powder diffractometer with MoK_α radiation. Details of the operating conditions of X-ray diffractometer are shown in Table 3.1

Table 3.1.Operating conditions for X-ray Diffraction

Radiation	: MoK_α
Filter	: Zr
Voltage	: 30kV
Current	: 20mA
Scanning speed	: 1°/min
Chart speed	: 10mm/min
Range	:5°-35°

3.2 DETERMINATION OF SIZE AND NUMBER OF BRASS PARTICLES

The test sample with the dimensions of 25.4 mm x 25.4 mm x 8 mm was taken to determine the number of brass particles and their sizes. The samples were successively polished by the emery paper of grit no. 1, 1/0, 2/0, 3/0, and 4/0. Final polishing was done with 1μm γ-alumina on velvet cloth. After polishing, the sample

was washed with water and dried in acetone. The sample was then placed under steriographic microscope and examined at 20x magnification. The two larger faces (25.4 mm x 25.4 mm) of each sample were examined. The total number of brass particles was counted and particles per unit area calculated. The size of the particles was measured using a micrometer eyepiece.

3.3 DETERMINATION OF FIBER CONTENT

The technique of fiber content determination is based on the digestion of the matrix resin by liquid media (sulfuric acid and hydrogen peroxide), which did not attack the fiber excessively. This technique was conducted according to ASTM D3171-76.

Three samples of each specimen were weighted 0.3g with a digital balance precision of 0.001g. The sample was separately taken in 250 ml beaker and 30 to 40 ml (not less than 20 ml) of concentrated sulfuric acid was added to the samples. The beakers with the acid-sample mixture were placed on a hot plate and heated until the sulfuric acid begun to fume. After the solution had become dark, 50% of hydrogen peroxide solution was added drop wise down the side of the beaker and the addition continued until about 35 ml had been added. At that time, to confirm the complete oxidation of the resin, more hydrogen peroxide was added and digestion continued for about 45 hours. The beakers were then removed from the hot plate and the solution allowed to cool in an ambient air. The contents of each beaker was filtered through a filter paper which was weighted in an analytical balance nearest to 0.001g and consequently the fiber was washed three times with distilled water and followed by acetone once. The fiber content filter papers were placed in an oven at 100°C for 1 hour to remove residual water and acetone. The filters containing fiber residue were cooled to room temperature and weighted. The percentage of fiber of each sample was calculated from the weight difference of fiber content filter paper to the filter paper divided by weighed sample.

3.4 BULK DENSITY

It is mainly a nondestructive test used as a quality control check of the consistency of formulation and processing of brake lining. Bulk density was measured by the water displacement technique recommended by SAE J380. In this experiment, two samples of each specimen of rectangular bar were taken. The test samples were not drilled only, because there is a tendency for air bubbles to become trapped in the drilled holes. The samples were weighted in an analytical balance with a precision of 0.001g. A container of distilled water (at room temperature), large enough to hold a completely submerged sample without contacting the inside surfaces of the container was taken. A monofilament cord was fastened to the weighing mechanism from which the sample was suspended and was completely immersed in water. Under the immersed condition, the sample was weighed in water within 30 seconds to minimize the absorption of the water by the sample. Bulk density was measured by the method of subtracting the "weight in water" from the "weight in air" and dividing the "weight in air" by the difference.

3.5 WATER ABSORPTION

Water absorption of the friction material was measured following the method described in ASTM D570-77. The test samples for water absorption were sawed and machined to form a bar of dimension 76.2 x 25.4 x 3.2 mm^3. The cut edges of the samples as well as surfaces were smoothed by finishing with emery paper of grit No. 0. Sawing, machining and emery polishing operations were done slow enough to avoid the appreciable heating of the materials. During the sawing or machining operations, the surfaces of sample were free from oil or any other grease. The presence of oily substances on the surfaces of the specimen hinders the absorption of water. So to avoid the presence of any oily substance, the specimens were washed with a cloth wet with gasoline, wiped with dry cloth and allowed to stands in air for two hours to permit evaporation of the gasoline. After preparing the specimens, these were cleaned and dried in an oven for one hour at 105 to 110°C and weighed in a digital balance nearest to 0.0001g. These specimens are called "conditioned".

The conditioned specimens were placed in separate containers of distilled water maintained at room temperature and were rest on edge and were entirely immersed. After 24 hours of immersion, the samples were removed from the water one at a time and all surface water wiped off with a dry cloth and weighed immediately. Water absorption was then calculated from the weight difference according to the equation 2.5.2.

3.6 SWELL TEST

The scope of this test was designated to check the thermal dimensional stability of brake linings in this department under controlled condition (SAE J160 JUN80). Four different samples were taken at room temperature and measured thickness at least on ten points located approximately 12.7-19.5 mm in from the lining edge. In this experiment a digital micrometer with the precision of 0.001 mm was used to measure the thickness. The unconfined specimens were placed in an oven at room temperature and the oven temperature increased to 204 ± 2.8°C. Rising time to 204 ± 2.8°C was recorded for one hour. The specimens were allowed to remain in oven for 30 minutes at 204 ± 2.8°C. The specimens were then removed from the oven and while still hot, thickness was measured at the same points where the initial thickness was measured. Difference of thickness was recorded as swell.

3.7 WEAR AND FRICTION COEFFICIENT

Wear and frictional measurements were performed in a pin-on-disc type apparatus (Fig 3.1) at room temperature in the ambient air. Figure 3.2 shows the arrangement of the wear testing machine for the measurement of friction force. The load cell was arranged in such a way that it just only touches the load arm. The load cell was connected to an amplifier which is calibrated to display tangential force on the pin directly. The amplifier also connected to an X-Y recorder. This allowed the on-line recording of friction force during testing. The size of the transducer and resolution used was 40 mm x 35 mm x 15 mm and 0.1gm respectively. The materials that were tested, machined in the form of cylindrical pins of diameter 8 mm and length 6.5 mm and were pressed against a rotating gray cast iron disc (hardness RB 84) which

acted as the counter body. Before the tests, the counter body was polished with the emery paper of grit no.3. Surface preparation of the counter body was completed by the running of a reference sample continuously at constant normal load of 15N and 900 rpm until the coefficient of friction has stabilized. During the tests. the curved surface of the cylindrical pin made contact with the flat surface of the counterbody which was 80 mm in diameter and 10 mm in thickness. For wear and frictional measurements, the disc was rotated at 900 and 1650 rpm respectively that yielded linear speed of 1.88 and 2.97 ms^{-1}. The weight of the pin was measured before and after the test and the weight loss due to wear was calculated after sliding for a distance of 6768 meter. After each test, wear scar morphology of the pin was examined under an optical microscope of 100 magnification.

Friction coefficient was also calculated from on-line measurement of friction force on the sample using a load cell. During the test, friction force versus time was recorded on the on-line recorder. The X axis of the curve represents the chart speed and Y axis represents the distance in mm corresponding to friction force. Coefficient of friction of the sample was measured by dividing the friction force with normal load at two minutes interval. From this experimental data, graph was plotted against the coefficient of friction versus time.
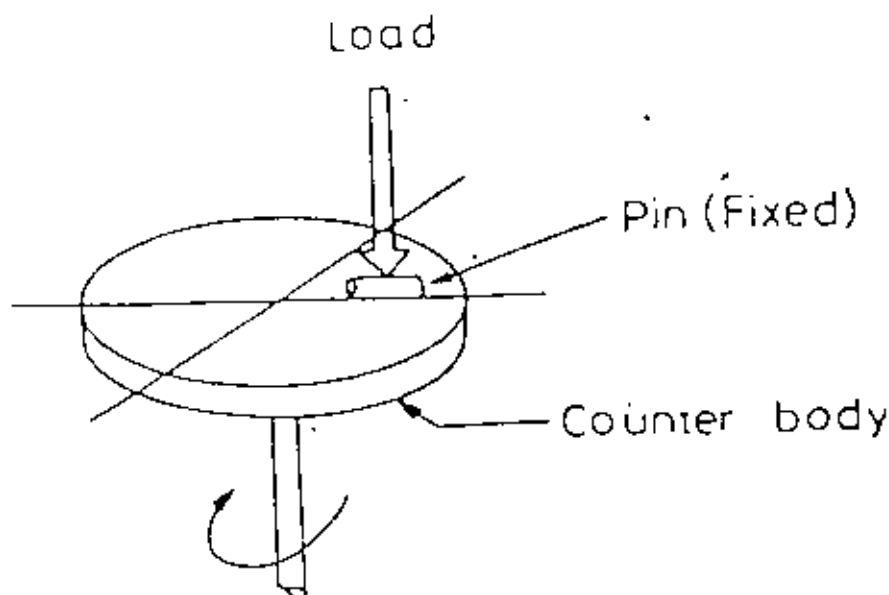
Fig. 3.1 Schematic diagram of pin-on-disc type wear testing machine
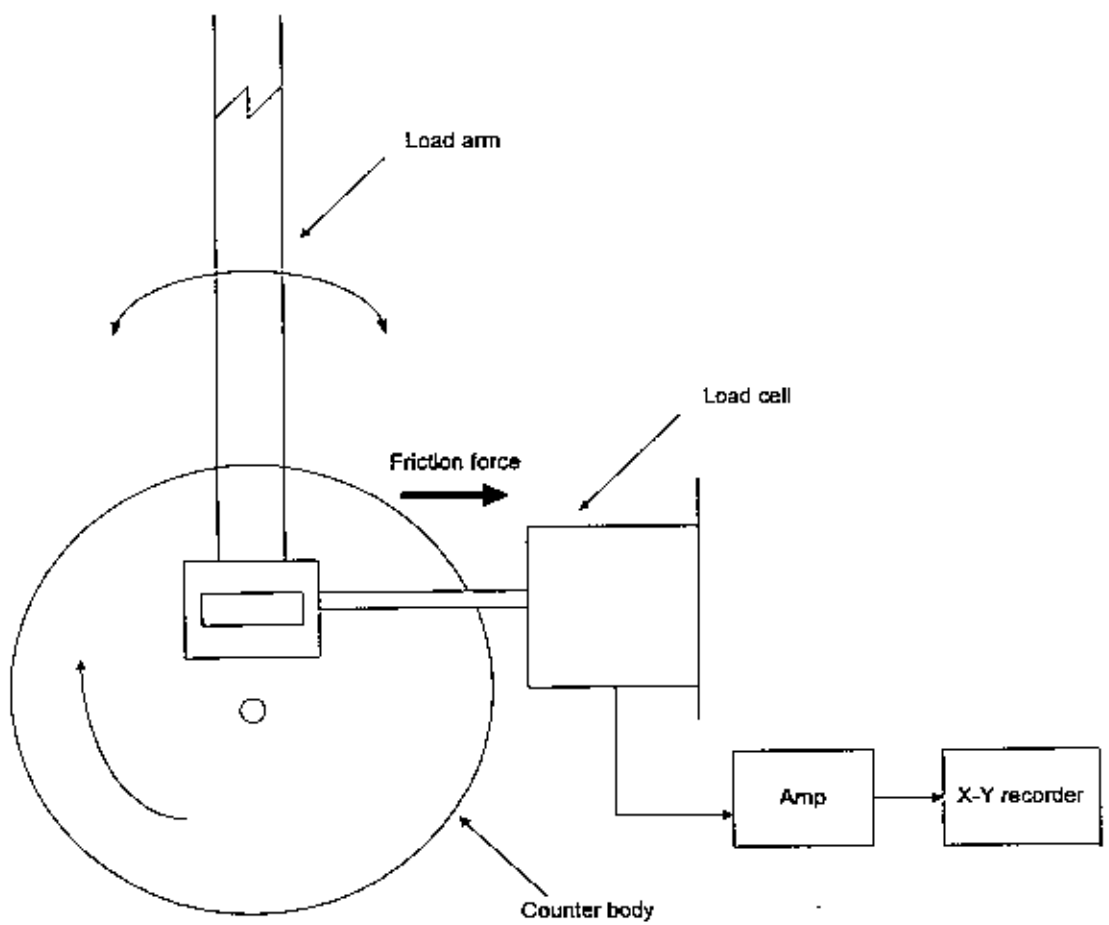
Fig. 3.2 schematic diagram of the pin-on-disc type friction testing machine

Chapter Four

4. DESIGN AND CONSTRUCTION OF A BLOCK-ON-RING TYPE WEAR TESTING MACHINE

4.1 PRINCIPLE OF THE MACHINE

In this machine, a brake lining test sample with a shape of square block (25.4 mm x 25.4 mm x 8 mm) is pressed against a cast iron ring which rotates in the vertical plane at a constant speed. The block is placed in a specimen holder which is supported by a load arm. One end of the load arm is held by a pivot arrangement so that it can swing in
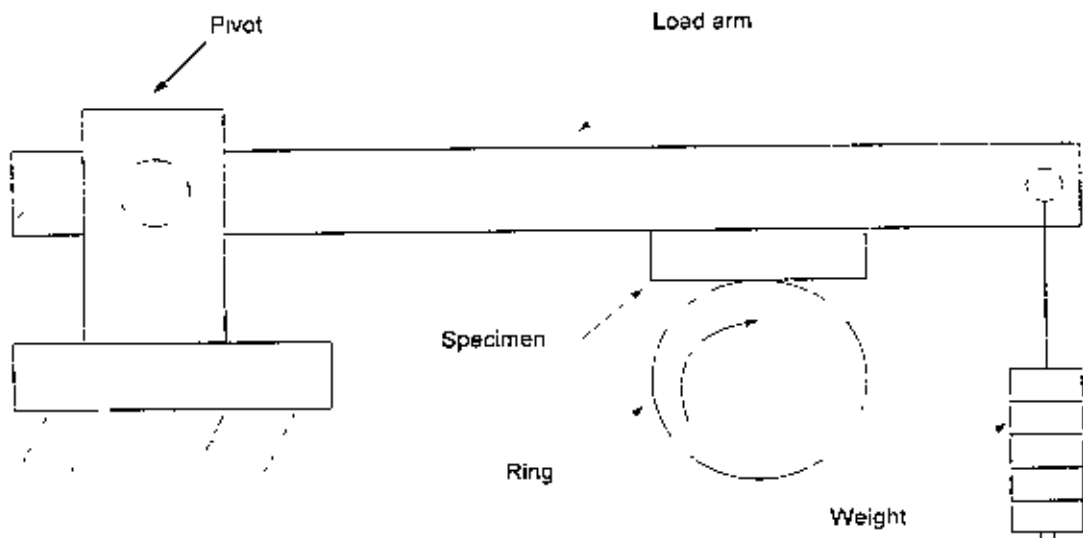
Fig.4.1 Schematic diagram of block-on-ring wear testing machine

the vertical plane. Weights are suspended at the other end of the load arm in order to press the block sample against the ring shaped counter body under a desired normal load. This machine can be used for the measurement of the wear damage of brake shoe lining by measuring the weight loss. This machine is essentially a modified version of the wear testing machine described in SAE J661a standard for brake shoe lining material. The major difference is : in the present machine the brake lining sample is pressed on the outer side of the ring-shaped counter body rather than on the inner side as suggested in the standard. This has been done to simplyfy the construction. The rpm

of the counter body is designed to 417 and load can be varied from 50 Psi (334 kPa) to 100 Psi (689 kPa) as per standard.

4.2 DIFFERENT PARTS USED IN THE CONSTRUCTION OF THE MACHINE

The parts which were used in construction of the block-on-ring wear testing machine are listed below.

A. Table assembly
a. Table frame
b. Table plate
c. Nuts and Screws

B. Load arm assembly
a. Small bearings
b. Bearing houses
c. Load arm
d. Pivot
e. Specimen holder
f. Rod
g. Load
h. Screws

C. Rotating ring assembly
a. Cast iron ring
b. Flange
c. Shaft
d. Pulley
e. Large bearings
f. Bearing cases
g. Base
h. Rubber belt
i. Motor
j. Nuts and Screws

4.3 BRIEF DESCRIPTION AND DESIGN OF THE PARTS OF BLOCK-ON-RING WEAR TESTING MACHINE

Table frame: The table frame was made of mild steel angle with required dimension (927 mm x 464 mm x 686 mm) and the total arrangement of the machine was mounted with it (Fig. 4.1).

Top plate: Made of mild steel, containing a rectangular groove (267 mm x 82.5 mm) located at 140 mm from the long edge and 127 mm from the short edge of the plate respectively. The purpose of this groove was to place externally the outer surface of the rotating ring. The plate also contains four holes of required diameter to support the bearing houses (Fig. 4.2).

Bearing house: The bearing house made of mild steel was used for the purpose of fixing up the load arm and was mounted on the table plate (Fig. 4.3).

Pivot of the load arm: It was used to hold the load arm with the bearing houses (Fig. 4.4).

Load arm: Made of mild steel and was supported by the bearing house. A rectangular chamber made of its bottom position which supported the specimen holder (Fig. 4.5).

Specimen holder: Made of stainless steel which contained the specimen. It was placed at the bottom position of the load arm for contacting the sample with the rotating ring (Fig. 4.6).

Load: Some variable loads were used at the end of the arm for determining the wear and friction coefficient (Fig. 4.7).

Shaft: It was made of alloy steel and supported by the large bearings, flange, pulley and the rotating ring (Fig. 4.8).

Bearing case: The purpose of this case was attached the large bearing.

Rotating ring: Made of cast iron used to contact the specimen for measuring the wear damage by the measuring the weight loss (Fig. 4.9).

Motor: A 3 phase (5HP) AC motor was used for rotating the shaft by pulley.

4.4 ASSEMBLING BLOCK-ON-RING TYPE WEAR TESTING MACHINE

A table frame of dimension 927 mm x 464 mm x 686 mm was constructed first with mild steel angle (76.2 mm x 76.2 mm x 8 mm). A mild steel top plate containing a rectangular groove of dimension 267 mm x 82.5 mm was mounted over the table frame and screwed to it. Two bearing houses were placed on the top plate and attached with it using screws of required size. Two bearings (15 mm diameter) were tightly fixed into the housing.

The mild steel load arm was connected to the bearings by a pivot. The specimen holder was screwed to the rectangular groove of the load arm. A cylindrical long rod was screwed at the opposite end (near the specimen holder) of the load arm. This rod was used to support the variable loads for the testing purpose. The whole arrangement of the load arm with bearings and bearing houses was shown in Fig. 4.10.

A round flange made of alloy steel was welded with the shaft. The flange was fixed to the cast iron counter body by nuts and screws. A pulley was attached to the shaft. The shaft containing the cast iron counter body and the pulley was supported on two bearings. The bearing housings were placed below the table top on mild steel angle by means of screws. Two metal angles called bases were welded horizontally with the table

leg under the table. The bearing houses were then tightly screwed with these bases. A rubber belt was used to connect between the motor and the pulley. The over all arrangement was shown in Fig. 4.11.
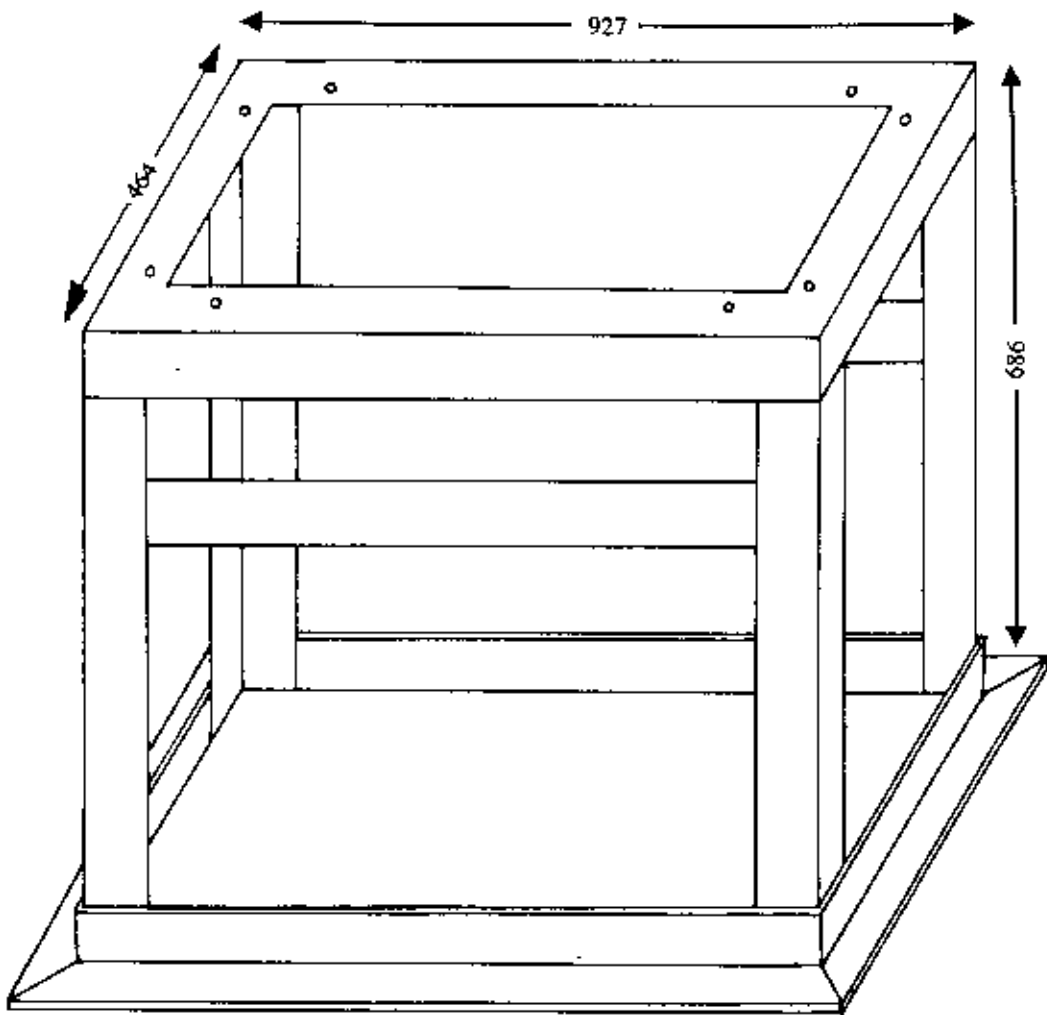
Fig. 4.1 A schematic diagram of table frame.

927

464

Top View

267

Front View

140 82 5
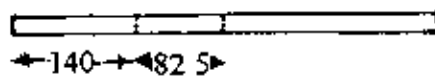
Side View

Fig. 4.2 A schematic diagram of top plate.
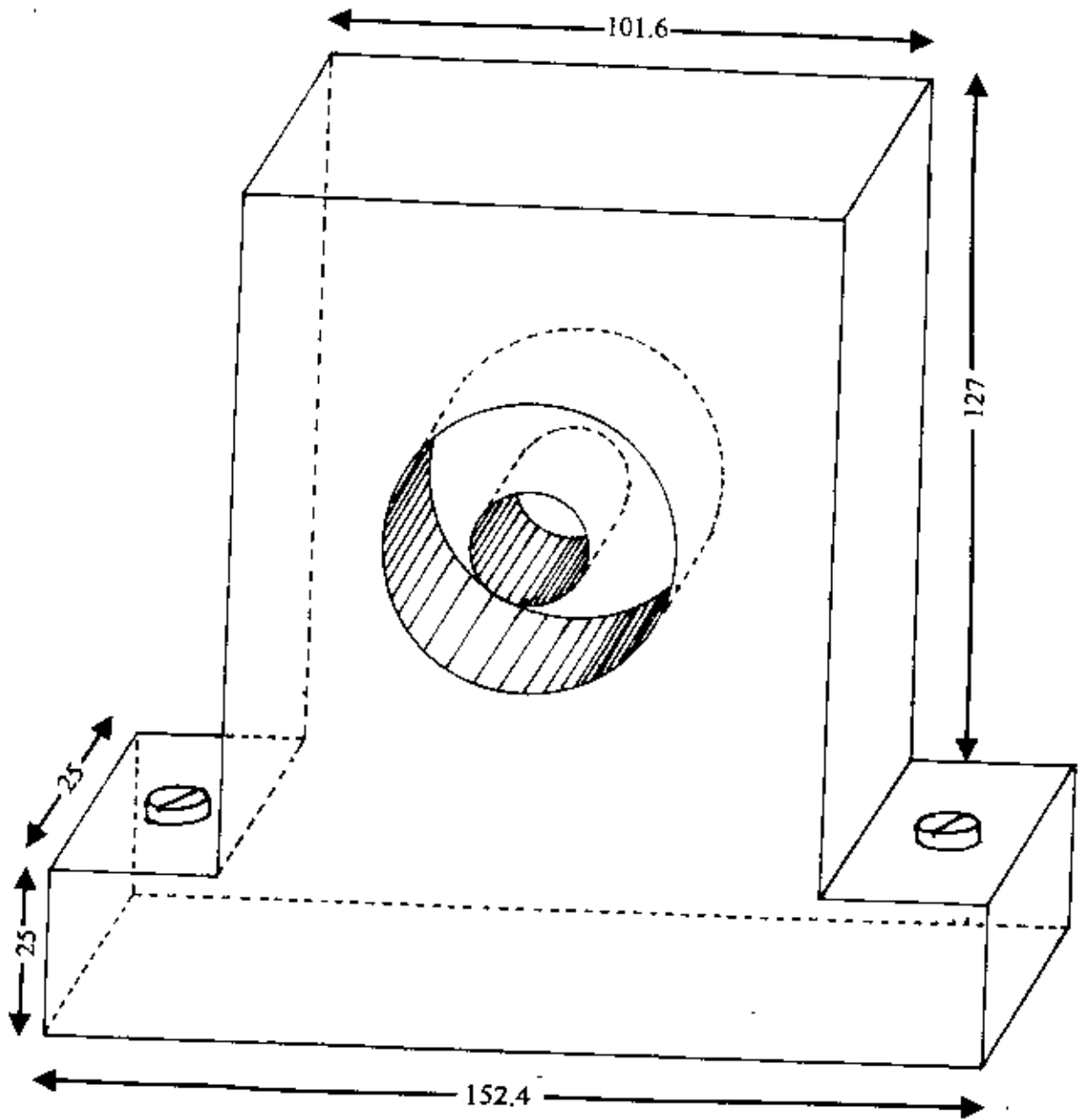
Fig. 4.3 A schematic diagram of bearing house.

Top View

φ 25

φ19
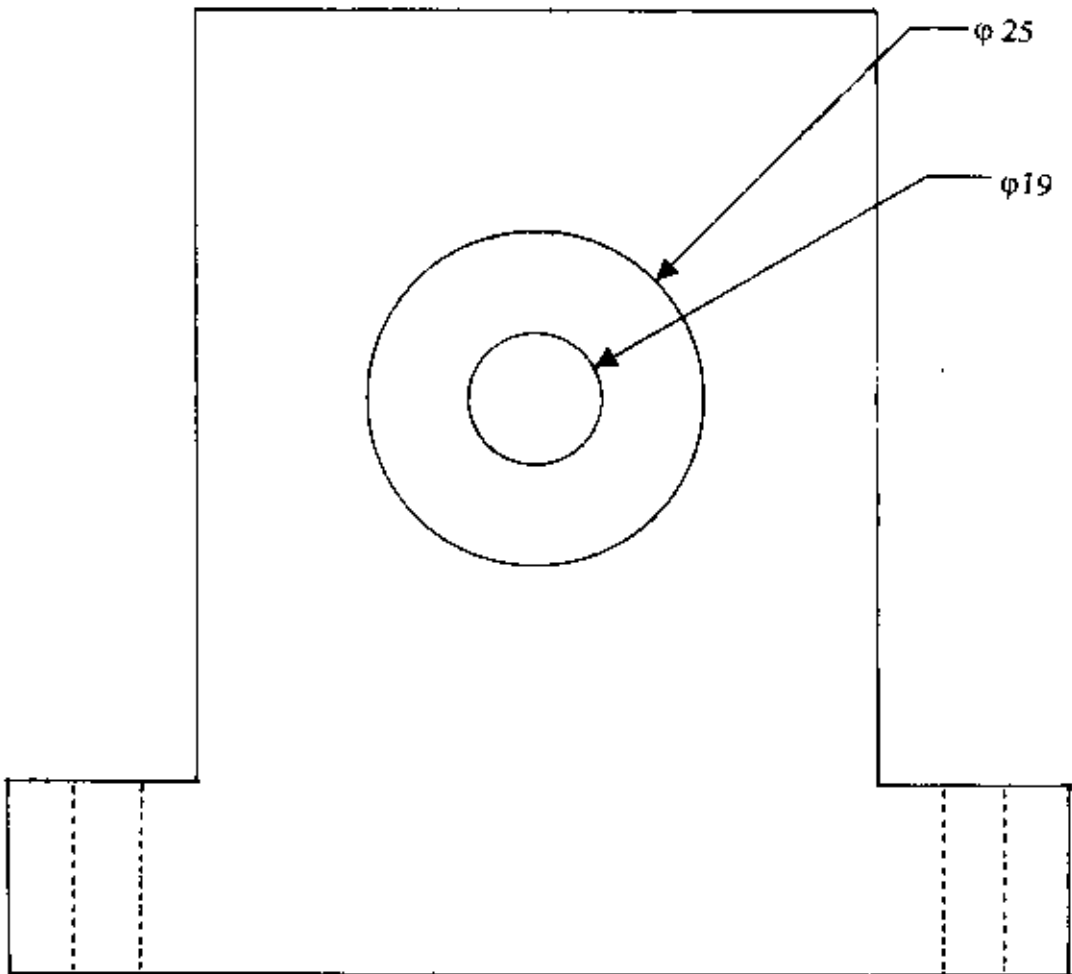
Front View

Fig. 4.3 (continued)
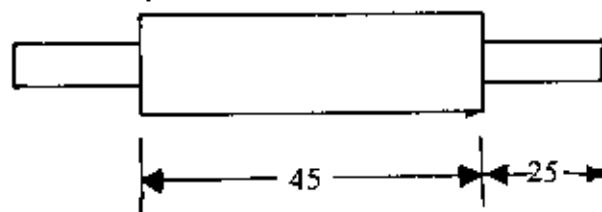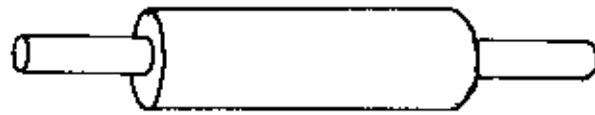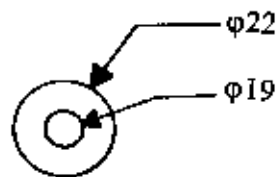
Front View

Side View

Fig. 4.4 A schematic diagram of pivot of the load arm.

Side View

Front View

Top View

30

22

420

63.5

304.8

φ12
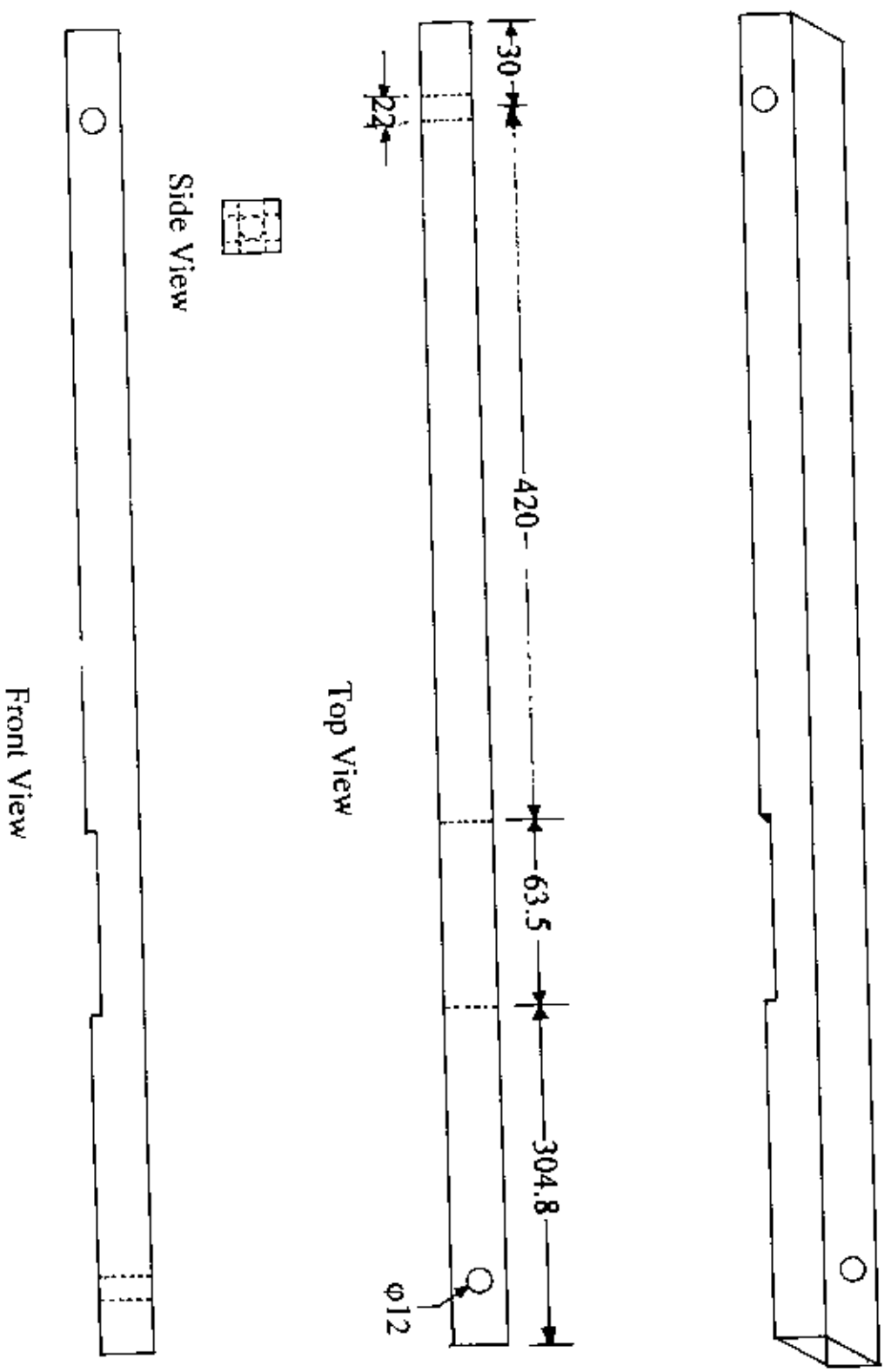
Fig. 4.5 A schematic diagram of load arm.

25.4

38.1

63.5
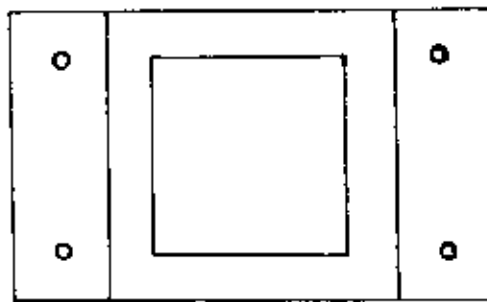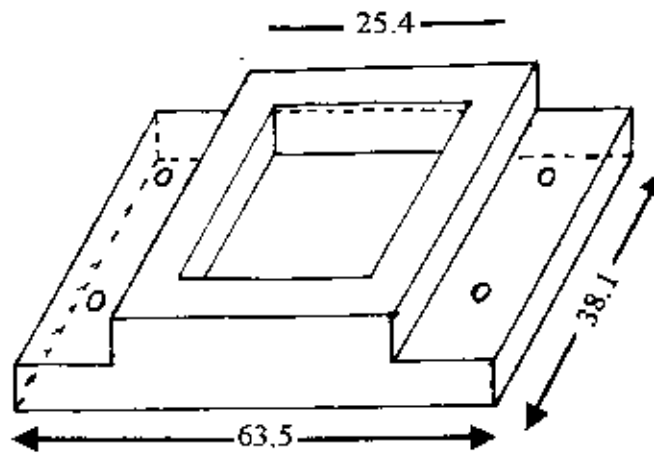
Top View

Front View

6

6
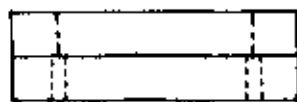
Side View

Fig. 4.6 A schematic diagram of specimen holder.

φ 127

φ 50 8

12

Top View

16

50

127

Front View

12

50.8

127
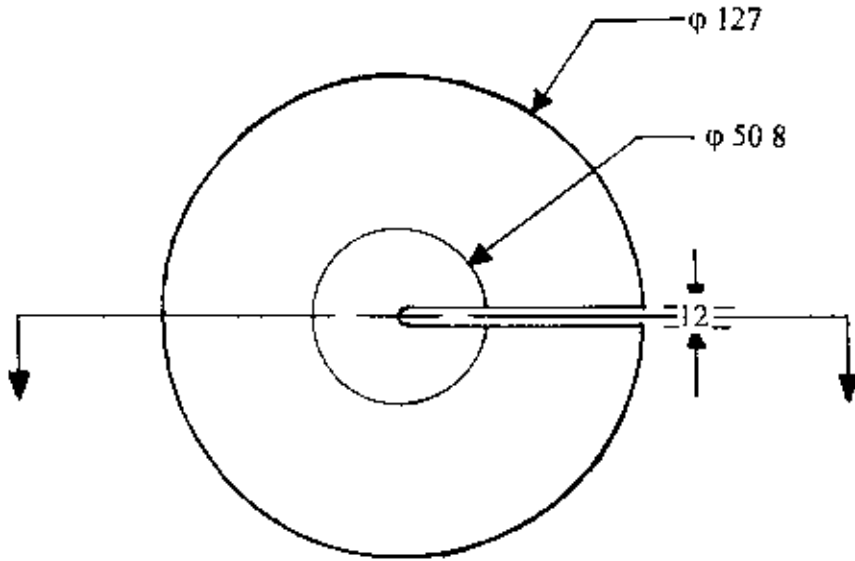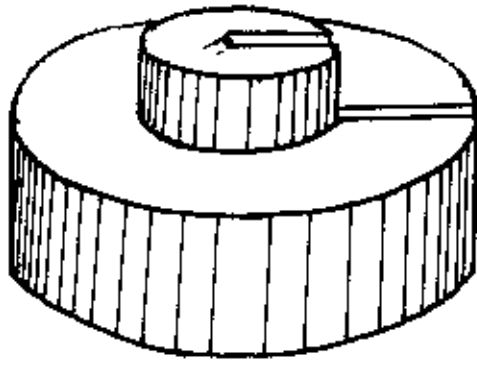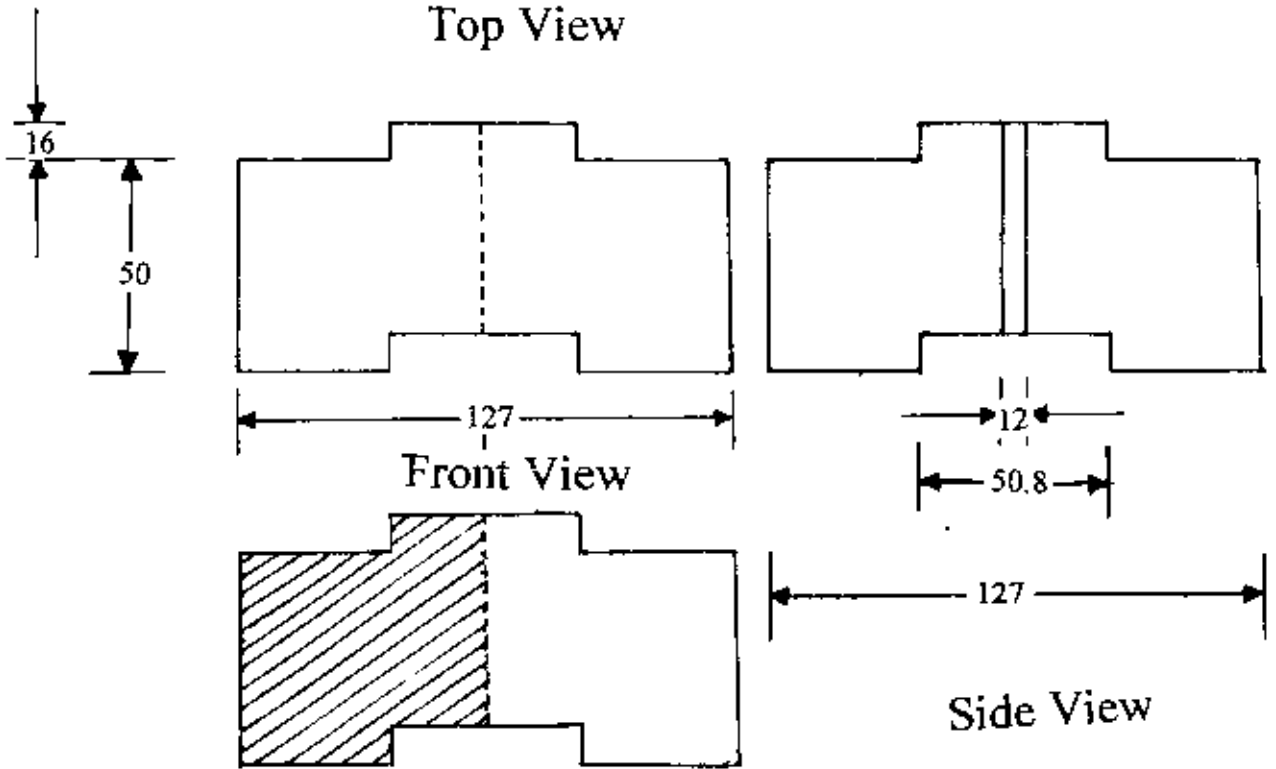
Side View

Cross sectional View

Fig. 4.7 A schematic diagram of load.

457 2

Top View

φ 171.45

φ152.4

φ 50.8

φ 28
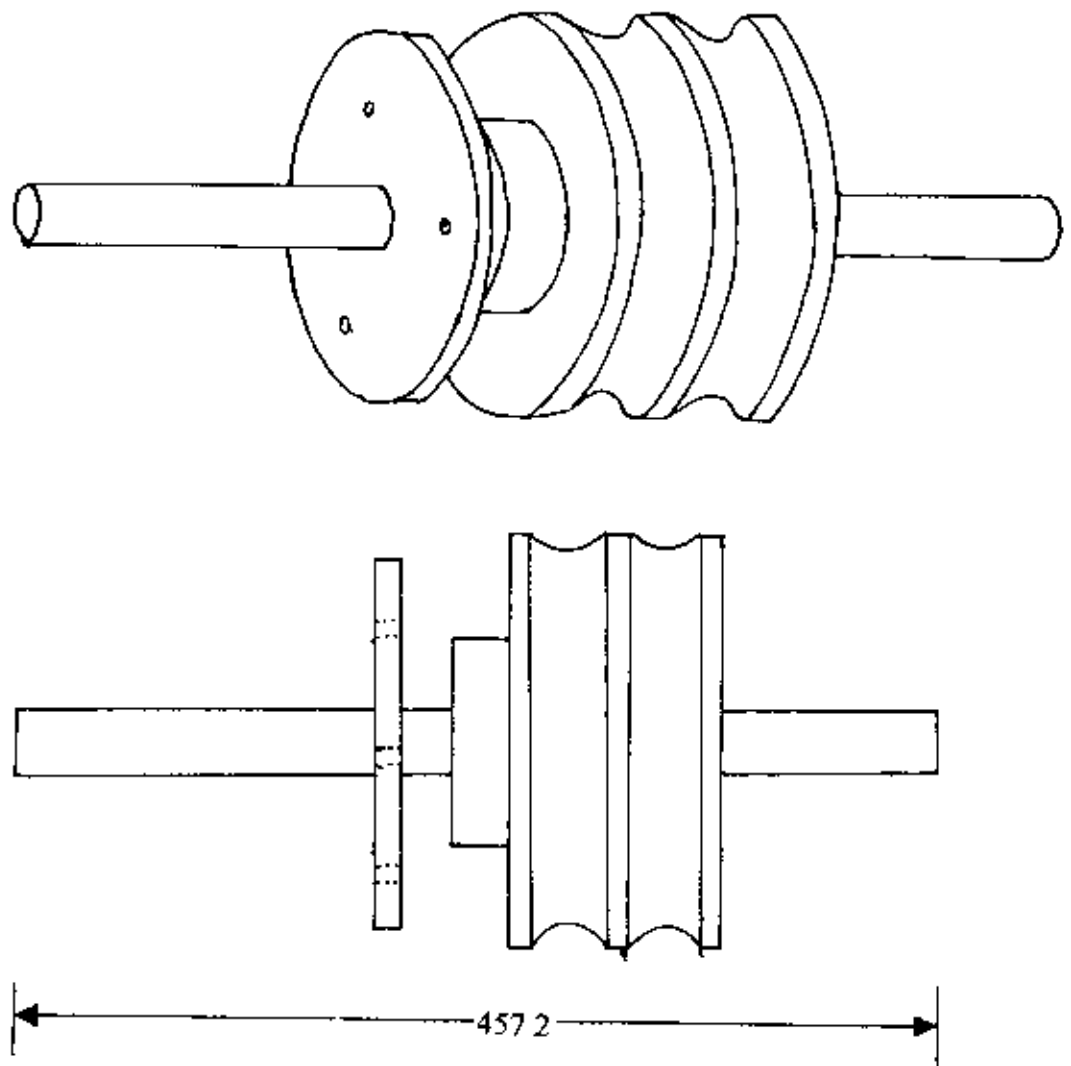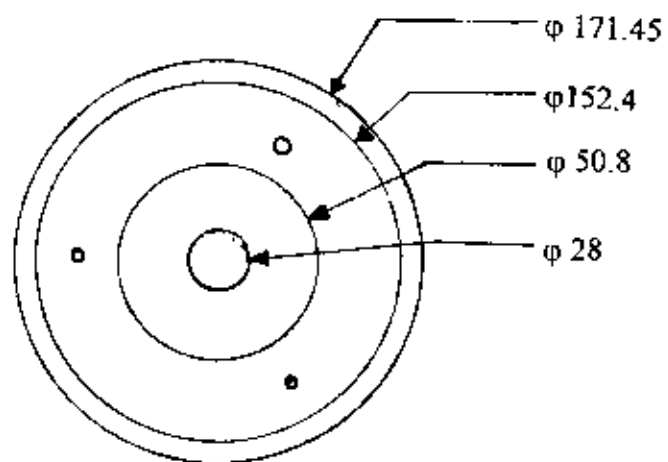
Side View

Fig. 4.8 A schematic diagram of shaft attached with pulley and flange.

φ 355.6

φ330

φ 28

φ303

Top View

330

355.6

Front View

25.4

303
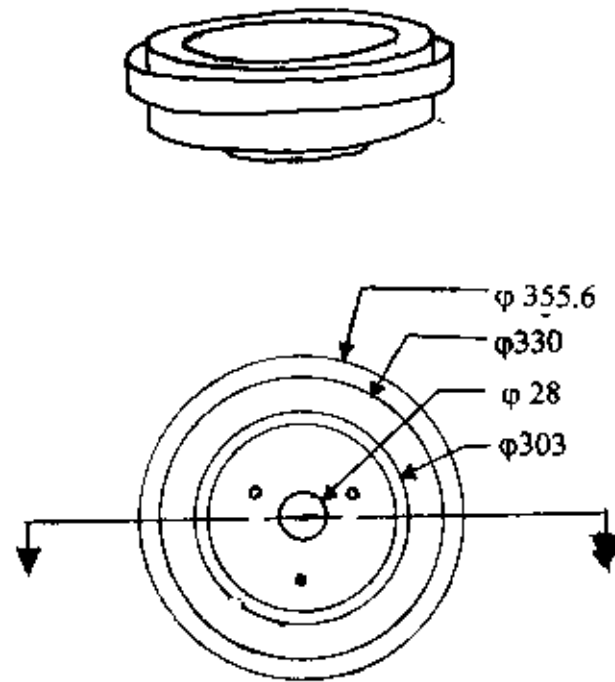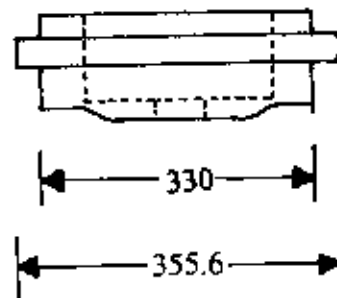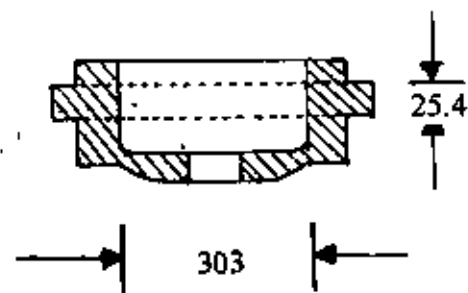
Cross Sectional View

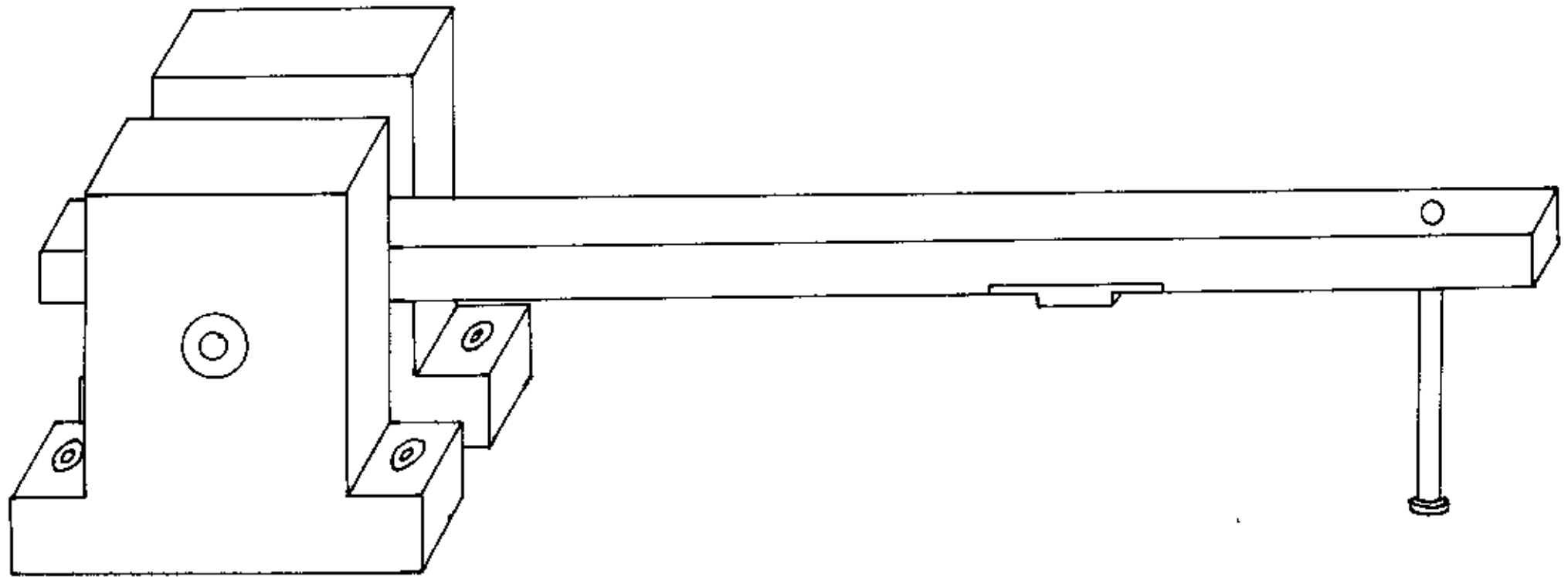Fig. 4.9 A schematic diagram of rotating ring.

Fig. 4.10 A schematic diagram of assembling of the load
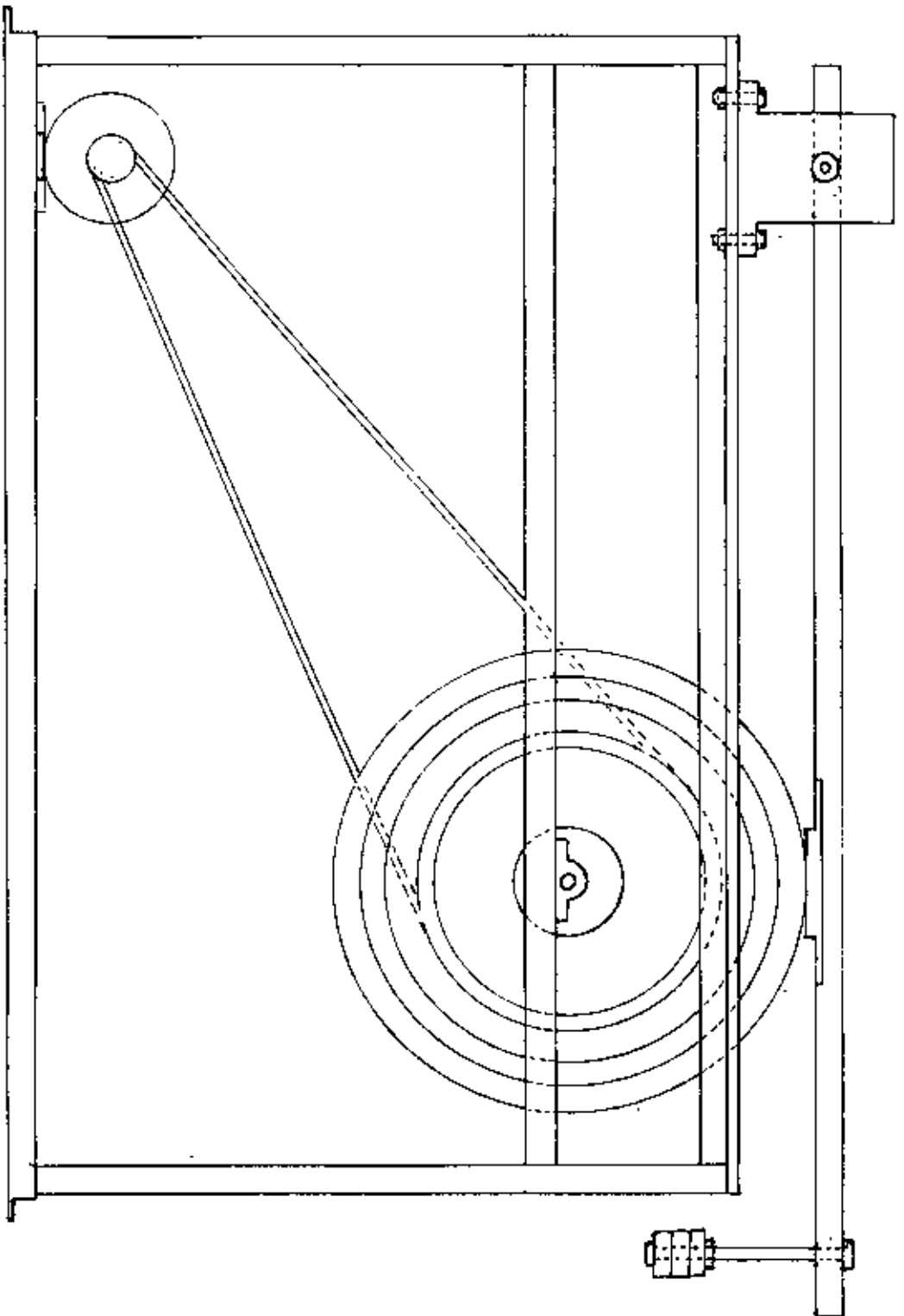arm, specimen holder and rod with bearing house

Fig. 4.11 A schematic diagram of block on ring wear testing machine

Chapter Five

5. RESULTS AND DISCUSSIONS

5.1 CHARACTERIZATION OF BRAKE SHOE LINING MATERIAL

5.1.1 X-ray diffraction (XRD)

Fig. 5.1-5.4 shows the diffraction patterns of these samples. In addition to a number of relatively sharp peaks, the patterns also contain a broad diffused peak at approximately 8 to 15^0 2θ positions. The d-spacing values of different crystallographic phases corresponding to the peaks of the XRD patterns are given in Tables 5.1-5.4 for all the materials. Observed d-spacings are compared with standard d-spacings [34] of probable phases. These are also summarized in Tables 5.1-5.4. In the case of all the four samples, the presence of asbestos and barium sulphate is positively identified. The observed d-spacings are found to differ slightly from the standard d-spacings. This is thought to be related to the presence of other minor constituents in the phases. The occurance of a broad peak in the XRD patterns is indicative of the presence of an amorphous phase in all the samples [35]. However XRD does not allow the identification of this phase. The identification of this phase is further discussed in the next section.

Table 5.1 Comparison of the observed peak position and the respective standard peak position of sample B.

Observed peak position (2θ)	Observed d-spacing A^0	Standard d-spacing A^0	Plane (hkl)	Type of constituents
5.6	7.274	7.40	001	Asbestos
9.2	4.430	4.44	020	$BaSO_4$
10.5	3.803	3.90	021	Asbestos
11.1	3.674	3.67	002	Asbestos
12.3	3.317	3.319	210	$BaSO_4$
13.1	3.115	3.103	121	$BaSO_4$
14.3	2.855	2.875	022	Asbestos
14.9	2.74	2.735	130	$BaSO_4$
17.1	2.390	2.41	003	Asbestos
19.3	2.12	2.156	202	Asbestos
20.4	2.006	1.9486	222	$BaSO_4$
26.8	1.533	1.538	060	Asbestos
27.8	1.479	1.475	412	$BaSO_4$

Table 5.2 Comparison of the observed peak position and the respective
standard peak position of sample F1.

Observed peak position (2θ)	Observed d-spacing A°	Standard d-spacing A°	Plane (hkl)	Type of constituents
5.6	7.274	7.40	001	Asbestos
9.3	4.383	4.339	101	BaSO$_4$
11.1	3.674	3.67	002	Asbestos
13.4	3.045	3.103	121	BaSO$_4$
15.7	2.60	2.663	200	Asbestos
17.7	2.309	2.307	040	Asbestos
18.4	2.222	2.211	123	BaSO$_4$
21.3	1.922	1.9317	132	Asbestos
25.3	1.622	1.625	340	BaSO$_4$
26.7	1.5389	1.538	060	Asbestos

Table 5.3 Comparison of the observed peak position and the respective standard
peak position of sample F2

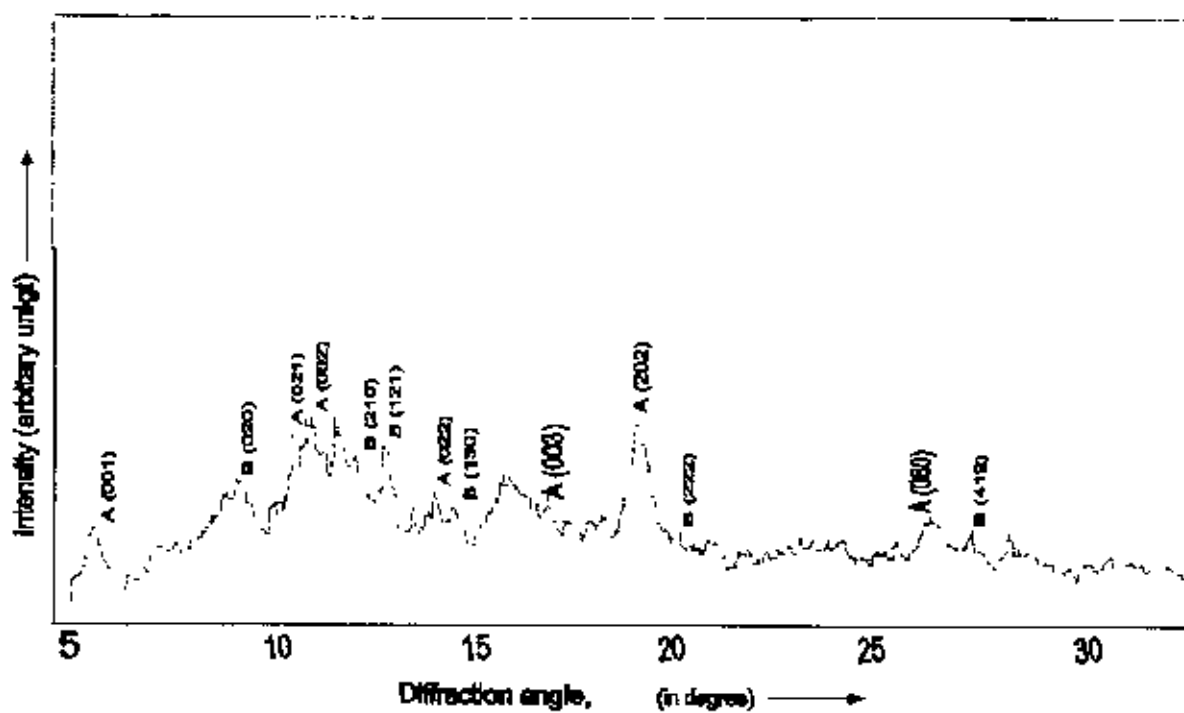| Observed peak position (2θ)	Observed d-spacing A°	Standard d-spacing A°	Plane (hkl)	Type of constituents
5.4	7.543	7.40	001	Asbestos
9.0	4.529	4.60	020	Asbestos
11.1	3.674	3.67	002	Asbestos
13.3	3.068	3.103	121	BaSO$_4$
14	2.915	2.875	022	Asbestos
16.1	2.537	2.482	221	BaSO$_4$
18.4	2.222	2.211	123	BaSO$_4$
22.7	1.805	1.799	203	Asbestos
26.6	1.5446	1.535	332	BaSO$_4$
27.3	1.5057	1.4958	402	BaSO$_4$

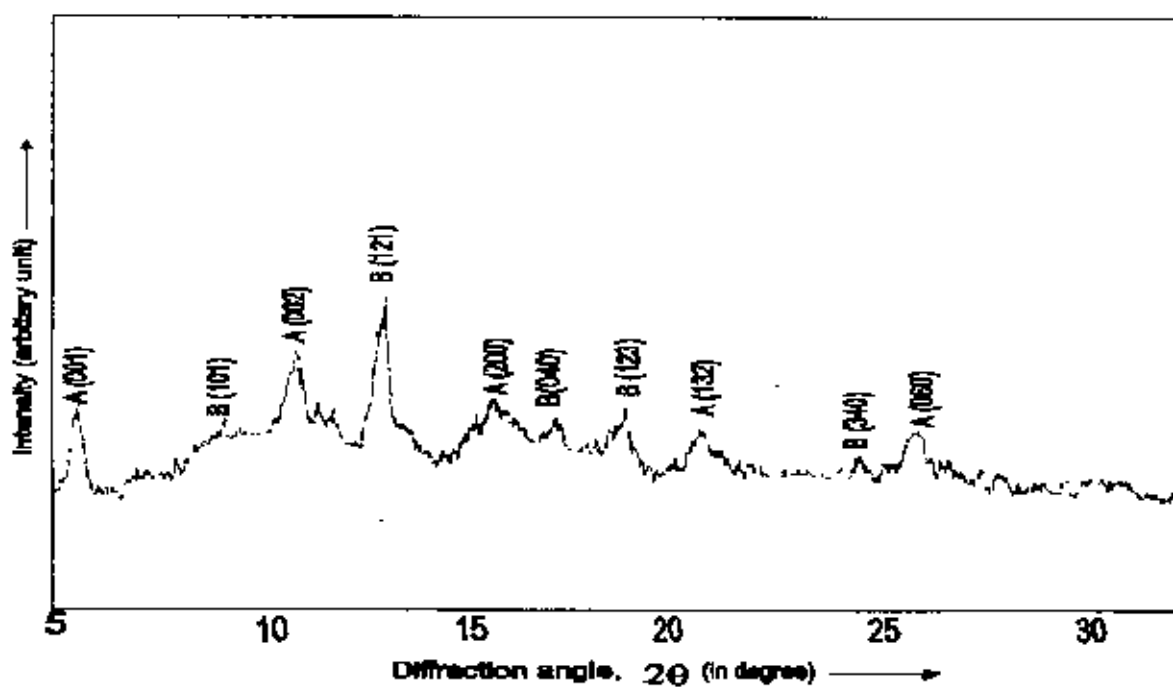Fig. 5.1 X-ray diffraction pattern of sample B

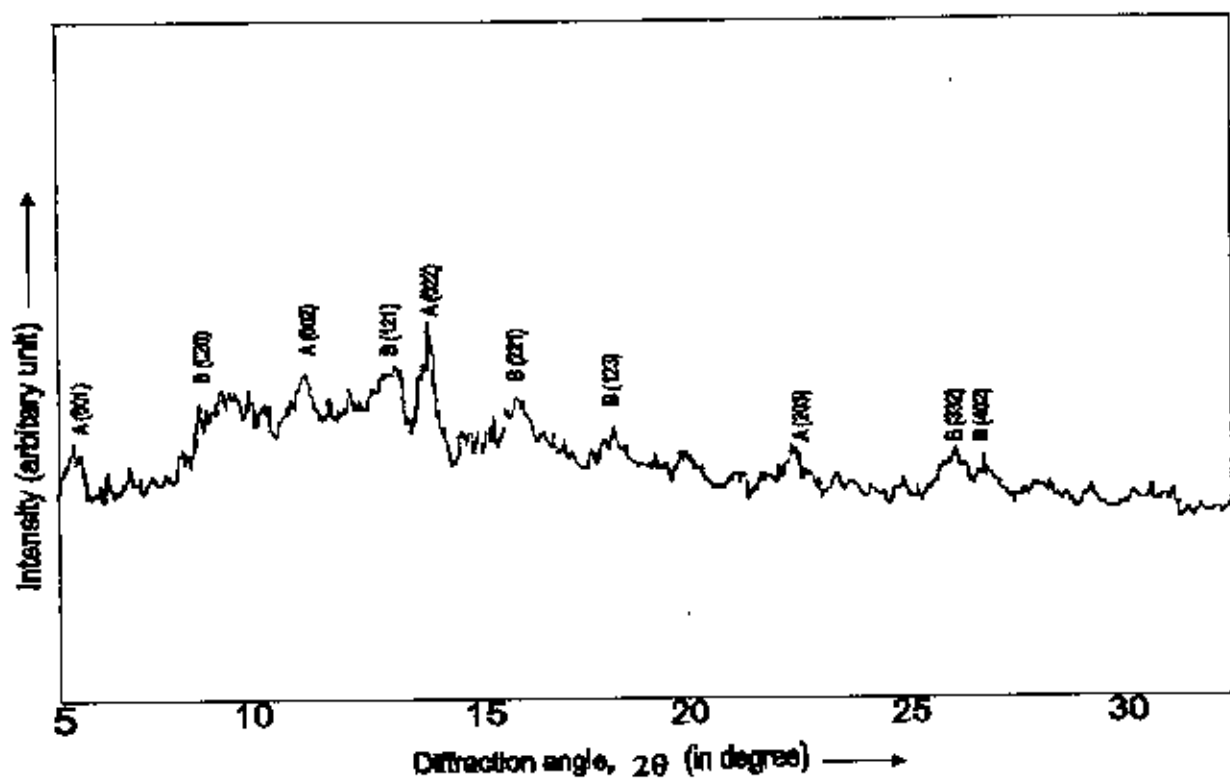Fig. 5.2 X-ray diffraction pattern of sample F1

74

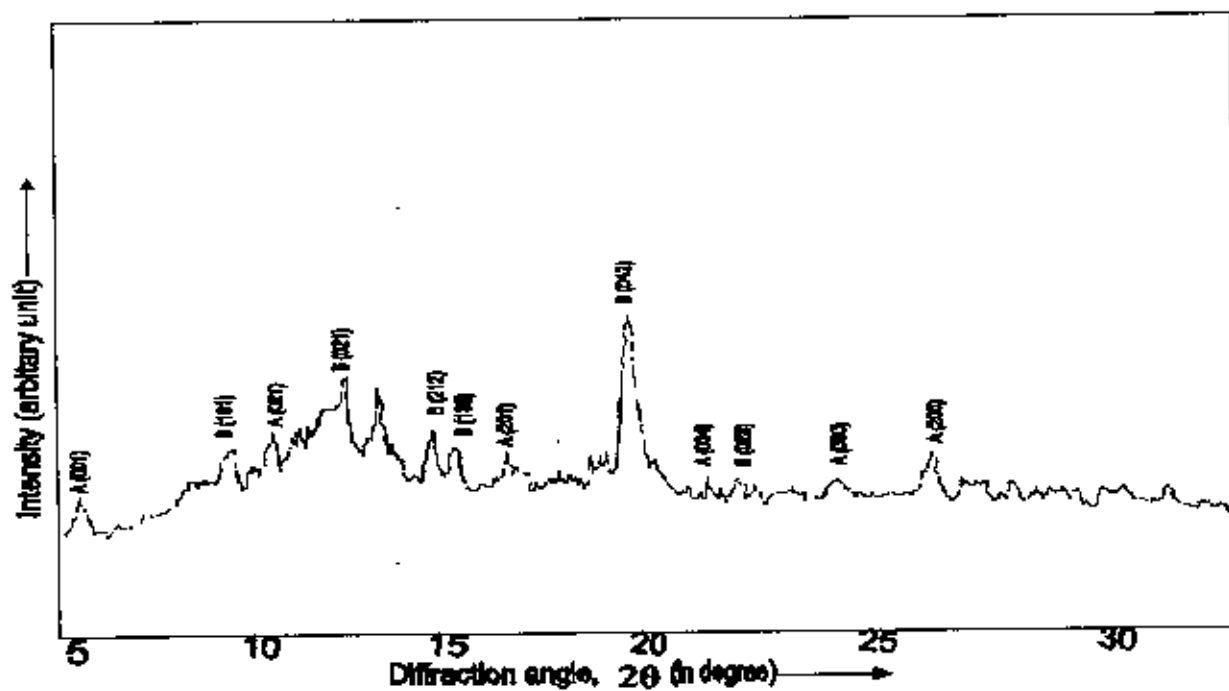Fig. 5.3 X-ray diffraction pattern of sample F2

Fig. 5.4 X-ray diffraction pattern of sample F3

Table 5.4 Comparison of the observed peak position and the respective standard peak position of sample F3.

Observed peak position (2θ)	Observed d-spacing A^o	Standard d-spacing A^o	Plane (hkl)	Type of constituents
5.5	7.406	7.40	001	Asbestos
9.4	4.336	4.339	101	$BaSO_4$
10.4	3.94	3.90	021	Asbestos
11.8	3.456	3.445	021	$BaSO_4$
12.3	3.316	3.319	210	$BaSO_4$
13.1	3.115	3.103	121	$BaSO_4$
14.4	2.835	2.836	212	$BaSO_4$
14.9	2.74	2.735	130	$BaSO_4$
16.1	2.537	2.505	201	Asbestos
21.1	1.94	1.945	042	Asbestos
21.9	1.87	1.835	004	Asbestos
24.3	1.688	1.682	023	$BaSO_4$
26.6	1.544	1.538	060	Asbestos
32.4	1.273	1.281	205	Asbestos

5.1.2 Infrared spectroscopy

Infrared spectra contain absorption peaks corresponding to different vibration/bending modes of atomic pairs present in samples. By recognizing the vibration/bending of atomic pairs, identification of the organic compounds present in the sample can be made. In the present study all of the four brake lining materials viz. B, F1, F2, F3 were investigated by infrared spectroscopy. The infrared spectra of the samples are shown in Fig. 5.5-5.8. It is observed that the higher wave number regions of all the spectra show a similar appearance. The positions of major absorption peaks of the four spectra are shown in Table 5.5. These peak positions are compared with the standard peak positions of different streching/bending vibration of different organic compounds. The standard peak positions of most closest compounds are given in Table 5.6. By comparing the observed peak positions with the standard ones, possible identification of functional group present in the samples are made in the last colum of Table 5.5. It may be mentioned that certain shift in observed peak position can occur, reasons of which are discussed in reference 33. It is seen that all the spectra contains a sharp peak at 3650 cm^{-1} which corresponds well with the standard peak position for the O-H stretching vibration in

phenol. Aromatic C-H stretching occurs at higher wave numbers (3400-3450 cm^{-1}) in all the samples. Absorption peak due to aldehyde C-H stretching vibration is found to be present in all the four samples at a slightly higher value. The presence of a series of peaks in the range of 1410-1630 cm^{-1} in the samples corresponds to the characteristic $C = C$ stretching of benzene skeleton. Para and ortho substitutions are also observed by the peaks in the range of 820-870 cm^{-1} and 710-750 cm^{-1} respectively. From the presence of benzene skeleton, O-H stretching of fhenol, C-H and C=O stretching of aldehyde, it is concluded that all the four samples tested contain Phenol formaldehyde as a major constituent. It may be mentioned that formaldehyde condenses preferentially at the ortho and para position of phenol [36] which has indeed been observed in the IR spectra of all the samples. Phenol formaldehyde is a highly crosslinked thermosetting polymer having no/little crystallinity. The presence of a broad peak in the XRD pattern of each sample presented in the previous section also supports the fact that each of the samples contains phenol formaldehyde. This thermosetting polymer is nowadays widely used as the matrix in brake friction material because of its good mechanical properties, excellent thermal resistance and low cost.

5.1.3 Microscopic examination

Optical micrographs of the brake shoe lining materials under both normal and oblique illuminations are presented in Figs. 5.9-5.12. The micrograph of sample B taken at oblique illumination shows a number of light brown particles embedded in a matrix. Under normal illumination, the sample in general shows a deeper tent, and the particles become more translucent. Sample F2 (Fig. 5.11a and 5.11b) shows similar features, although the size of the particles is bigger in sample F2. The particles in sample B and F2 are somewhat rounded in shape. The particles in sample F1 and F3 (Fig. 5.10 and 5.12) are similar and their colour and shapes are different from those in samples B and F2.

In phenolic based friction material, cashew nut shell powder and/or pre cured phenolic powder are nsnally added as friction modifier. It may be mentioned that cashew nut shell, which is naturally occurring, is a modified phenolic based organic

Table 5.5 Observed absorption peaks and their identification

Observed absorption peak position, cm^{-1}				Possible Functional group
B	F1	F2	F3	
3650	3650	3650	3650	O-H Str. (Phenol)
3400	3450	3400	3450	C-H Str. (aromatic)
2900	2900	2900	2900	C-H Str.(aldehyde)
2850	2850	2850	2850	C-H str. (aldehyde) (shoulder)
	2530			
2300	2370	2350		
	1790			C = O Str. (adlehyde)
1630			1630	C = C str. (Characteristic benzene skeleton)
1600	1600	1600	1600	C = C str. (Characteristic benzene skeleton)
			1500	C = C str. (Characteristic benzene skeleton)
1440	1410	1430	1440	C = C str. (Characteristic benzene skeleton)
1260	1260	1240	1250	
1170			1180	
1080	1080	1080	1070	(C-O) str. (Phenol)
1020	1020	1029	1020	(C-O) str. (Phenol)
950	950	960	950	
820	870	880	830	Para substitution (benzene ring)
750	710	750	760	Ortho substitution (benzene ring)

Table 5.6 Standard IR absorption peak position for different compounds [33,37].

Aromatic hydrocarbon		Position
C – H str	:	$3050 - 3000 \text{ cm}^{-1}$
C = C str	:	$1650 - 1450 \text{ cm}^{-1}$
C –H def.	:	$900 - 700 \text{ cm}^{-1}$
Characterise C=C	:	$1600, 1580, 1500, 1450(m) \text{ cm}^{-1}$
Ortho		$770 - 735 \text{ cm}^{-1}$
Para		$840 - 800 \text{ cm}^{-1}$

Phenol:		
OH str.	:	$3700 - 3500 \text{ cm}^{-1}$
C – O str.	:	$1440 - 1300 \text{ cm}^{-1}$
		1200 cm^{-1}
C – O str.	:	1080 cm^{-1}
		1010 cm^{-1}

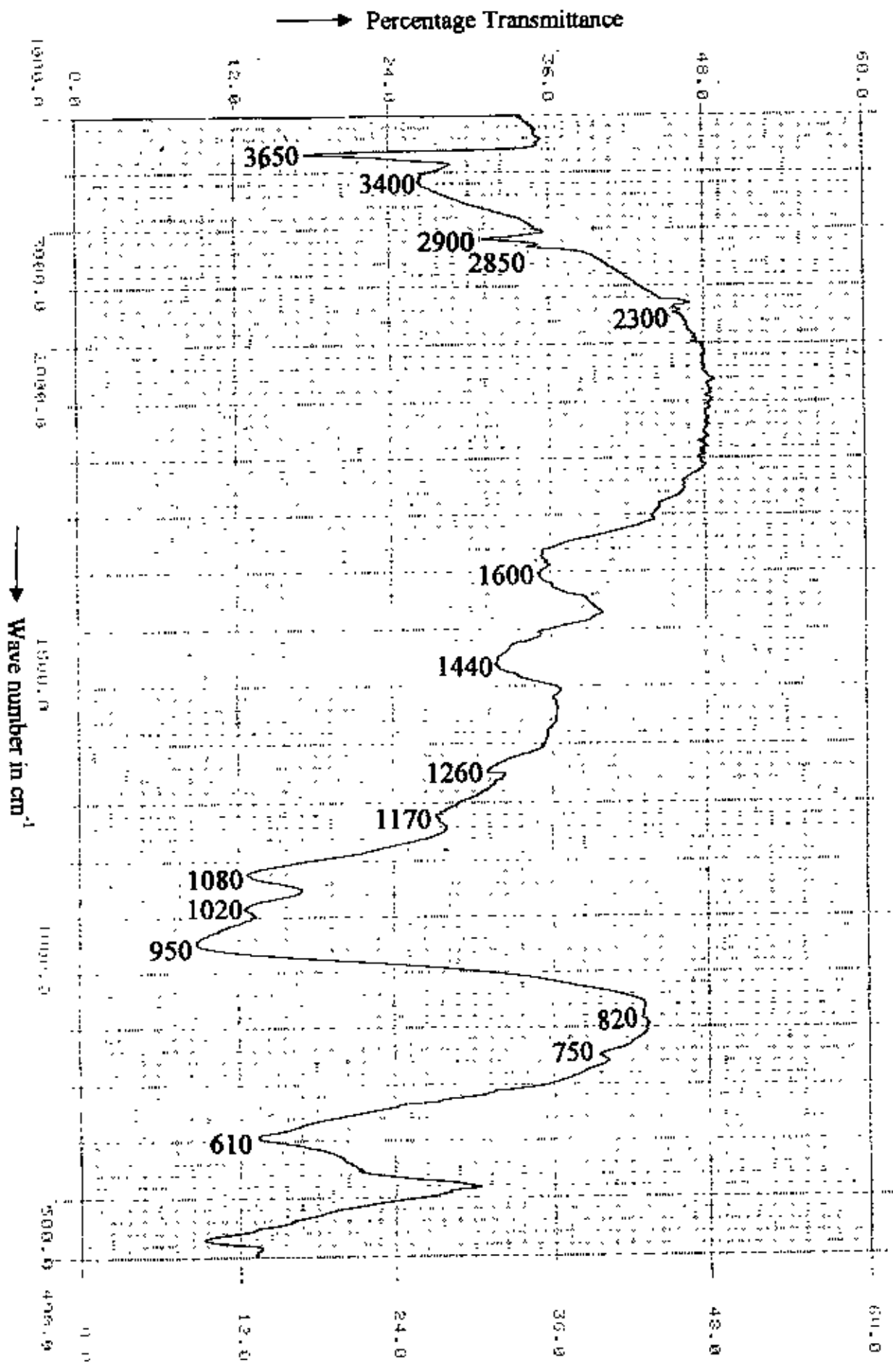| ldehydes		
C = O str.	:	1750 cm^{-1}
C – H str.	:	2820 cm^{-1}
		2720 cm^{-1}

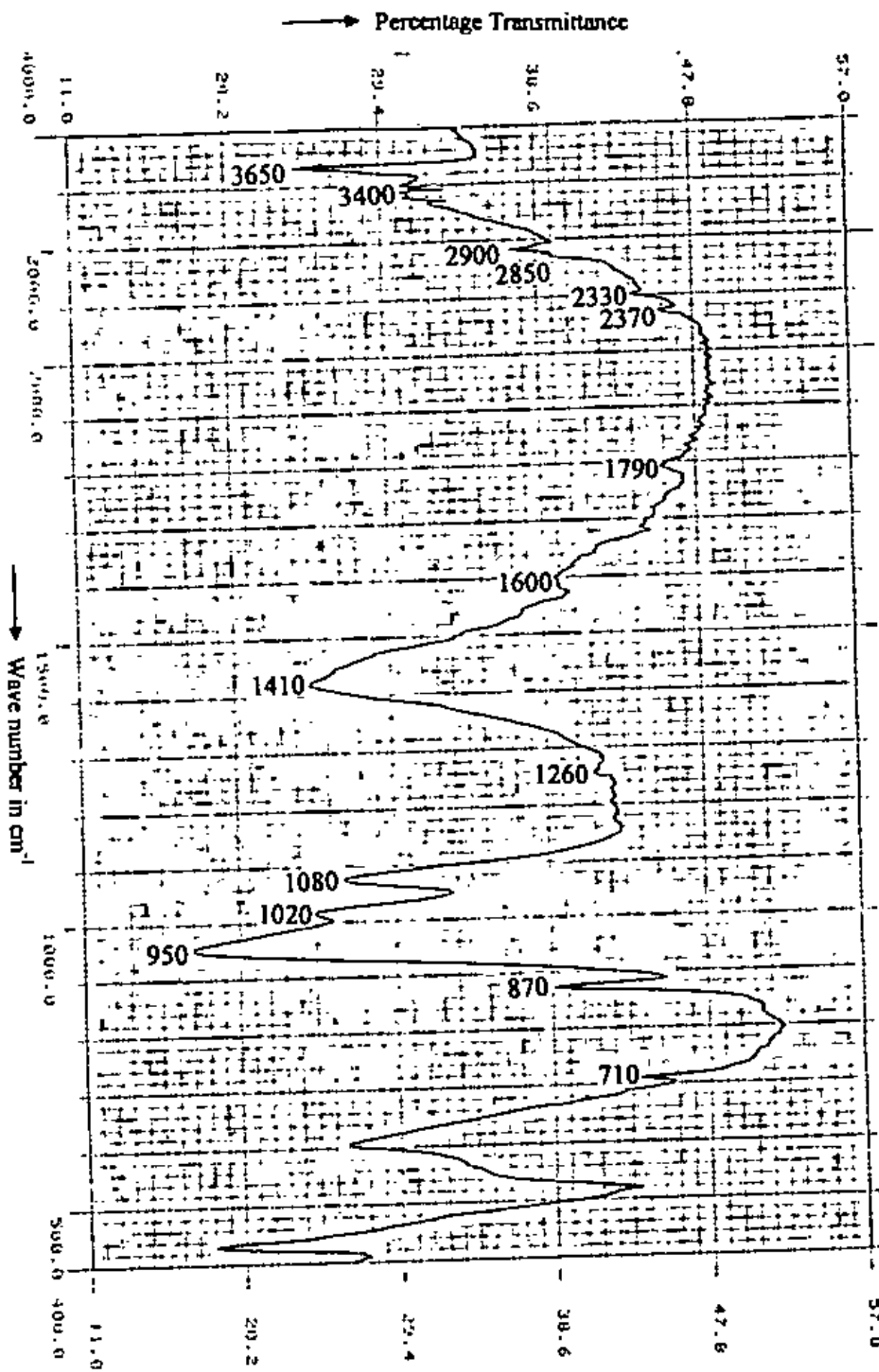Fig. 5.5 Infrared spectrum of sample B
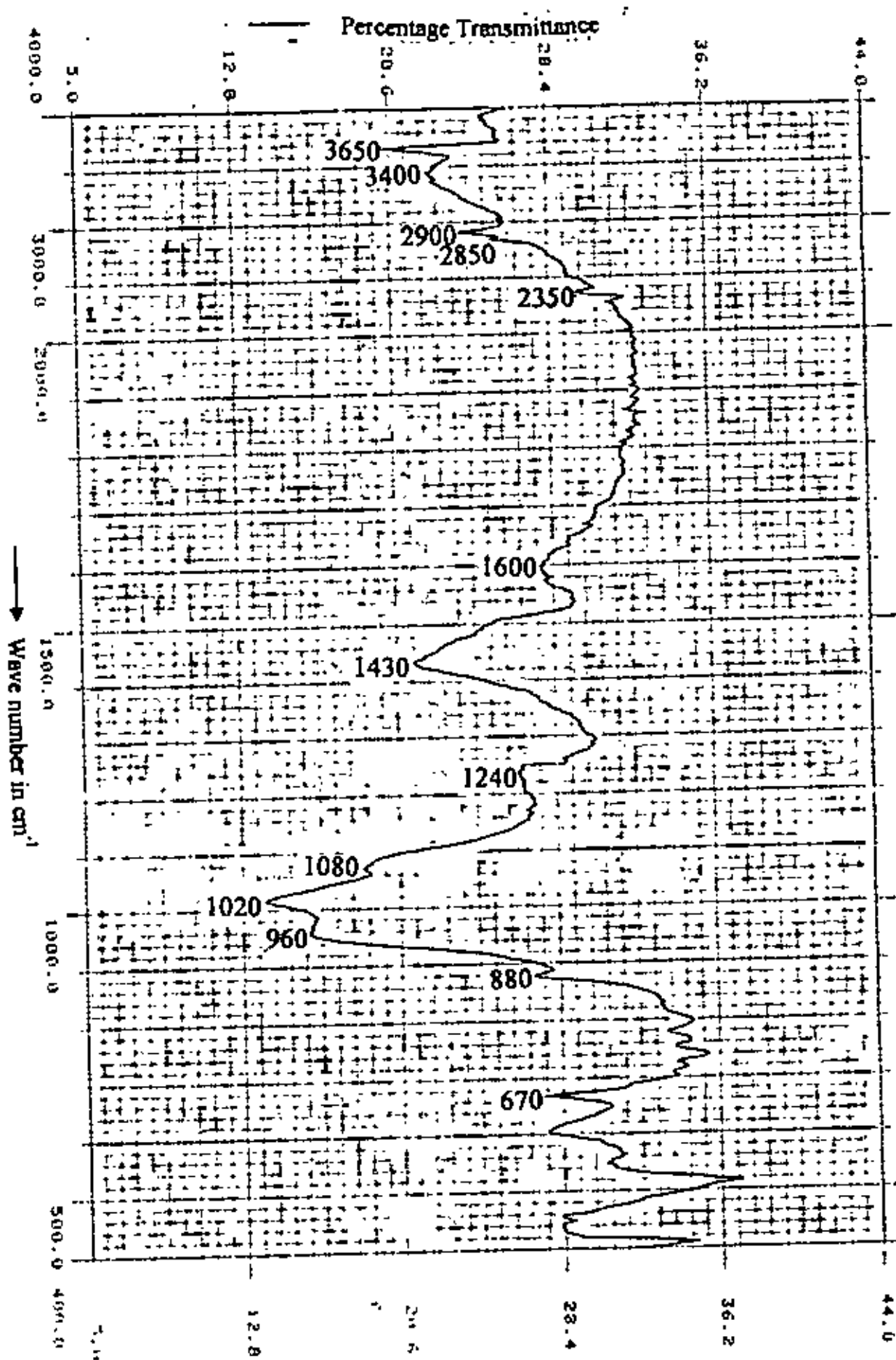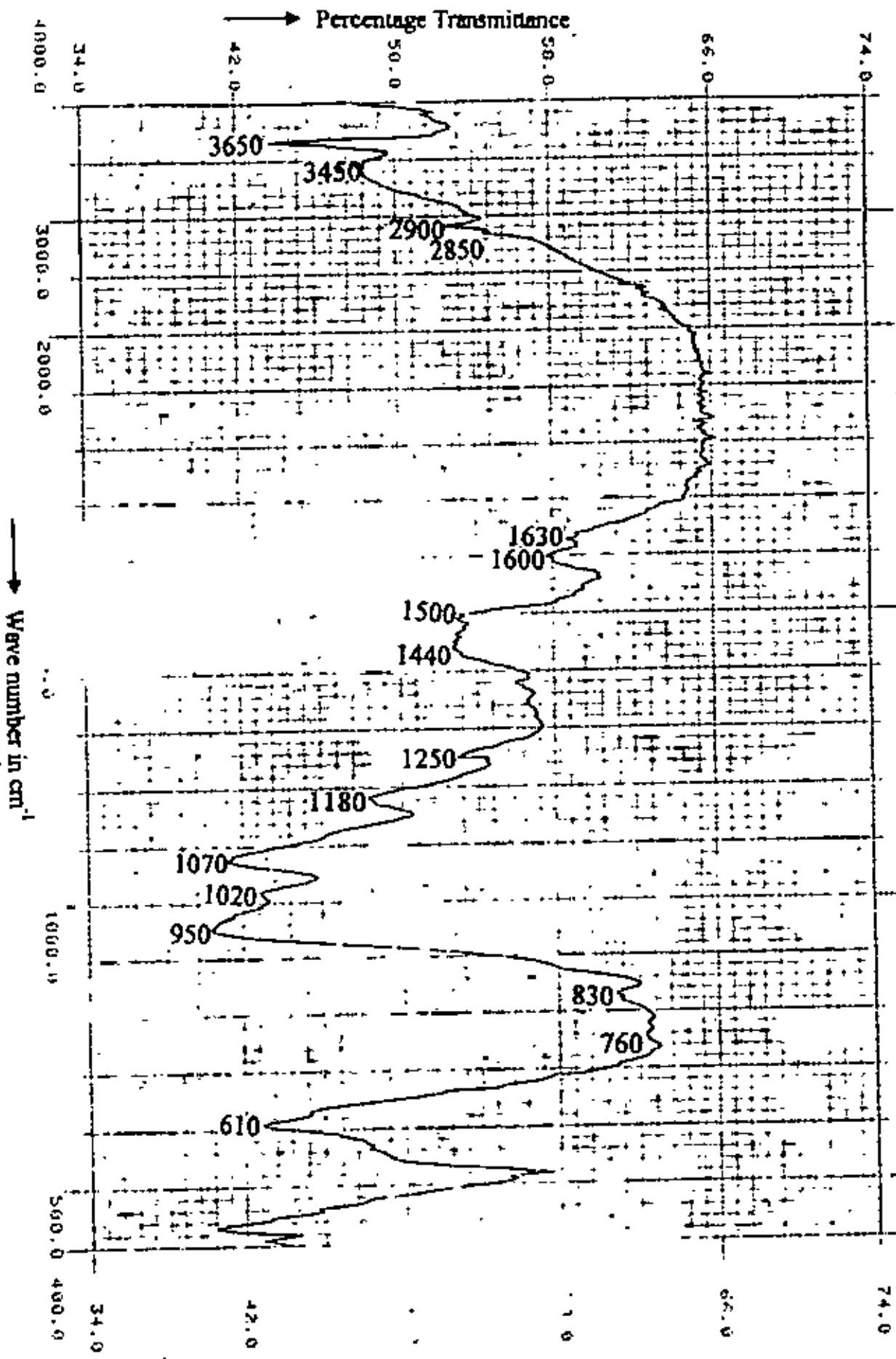
Fig. 5.6 Infrared spectrum of sample F1.

Fig. 5.7 Infrared spectrum of sample F2

Fig. 5.8 Infrared spectrum of sample F3

material. These can exist as distinct particles in the micrograph. It is thus seen that all the four materials examined contain particles of friction modifier (cashew nut shell and/or pre cured phenolics). It is at present difficult to distinguish between the cashew nut shell and the pre cured phenolic particles.

Besides the friction modifier, existence of lumps of asbestos fibers are also seen in some samples (indicating by 'A'). In addition, the size and amount of brass particles vary from sample to sample. Brass particles are seen as very bright phase in sample F2 (Fig.5.11a indicated by 'B') and F3 (Fig. 5.12a). Samples B and F1 also contain brass particles but their size and amount are small. The average size and amount of brass particles (numbers/cm^2) were determined under the microscope and are presented in Table 5.7 and 5.8 respectively. It is seen that both F2 and F3 contain brass particles that are significantly larger in size and higher in amount as compared with those of the other samples.

5.1.4 Fiber content

The asbestos fiber contents of the four samples were determined by dissolution of the matrix resin and other ingredients. Table 5.9 shows the fiber content of the samples. It is seen that the fiber contents of the samples are in the range of 30-50 wt.%. The Bangladeshi material (sample B) contains a moderate amount of asbestos fiber (44%).

Table 5.7 Average brass particle size of B, F1, F2, and F3 samples

sample	Particle size (μm)
B	30
F1	48
F2	343
F3	422

Table 5.8 No.of brass particles/cm^2 of B, F1, F2, and F3 samples

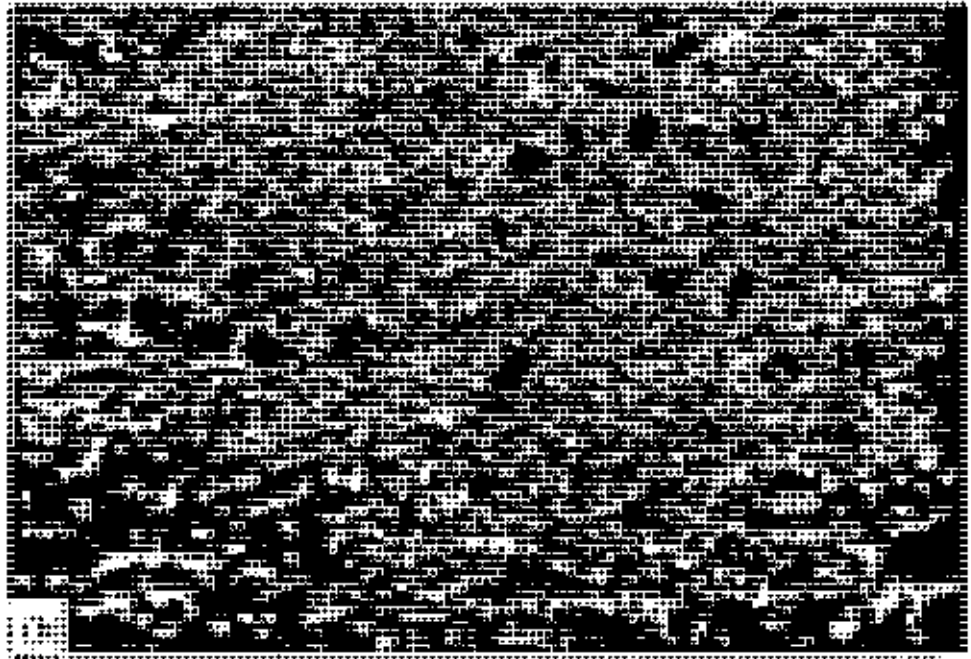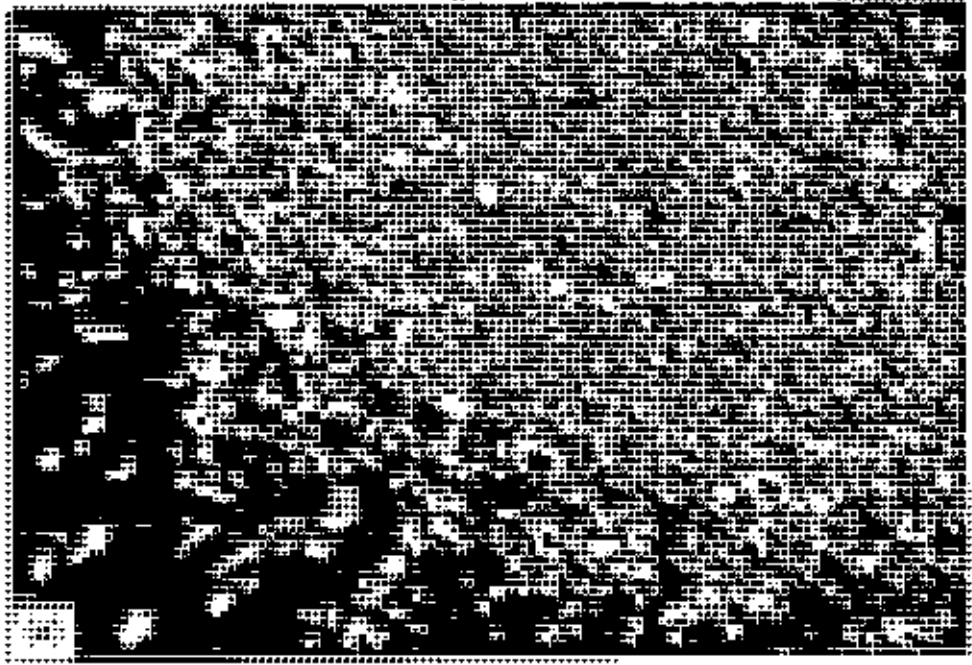| sample	No. of particles/cm^2
B	7
F1	4
F2	11
F3	27

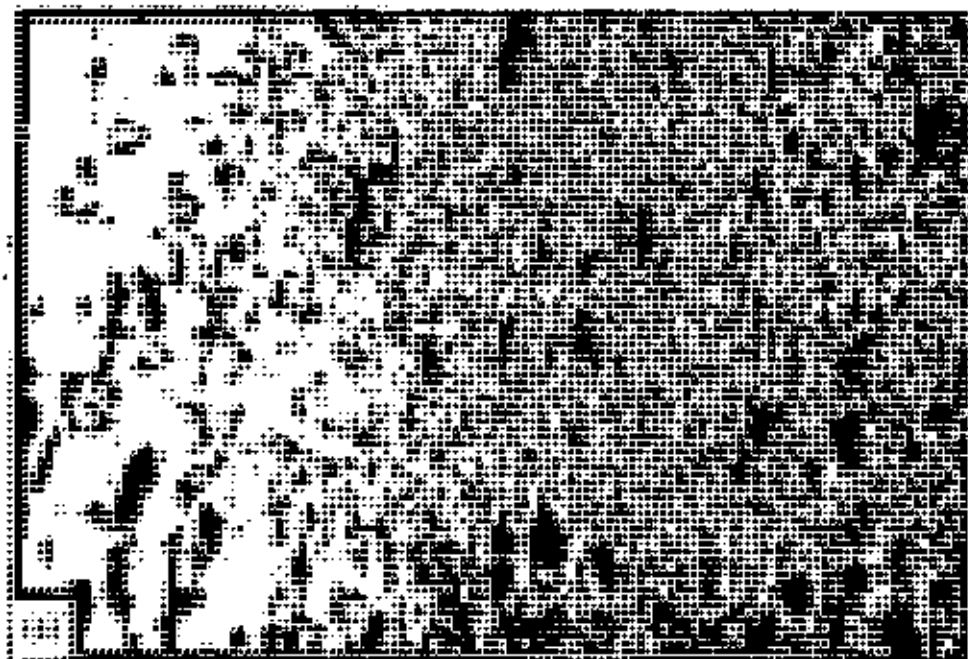Fig. 5.9 Micrograph of sample B (×200), (a) oblique illumination and (b) normal illumination.

Fig. 5.10 Micrograph of sample F1 (×200), (a) oblique illumination and (b) normal illumination.

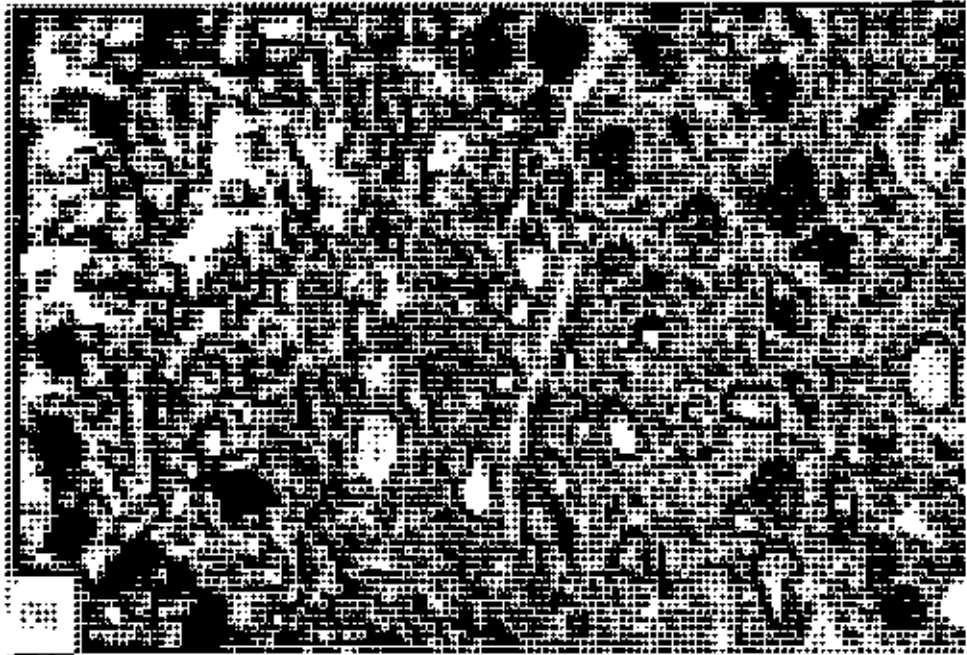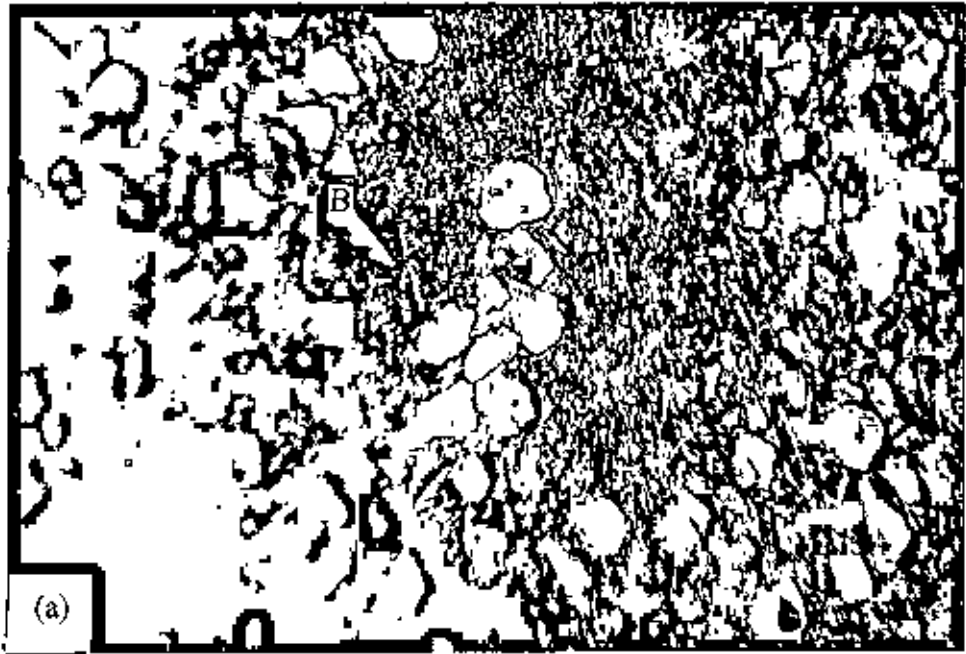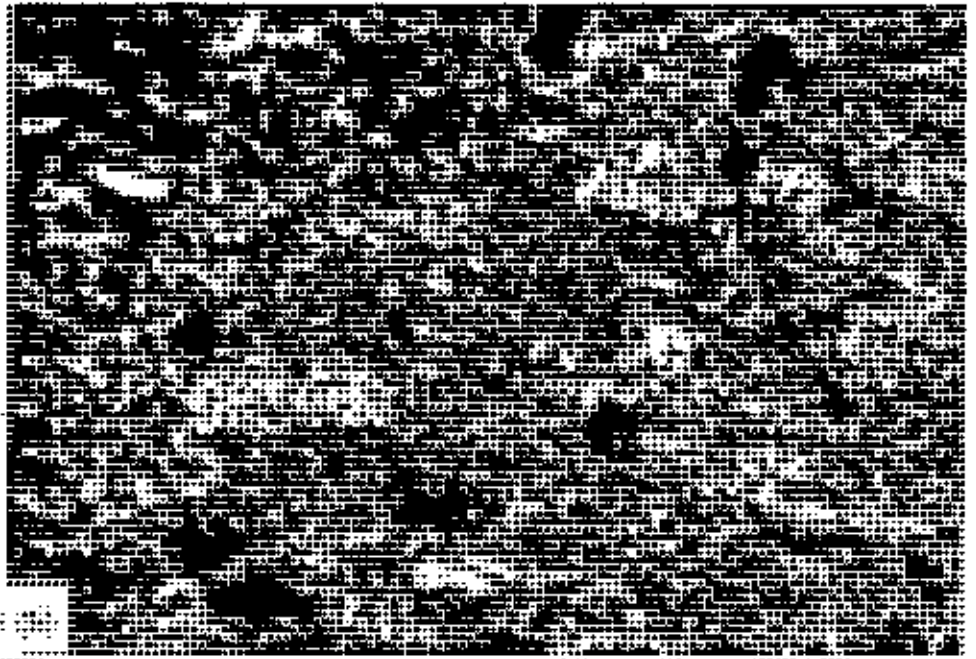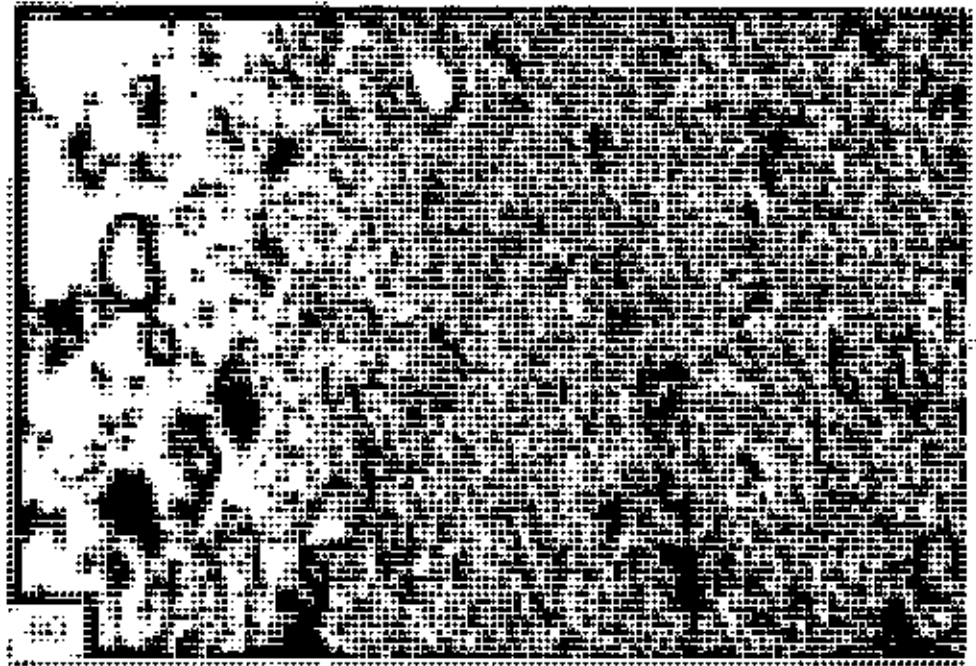Fig. 5.11 Micrograph of sample F2 (×200), (a) oblique illumination and (b) normal illumination.

Fig. 5.12 Micrograph of sample F3 (×200), (a) oblique illumination and (b) normal illumination.

Table 5.9 Asbestos fiber content of B, F1, F2, and F3 samples

Sample	% of fiber (Weight basis)
B	44
F1	32
F2	50
F3	30

5.2 PHYSICAL PROPERTIES OF BRAKE SHOE LINING MATERIAL

5.2.1 Bulk density

The bulk density of the friction materials investigated is given in the bar chart in Fig. 5.13. It is observed that the friction material manufactured in Bangladesh (sample B) has a bulk density of 1.66 g/cc, while the three imported friction materials (F_1, F_2 and F_3) possess a density in the range of 1.92-2.09 g/cc. The Bangladeshi material is thus seen to have the lowest bulk density.
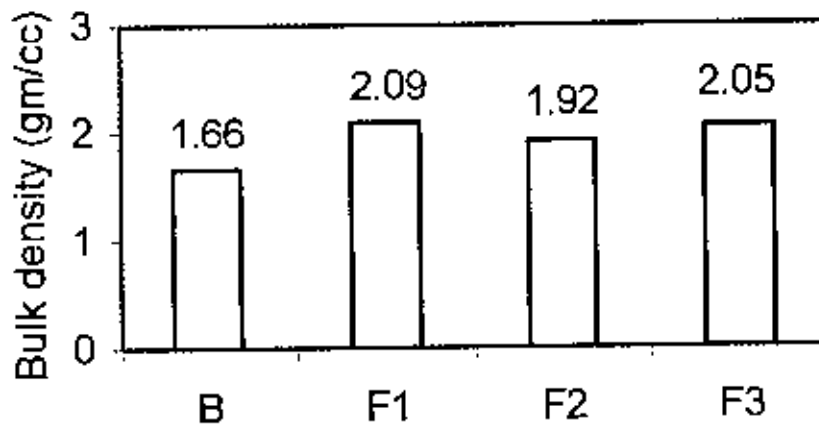

Fig. 5.13 Bulk density of automotive brake shoe lining materials. B: Materials manufactured in Bangladesh and F1, F2, F3: Imported materials of three different countries of origin.

5.2.2 Water absorption

Fig. 5.14 depicts the water absorption characteristic of the materials. Water absorbed by the imported materials is seen to be quite low (0.05 to 0.98%). In comparison, the friction material manufactured in Bangladesh absorbed as much as 4.57 % water which is rather high.
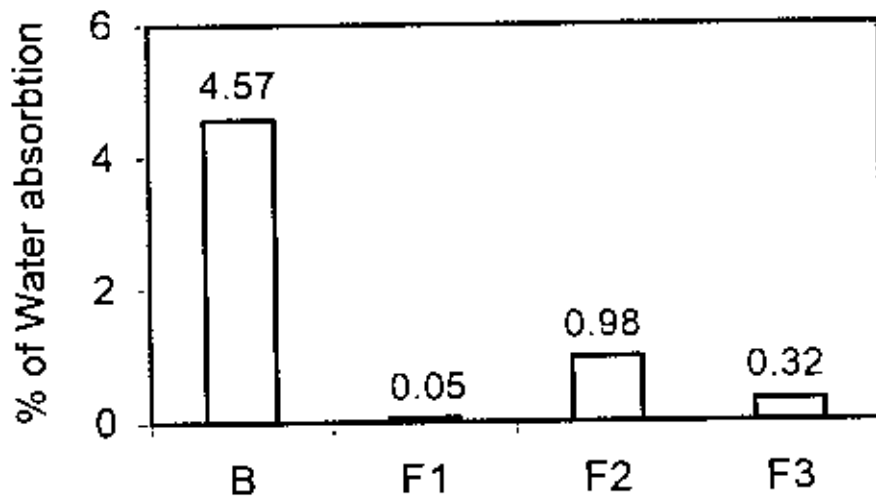

Fig. 5.14 water absorption characteristics of the lining materials.

For instance, Bangladeshi material contains a smaller amount of brass chips as compared with others. Calculation shows that this factor can not fully account for the low density of the Bangladeshi material. Presence of higher porosity in the Bangladeshi material is believed to be responsible for the low density. Higher water absorption of the Bangladeshi material also supports this, because higher percentage of voids has been found to increase water absorption [4].

5.2.3 Swell

The results of swell test performed on the four materials can be found in Fig. 5.15. During the test, the Bangladeshi material is found to swell by 0.39 %. This value is quite comparable with foreign samples F_1 and F_3. Sample F_2 is found to possess the worst swell resistance i.e., it exhibits the highest swelling during the test.
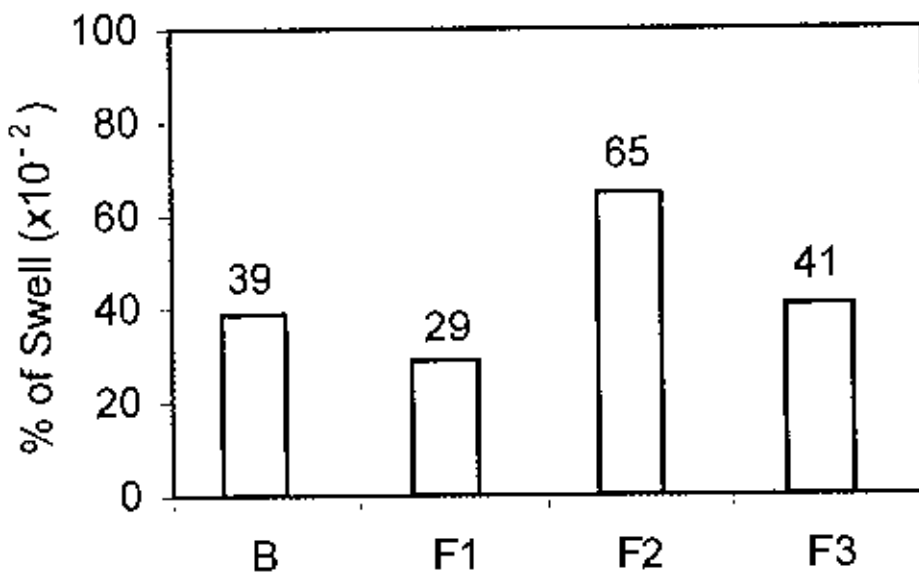

Fig. 5.15 Results of swell test on brake lining materials.

5.3 FRICTIONAL AND WEAR BEHAVIOR OF BRAKE SHOE LINING MATERIAL

5.3.1 Friction coefficient

For frictional measurements, the disc was rotated at 1650 rpm that yielded linear speed of 2.97m. The variation of friction coefficient (μ) during wear tests is shown in Fig. 5.16(a-d) for all the materials (B, F1, F2 and F3 samples respectively). The friction coefficient is shown in each case as a band that represents the variation of its value during different tests. The bands of friction coefficient values for all the

materials are more or less horizontal in all cases, indicating that the friction coefficient is rather stable during the tests [29,38]. The friction coefficient curve of Bangladeshi material tends to show a slightly higher fluctuation though. All the materials possess friction coefficient in the neighborhood of 0.4, Bangladeshi material has a slightly higher while the imported material F1 has a slightly lower value than 0.4. These values fall well within the range of friction coefficient of automotive brake lining material [31].

5.3.2 Wear

Fig. 5.17 presents the comparison of wear resistance of the friction materials. Bangladeshi material (sample B) exhibits the higher wear rate i.e., a lower wear
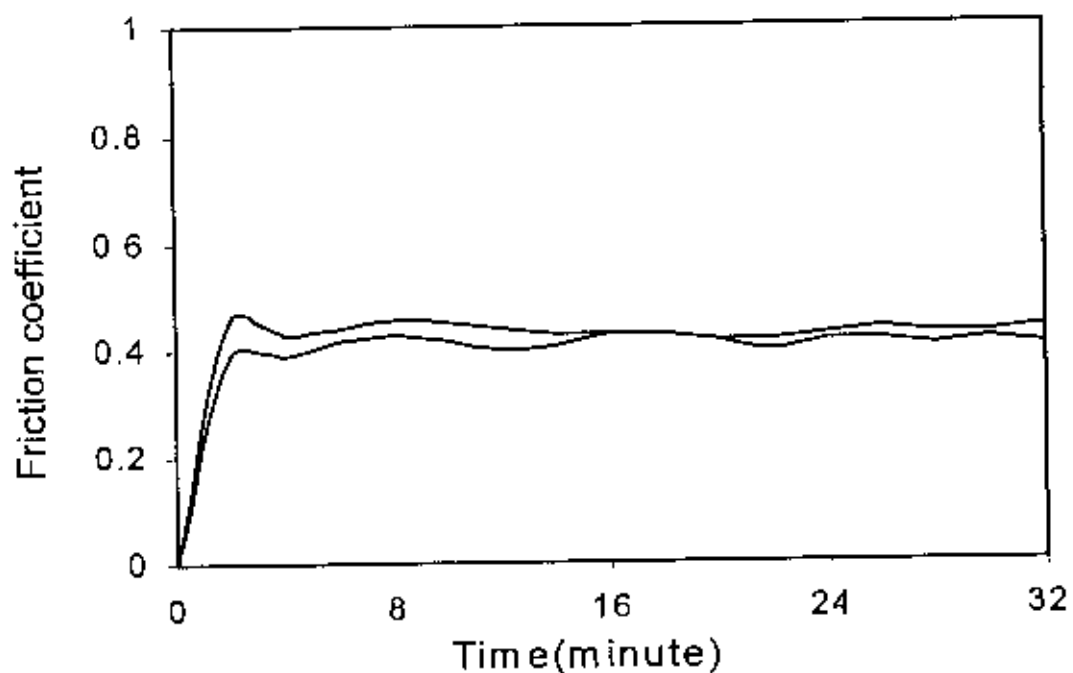

Fig. 5.16 Friction coefficient of break linings against gray cast iron as a function of testing time. (a) B, (b) F1, (c) F2 and (d) F3.

resistance than the imported materials F2 and F3. The Bangladeshi material is however superior to the material F1 in terms of wear resistance. Larger amount of brass particles (Table 5.8) present in the F2 and F3 samples are thought to be among the reasons for the much lower wear rate of these samples.
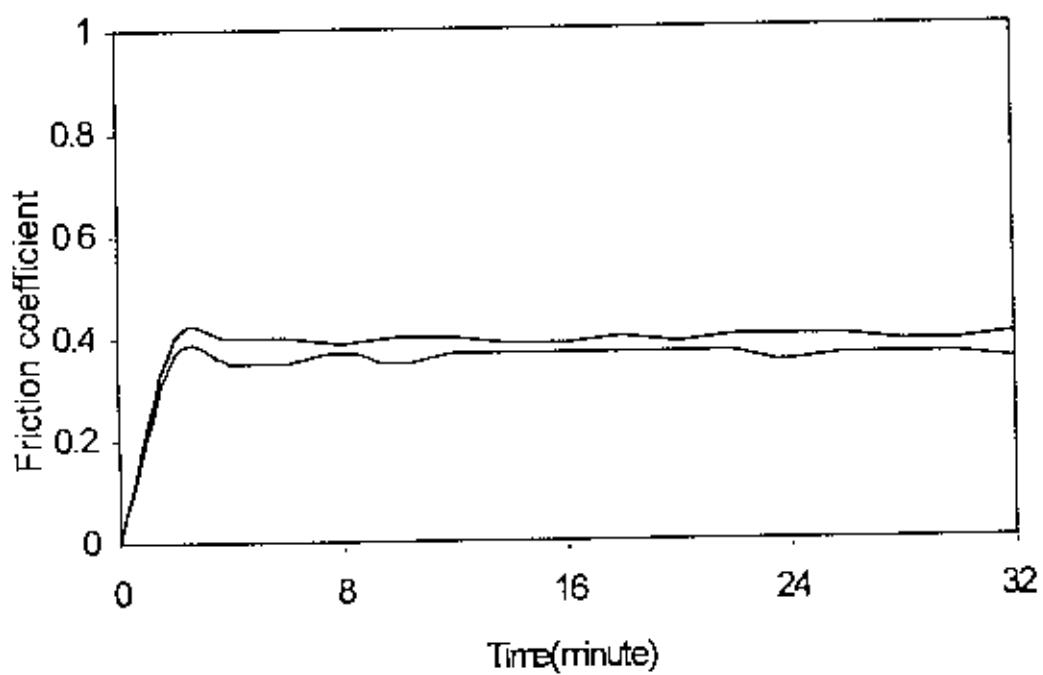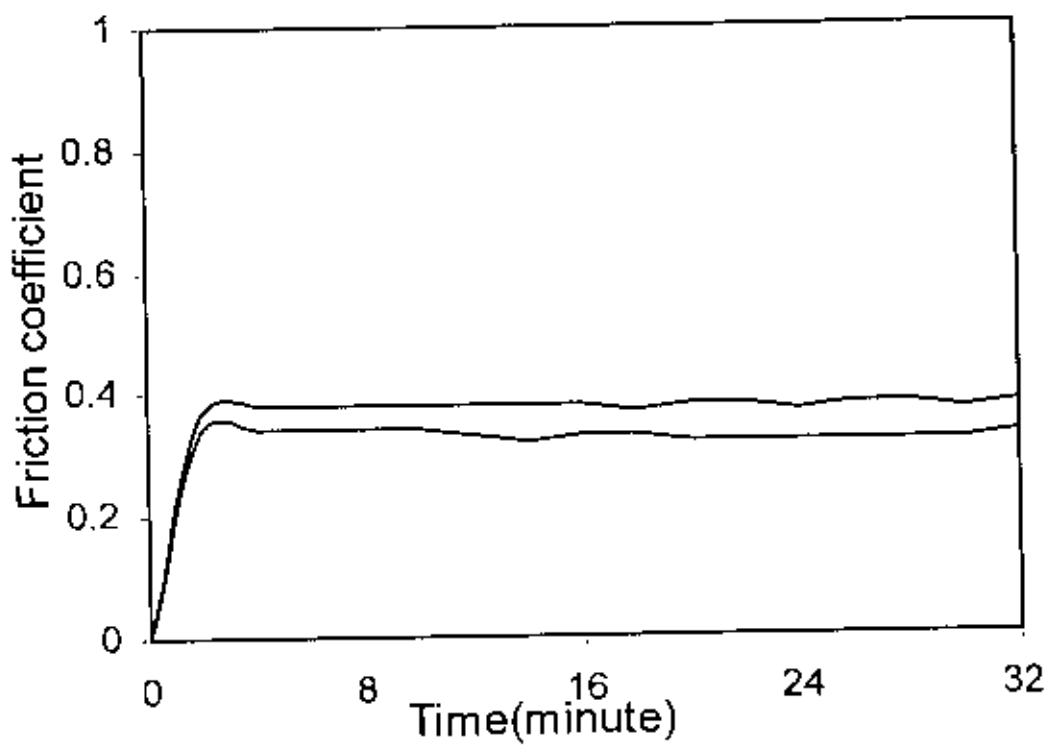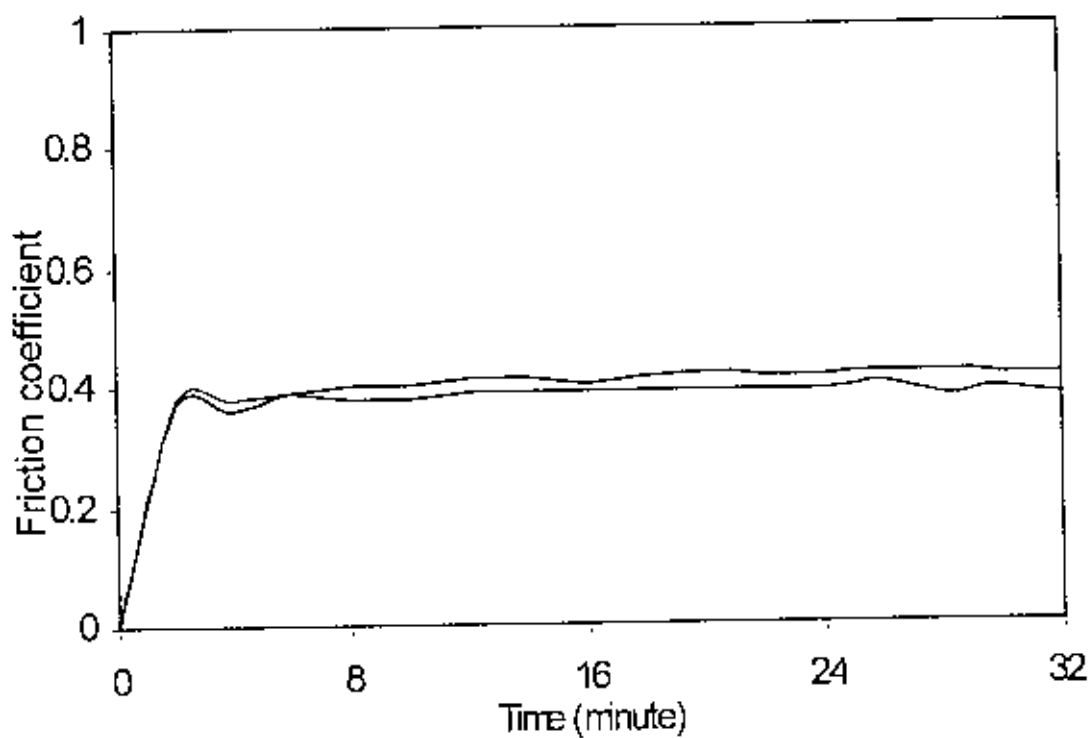
91

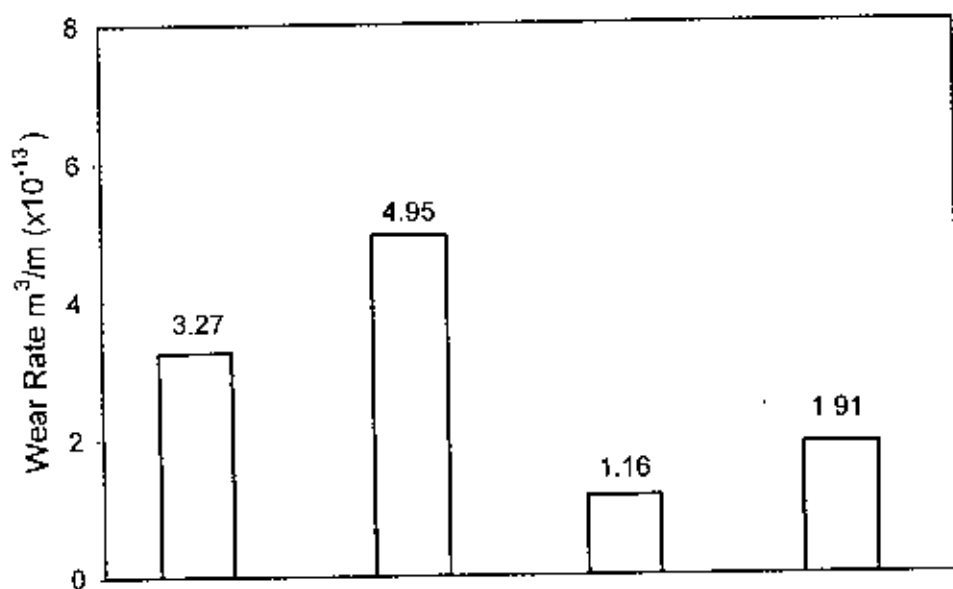Fig. 5. 16 (Continued)

Fig. 5.16 (Continued)

Fig. 5.17 Comparison of the wear of the lining materials

Fig. 5.18(a-d) shows the photomicrographs of wear scar on B, F1, F2 and F3 samples respectively tested for a sliding of 6768 m. The micrographs were taken immediately after the test without any cleaning. Sliding marks are visible on all the four samples. Sample B shows a smoother wear scar with closely spaced sliding marks. The wear scars on samples F1, F2 and F3 are relatively rough. Widely spaced deep grooves are visible In addition, some dark areas are easily visible on the scars of F1, F2 and F3. These dark areas are deep pits from which dislodgment of particles occurred. Such dislodgment is seen to occur to a much lesser extent in sample B. From the optical micrographs shown in Fig. 5.18(a-d), it is not possible to identify the wear mechanism(s) of the friction materials. Further study with SEM could shed some light on the exact mechanism [39].
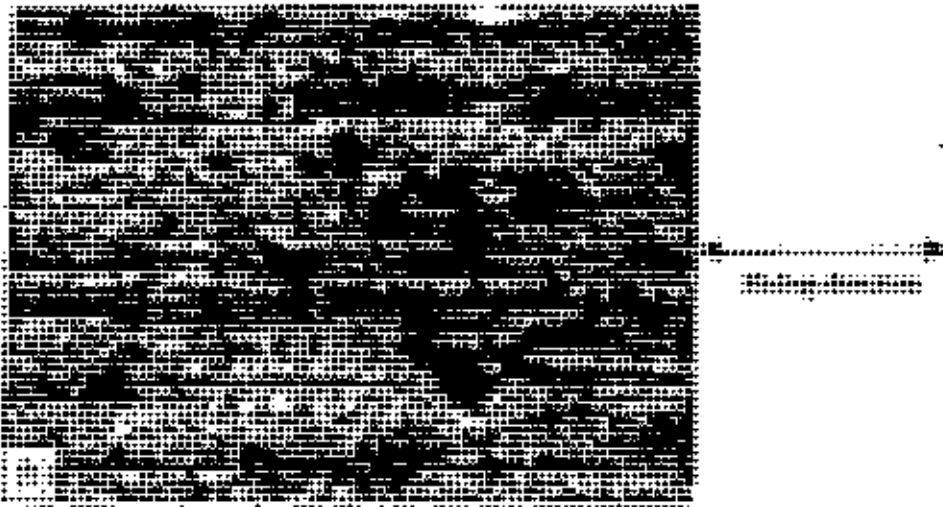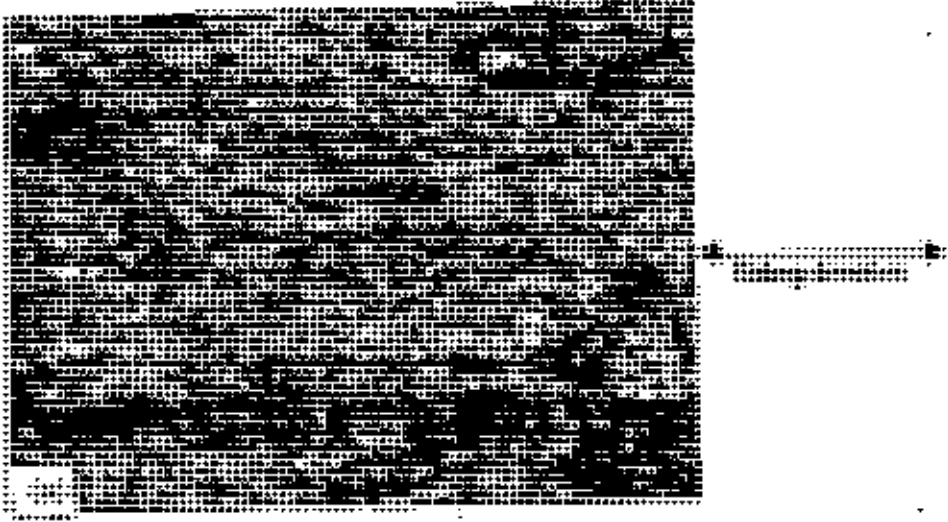
Fig. 5.18 Micrograph of wear scar of sample (a) B, (b) F1, (c) F2, and (d) F3. × 100 (Applied load 15N, sliding distance 6768m).
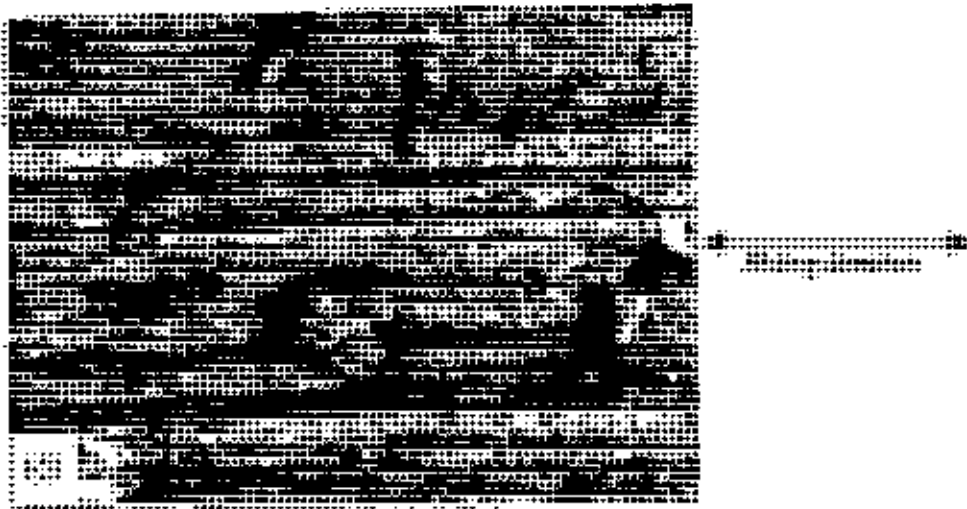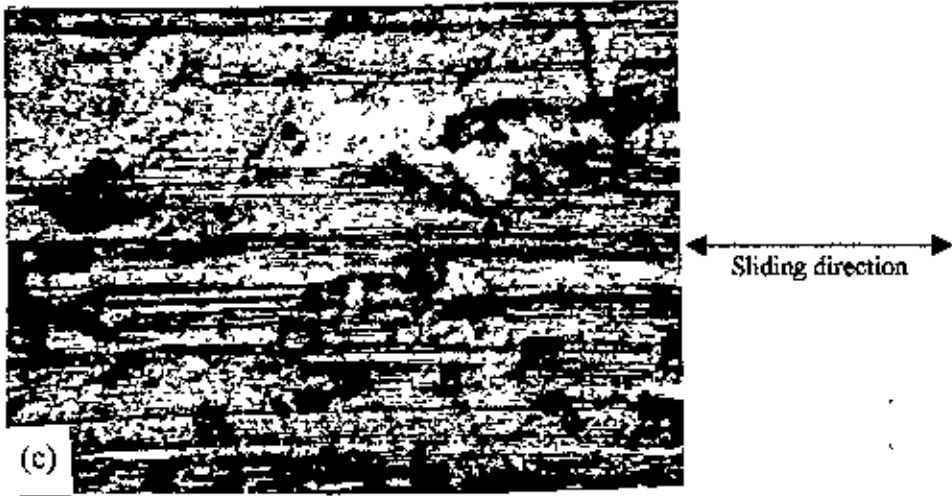
Sliding direction

Sliding direction

Fig.5.18 (Continued)

Chapter Six

6. SUMMARY AND CONCLUSION

A polymer based automotive brake shoe lining material manufactured in Bangladesh is compared with those of three imported materials sold in the local market. X-ray diffraction, infrared spectroscopy, gravimetric analytical techniques and metallographic examination of the four materials were carried out to identify the constituents. Relevant physical properties of the materials viz. Density, water absorption and swelling characteristics were also determined using standard methods. The friction and wear behaviour of the materials were tested in a pin-on-disc type apparatus under ambient conditions. (Linear speed and load employed were 2.97 and $1.88m^{-1}$ and 15N respectively.) X-ray diffraction was used to find out the phases that are present in the lining materials. A JEOL DX-GE-2P X-ray powder diffractometer with Mok_{α} radiation was used to identify the phases. Infrared spectroscope was used to identify the organic compounds present in the samples. A 460 shimadzu Infrared spectrometer with a scanning speed of 360 cm^{-1}/min in the range of 460–4000 cm^{-1} was used for this purpose. Presence of fiber in these materials were determined by ASTM D 3171-76 standard test method. Water absorption, bulk density and swell test were conducted by ASTM D570-77,SAE J380 and SAE J160 JUN80 respectively. For wear and frictional measurements, the disc was rotated at 900 and 1650 rpm respectively. Wear was measured by the weight loss after the sliding distance of 6768m. During the tests, friction force was measured by an on-line load cell. It has been observed that all of the four friction materials contain phenol formaldehyde as the matrix. Other major ingredients were also the same in all the samples. These include asbestos as fiber reinforcement, barium sulphate as filler, brass particles and cashew nut shell/pre cured resin as friction modifiers. It was found that swell resistance of the friction material manufactured in Bangladesh compares favourably with that of the imported materials, but the bulk density of the Bangladeshi material is the lowest and its water absorption highest. The room temperature friction coefficient of the Bangladeshi material was found to be about 0.4 which lies well within the acceptable range. Among the four materials tested the Bangladeshi material was found to rank third in respect of wear

resistance. It is concluded that the physical and room temperature wear and frictional characteristics of the brake shoe material manufactured in Bangladesh are reasonable. However, in order to make a complete evaluation of the performance of the Bangladeshi friction material vis-a-vis the imported ones, their fade and recovery characteristics as well as other properties should be determined. It is believed that there are ample scopes for further improvement of the quality of Bangladeshi material through improved formulation and manufacturing process control. Besides the above, a wear testing machine based on SAE J661a has been designed to correspond closely to the wear and frictional condition of an actual automobile.

Chapter Seven

7. REFERENCE

1. S. K. Rhee, M. G. Jacko and P. H. S. Tsong, Wear, 146 (1991) pp. 89-97.

2. P. Lukin, G. Gasparyants and V. Rodionov, Automobile Chassis: Design and Calculations, Mir Publishers, Moscow, (1989).

3. Yu. M. Tarnopol' Skill and T. Kincis, Static Test Methods for Composites, Van Nostrand Reinhold Company Inc., (1981).

4. P. K. Mallick, Fiber-Reinforced Composites, 2nd Ed., Marcell Dekker Inc., New York (1993), p. 372.

5. W. W Wright, The Effect of Diffusion of Water into Epoxy Resins and Their Carbon Fiber Reinforced Composites, *Composites*, 12:201 (1981).

6. G. Marom and L. J. Broutman, Moisture in Epoxy Resin Composites, *J. Adhesion.* 12:153 (1981).

7. E. L. McKague, Jr., J. E. Halkias, and J. D. Reynolds, Moisture in Composites: The Effect of Supersonic Service on Diffusion, J. Composite Mater., 9:2 (1975).

8. M. J. Adamson, A Conceptual Model of the Thermal-Spike Mechanism in Graphite/Epoxy Laminets, Long-Term Behavior of Composites, ASTM 813:179 (1983).

9. H. T. Hahn, Hygrothermal Damage in Grafhite/Epoxy Laminates. J. Eng. Mater. Tech. vol., 109:1 (1987).

10. J. R. Strife and K. M. Prewo, The Thermal Expansion Behavior of Unidirectional and Bidirectional Kevlar/Epoxy composites, J. Composites Mater., 13:264 (1979).

11. S. F. H. Parker, M. Chandra, B. Yates, M. Dootson, and B. J. Walters, The Influence of Distribution Between Fiber Orientation Upon the Thermal Expansion Characteristics of Carbon Fiber-reinforced Plastics, Composites, 12:281 (1981).

12. D. A. Rigney, Metallurgical Engineer, The Ohio State University, Coloumbus, Ohio.

13. N. Viswanath and D. G. Bellow, Wear, 181-183 (1995), pp. 42-49.

14. Z. Rymuza, Wear in Polymer Micro-Pairs, Proc. 3rd. Int. Conf. on Wear on Materials (1981), pp. 125-132.

15. S. B. Ratner, I. I. Farberova, O.V. Radyukevich and E.g. Lure, Connection Between the Wear Resistance of Plastics and Other Mechanical Properties, Sov. Plast., 7 (1964) 37.

16. R. B. Lewis, Predicting the Wear of Sliding Plastic Surfaces, Mech. Eng., 86 (1964) 32-35.

17. S. K. Rhee, Wear Equation for Polymers Sliding Against Metal Surfaces, Wear, 16 (1970) 431-445.

18. J. K. Lancaster, Friction and Wear, in A. D. Jenkins (ed.), Polymer Science (1972), Chapter 14.

19. J. R. Atkinson, K. J. Brown and D. Downson, The Wear of High Molecular Weight Polyethylene, pt. 1. Isotropic Polyethylene Against Dry Stainless Steel in Unidirectional motion, Trans. ASME, J. Lubr. Technol., 100 (1978) 208-218.

20. N. S. Eiss, Jr., K. C. Wood, J. A. Smyth, Model for the Transfer of Polymer to Rough Hard Surface, Trans. ASME. Technol., 101 (1979) 212-219.

21. D. Downson, S. Taheri and N. C. Wallbridge, The Role of Counterface Imperfections in the Wear of Polyethylene, Proc. 6th Int. Conf. On Wear of Materials (1987), pp. 415-425.

22. David A. Rigney and W. A. Glaeser, A Source Book on Wear Control American Society for Metals. Metal Park, Ohio, USA, (1978).

23. M. G. Jacko and S. K. Rhee, in M. Grayson (ed.), Encyclopedia of Composites Materials and Components (1983), pp.144-154.

24. B. J. Briscoe, I. Ramirez and P. J. Tweedle, Friction of Aramid Fiber Composites, Proc. Int.Conf.on Disc Brakes for Commercial Vehicles, Institution of Mechanical Engineers, London (1998), pp. 15-29.

25. P. H. S. Tsang, M. G. Jacko and S. K. Rhee, Comparison of Chase and inertial brake Dynamometer Testing of Automotive Friction Materials, in K. C. Ludema (ed.), Proc. Int. Conf. on Wear of Matelals, American Society of Mechanical Engineers, New York, (1985), pp. 129-137.

26. M.G. Jacko, Physical and Chemical Changes of Organic Disc Pads in Service, Wear, 46 (1976) 163-175.

27. J. M. Herring, Mechanism of Brake Fade in Organic Brake Linings, SAE Q. Trans., (1967) Paper 670146.

28. M. G. Jacko, W. M. Spurgeon, R.M. Rusnak and S. B. Catalano, The Thermal Stability and Fade Characteristics of Friction Materials, SAE Q. Trans., (1968) Paper 680417.

29. P. Gopal, L. R. Dharnai and Frank D. Blum, Wear, 174 (1994) pp.119-127.

30. Jisheng E and D. T. Gawne, Wear176(1994), pp.195-205.

31. W. C. Orthwein, Clutches and Brakes: Design and selection, Marcel Dekker Inc. N.Y., (1986).

32. Andersion, A. E., and Knapp, R. A., Brake Lining Mechanical Properties, Laboratory Specimen Studies, paper 790715, SAE, Warrendale, (1979).

33. Y. R. Sharma, Elementary Organic Spectroscopy: Principle and Chemical Application, S. Chand & co. Ltd., New Delhi, (1992).

34. Powder Diffraction File, Joint Committee on Powder Diffraction Standards, Pennsylvania, Second printing, October, (1980).

35. Cullity B. D., Elements of X- ray Diffraction, 2nd Ed., Addision-Wesley Publishing Company, Inc. London, (1977).

36. Wayne R. Sorenson and Tod W. Cambell, Preparative Methods of Polymer Chemistry, Second Edition, Interscience Publishers.

37. R. L. Pecsok, L. D. Shields, T. Cairns and I. G. McWilliam, Modern Methods of Chemical Analysis, 2nd Ed., John Wiley & Sons, New York, (1976).

38. P. Gopal, L. R. Dharnai and Frank D. Blum, Wear 181-183 (1995) pp. 913-921.

39. P. Gopal, L. R. Dharnai and Frank D. Blum, Wear 193 (1996) pp.199-206.